Flinders
UNIVERSITY

Adaptive MIMO Vibration Cancellation in Plate Structures

-- Design Online Controller based on PPF Control Strategy

by

Chuanyu Sun, M.Eng. (Biomedical)

Supervisor: Amin Mahmoudi, Fangpo He

Date of submission: December, 2019

Submitted to the College of Science and Engineering in partial fulfillment of the requirements for the degree of Master of Engineering (Biomedical) at Flinders University - Adelaide Australia

Acknowledgement

Firstly, I would like to express my profound appreciation to my supervisors, Dr Amin Mahmoudi and Associate Prof. Fangpo He who prompted the generation and accomplishment of this thesis. I am inspired by their dedicated work style. Especially Fangpo, she provided me with many valuable comments to encourage me to work better. Besides, she provided some life advice to me to make my mind free from distraction to finish my thesis.

Then, I also want to express my gratitude to PhD. Peng Zhang, his patience, inspiration and constructive criticism were accompanied me in the whole processing of the project, he helped me too much.

Finally, special thanks to my husband and my parents, thanks for your selfless and endless support, encouragement and understanding during the preparation of this thesis.

Declaration

I certify that this work does not incorporate without acknowledgment any material previously submitted for a degree or diploma in any university; and that to the best of my knowledge and belief it does not contain any material previously published or written by another person except where due reference is made in the text.

Chuanyu Sun

December 2019

Abstract

Flexible structures are widely used in many engineering systems due to their lightweight. This kind of structures is normally vulnerable to vibrations, especially when the system changes. To such systems, the fixed-parameter active vibration controllers cannot provide the best control performance and sometimes even help to excite the system. Therefore, a Real-Time Adaptive Control Scheme (RTACS) is highly demanded to maintain control performance in real-time. The RTACS is required to respond to changes in the system (adjust the parameters of controller online) and provide sufficient vibration attenuations.

In this thesis, a top thin plate bonded connected to a vibration base plate by three pairs of sensors/actuators is used as a research vehicle. The top plate can be mathematically modelled as a three-input three-output resonant flexible structure with an infinite number of modes near the natural frequencies of the structure itself. However, only the first three modes are in the concerned frequency range. Therefore, for the controller design purpose, a simplified State-Space Representation (SSR) model and Second-order Differential Model including these three modes are constructed (the D term is neglected for simplicity).

Positive Position Feedback (PPF) is one of the most effective active control algorithms and is widely applied to many MIMO flexible systems due to its advantages. The PPF utilizes a second-order low-pass filter that is insensitive to spillover effect and can control multiple modes through one pair of sensor/actuator. However, designing a PPF requires simultaneous optimization of all controller parameters for different modes and PPF also lead to a relatively large steady-state error for the closed-loop system. According to the above analysis, two new control methodologies based on the technique of PPF are proposed and implemented on the plate system.

The first proposed method is Independent Modal Positive Position Feedback (IMPPF) combining the advantages of the Independence Modal Space Control (IMSC) algorithm with the PPF. Thus, the parameters of IMPPF can be designed separately for each vibration mode. The structure of IMPPF is relatively simple as it only uses two controller parameters for each mode (i.e., the control gain and time constant are designed through error elimination method and root locus technology respectively). The computation load of the proposed IMPPF is low, therefore, IMPPF can easily realise online update parameters and be implemented in the proposed RTACS. The second method is the Modified Positive Position Feedback (MPPF),

which is developed by adding a first-order filter in parallel to the conventional PPF. The first-order filter has the potential to reduce the damping of the compensator, thereby reducing the steady-state error of the closed-loop system while maintaining the control performance of PPF. The parameters of MPPF can be optimized by utilizing the H_∞ norm and Genetic Algorithm. Finally, an RTACS is proposed based on a pre-designed frequency estimator that can select the better controller between IMPPF and MPPF and update controller parameters in real-time.

To validate the effectiveness of the proposed methods, numerical simulations are conducted on MATLAB Simulink©. Both IMPPF and MPPF are designed for the built SSR model. The simulation results show that the vibration attenuation effect of IMPPF can reach up to 13 dB, and MPPF can reach up to 20 dB. The simulation result of the RTACS clearly demonstrates its effectiveness in vibration attenuations of the given MIMO flexible plate-structure after the onset of system changes.

A real-time physical experiment is conducted upon successful validation of the proposed IMPPF, MPPF and RTACS in simulation. The experiment results show that the control performance of IMPPF and MPPF can reach up to 17dB and 20dB, respectively, that agrees with the results of simulation study. The experiment results also verify the effectiveness of the proposed RTACS to control the first three vibration modes of the given MIMO flexible plate-structure, especially after a system change is introduced to the original MIMO flexible plate-structure.

Table of Illustrations

Contents

Chapter 1: Introduction

This chapter introduces the motivation of the thesis, followed by the background of the research project. Finally, the research methodology with an outline of the thesis is shown.

1.1 Motivation

In order to enhance the efficiency and dynamic performance of machines, researchers are increasingly inclined to make the system design light. More and more designers are prompted to put lightweight materials to devices. Lightweight materials make the structures more flexible. The flexible structure offers many benefits, such as reduces weight, wind resistance, and space requirements. These have made it possible to achieve some outcomes in many fields, such as enhancing the agility of the robotic arm and reducing the energy consumption of vehicles. In the biomedical field, these outcomes have led to the creation of devices for micro-invasive surgery and the possibility of artificial mechanical limbs.

However, there is one big problem of flexible structures: it is susceptive to the environment changes which bring unwanted vibrations to the system. Due to the light and thin design of the flexible structure, it is easily damaged by the unwanted vibrations. Especially, the vibration frequency is close to the natural frequency of the structure, the resonance is derived. The resonance causes the structure oscillates with a large amplitude, which may lead to poor performance, short lifetime and the destruction. One classical example of the damage of resonance phenomenon is the collapsed of Tacoma Narrows Bridge in 1940. The narrow and thin bridge can be seen as a kind of flexible structure. The bridge was destroyed by the wind caused a resonance phenomenon. This shows the importance of vibration cancellation.

However, the problem becomes not simply to eliminate vibration, as the system tends to change over time. For example, an aircraft constantly burns fuel to provide energy during flight, its total mass also constantly reduces, and all the parameters of the flexible structure are varying with time accordingly. Therefore, controlling the dynamic system with a fixed controller often leads to poor control effects and even destabilizes the entire system. However, rather than rebuilding the structures or using non-lightweight materials, people are more willing to control vibration with the environment changing which is known as adaptive online control.

Adaptive online control is not an easy task, that because of several difficult points:

1. The flexible structure has very large amounts of modes, which means the mathematic model is nearly infinity orders. It is extremely tough to build the mathematic model. It is impossible to design a controller or algorithm to control all of the modes. Hence, researchers always only consider several significant modes. Generally, the modes with low frequencies influence the structure most. Hence, the mathematic model is built for several low frequencies modes to realise simplified to low order substitute function. Nevertheless, the system is still affected by the ignored modes. That causes the spillover effect which may lead to low performance and unstable of the system.

2. The controller of the flexible structure is requested to control multiple modes in a wide band. It is hard because researchers need to balance the better attenuation control effect for one mode or sensitive to control several modes.

3. The parameters of the flexible structure are varying with time. The variation is usually small but continuous. As the aeroplane in the previous example, the controller has to change the parameters in time to ensure a smooth flight. Unfortunately, most parameters are unknown or request large computations.

4. The controller needs to respond to the flexible system quickly enough. Since the system is changing continuously, the previous parameters may make the system work poorly or even unstable. Therefore, the controller needs to calculate and replace new parameters quickly. But less time means less accuracy. The trade-off between time and accuracy is also a major topic of the research.

These four points can assist to determine the requests of the research and design an appropriate controller to cancel the vibration for a flexible structure. The research of flexible system controller has always been a research hotspot, so many researches have been established. The motivation of this thesis is to find solutions to these difficulties so that to get an effective online control method for plate structure which is a common flexible structure.

1.2 Project Background

The project is centred on a plate system. The plate system is a multi-input-multi-output (MIMO) system. The physical setup can be seen as Figure 1.1. This system consists of a top plate, a base plate, three coupled sensor/actuator transducers and a disturbance transducer. They are presented as a grey area, yellow area, T1-T3 and T4 respectively in Figure 1.1. The sensor/actuator banded the top plate and base plate together by screws. Assume the plate system

initial state is static without vibration. The disturbance T4 received a signal which causes the vibration of the base plate, the vibration transfer to three sensors, then to the top plate by screws on the three actuators. Since the T1, T2 and T3 are sensors and also actuators, the system can be seen as three inputs and three outputs system. The goal of the thesis is to design a controller that can effectively reduce the vibration of the top plate, even if the base plate vibration exists, and still have a good control effect when the environment (load, etc.) of the top plate changes.

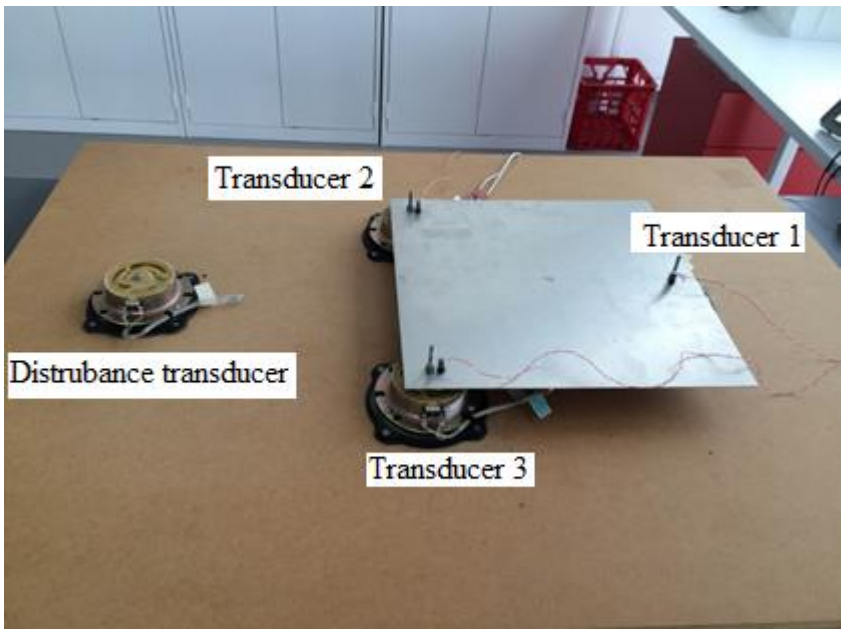

Figure 1-1 - Physical Model

1.3 Methodology and Outline of the Thesis

The research can be divided into 5 steps.

In the first step, a literature review is summarized by reading a large number of relevant flexible system control algorithm works of literature, to analysis the advantages and disadvantages of each method. With the process, the scope of the thesis worked on is continuously narrowed down and determined until the appropriate control algorithms are selected. Based on the gaps in the suitable algorithms, the new control methods are proposed in follow. This part is presented in detail in Chapter 2.

The second step is to build a mathematical model of the plate system. Since some studies have done by previous researchers, the second step focuses on building a State-Space Representation and Second-order Representation that are simpler and available to extract data faster than the

transfer function. However, since the laboratory plate system has amended after the previous researches, the data is obtained again for the new plate system. This part is indicated in Chapter 3.

In the third step, the analysis of the controller strategies to be explored is interpreted by gradually expanding from the systems under tight conditions in original literature to the relatively loose conditions for general systems. Then according to the characteristics of the plate system, it is simplified to achieve high-efficiency and effective online control. The details of this part are in Chapter 4.

In the fourth step, the controllers established in the third step are simulated numerically in MATLAB Simulink© to verify the analysis results and observe the control effects. This content of this step will be described in Chapter 5.

The final step verified the effects of designed new controllers experimentally, which starts with the offline experiments, then do the online experiments. This step is shown in Chapter 6.

Finally, conclusions are presented in Chapter 7.

Chapter 2: Literature Review

This chapter outlines large amounts of literature on adaptive MIMO vibration cancellation, it can be divided into four parts. Section 2.1 will focus on the previous work of the project related to the theme of this thesis. Section 2.2 analyses several algorithms of the adaptive controller with their advantages and disadvantages. In Section 2, three control methods (PPF, IMPPF and MPPF) which are appropriate for the plate system are summarized. These three control algorithms are very important in the entire thesis. Section 2.3 will introduce methods of frequency estimator generation. The frequency estimator is the key to detecting system changes while obtaining useful controller parameters that make online adaptive controllers possible. Section 2.4 summarizes the original contributions of this thesis.

2.1 Previous Work

The project has been undertaken by several researchers and they achieved certain results, but there are still some deficiencies. This part will indicate previous related work.

2.1.1 System Modelling

The mathematic modelling of the physical system is made by Zhang and He [1], who simplified the plant system by changing each infinity-order nonlinear transfer function to be three added second-order linear functions, which is 6-order transfer function. The system can be simplified because the high-frequency modes affect the vibration of the system slightly, in this project, it only considers the first three modes, so there are three second-order functions. Due to this breakthrough work, the controller design is much easier. However, due to the physical system has already replaced also, the data need to be acquired again. In addition, as the research plate system is a MIMO system, the matrix-based expression model is clearer and more concise. Therefore, a State-Space Representation and a Second-order Differential function representation can be constructed to upgrade the original transfer function model.

2.1.2 Controller Optimization Design

Chen [2] researched the online optimization problem of PPF controller. He compared several optimization methods and finally selected the genetic algorithm (GA) for calculating the H_∞ norm as the limit or constraint to select the appropriate parameters. The results showed that the optimization method can further cause up to 5 dB of attenuation. Chen's work can provide an optimization method that is noise-free and has no spillover. But it needs to be improved because

it is not ready to optimize parameters in the system with unknown changes, and the optimization parameters provided by GA are too slow, which can reach up to more than 40 minutes [3]. Thus, it cannot be used directly to the online adaptive control scheme.

2.2 Controller Algorithms

The control algorithm is the key to the adaptive online control system. To explore the control algorithm suitable for the board system, this section indicates several controller design methods.

2.2.1 Least-Mean-Square (LMS) Algorithm

Considering the harmful effects of unwanted vibration from vehicle seats on human health, Gan [4] built an active seat system which can reduce vibrations through the LMS adaptive algorithm. LMS algorithm has a signal filtering process and a filter coefficients adaptive process. Gan [4] tried to use finite impulse response (FIR), shown in Figure 2-1, to be the filter structure for adaptive filtering in digital signal processing, because FIR is always stable. After mathematic modelling the filter and using the LMS recursive algorithm, the weight equation can be indicated as:

$$\boldsymbol{w}(n+1) = \beta \boldsymbol{w}(n) + \mu \boldsymbol{x}(n) e(n)$$

where:

$\boldsymbol{w}(n)$ is the filter coefficient vector, $\boldsymbol{w}(n) = [\mathrm{w}_0(\mathrm{n}), \mathrm{w}_1(\mathrm{n}), \dots, \mathrm{w}_{\mathrm{L}-1}(\mathrm{n})]$, which can be adjusted by LMS adaptive algorithm to minimise the error signal;

$\boldsymbol{x}(n)$ is input vector, $\boldsymbol{x}(n) = [\mathrm{x}_0(\mathrm{n}), \mathrm{x}_1(\mathrm{n}), \dots, \mathrm{x}_{\mathrm{L}-1}(\mathrm{n})]$;

$e(n)$ is error signal, $e(n) = filter\ output\ y(n) - desired\ response\ d(n)$;

μ is a positive real constant which can be calculated by stability condition of the LMS algorithm;

β is leakage factor which is used to control the weight update of the LMS algorithm. The leakage factor can improve convergence and stability of the the LMS algorithm and solve the problem of drifting in the LMS algorithm [32], and can be chosen in the range of 0 to 1.

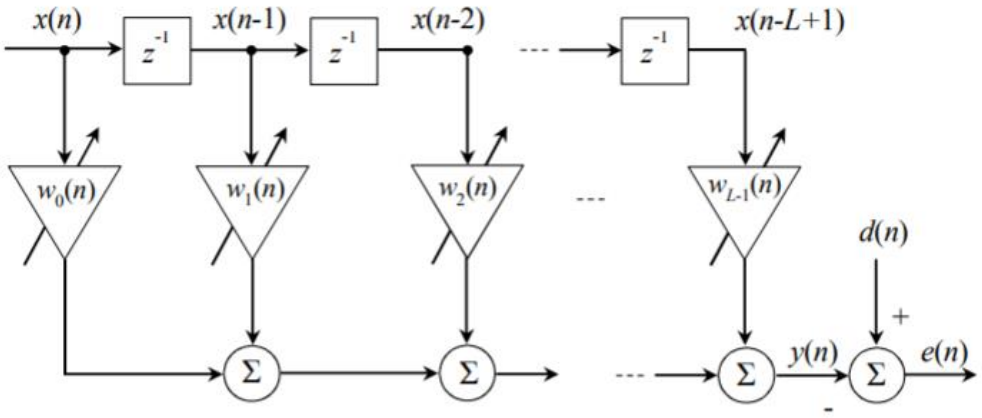

Figure 2-1 - Adaptive FIR filter structure

This method can give a simple way to design the controller and obtain parameters quickly. However, the added controller may cause secondary path dynamics. Although the Filtered-x LMS (FXLMS) algorithm and a secondary path identifier Fast-block LMS (FBLMS) system were derived to compensate the secondary path effect, the added elements made the structure very complex. If the method is used to a MIMO system, the complexity of designing structure increases exponentially. Also, the LMS method is a linear adaptive filtering algorithm. Using this method in non-linear system may cause unsatisfactory performance.

2.2.2 Backstepping Fuzzy Control

Adaptive backstepping fuzzy control strategy has been widely studied in flexible structures. Fuzzy control performs well in many different systems which were confirmed by experimental results. To indicate few, Fang et al. [5] using an adaptive backstepping sliding mode controller with a fuzzy system to control a cantilever beam structure. They presented an adaptive backstepping fuzzy sliding mode control approach can improve the tracking error. Zhao [6] et al. found that a fuzzy adaptive controller can effectively bound all signals and track the target signal in a small error for unknown nonlinear models of strict-feedback systems with unknown disturbances. Li et al. [7] presented a fuzzy adaptive controller with the hybrid parameter adaptive laws is useful for a MIMO nonlinear system. The backstepping fuzzy control not only independents on the system model improves the robustness of the plant system, but also can avoid the cancellation of useful nonlinearities and can relax the matching condition for the strict feedback system. In addition, [5]-[8] all verified this method can be used with state-space representation. It also has self-learning ability, so it is also widely used in artificial intelligent technology. However, the fuzzy logic needs large programming work to realize it, because the

less information fuzzy control may lead the system to reduce results accuracy and dynamic performance. Besides, fuzzy logic lacks the inherent systematisms to define control targets. The mathematical model of the system discussed in this thesis can be constructed, so there is no need to use a fuzzy algorithm.

2.2.3 Independent Modal Space Control (IMSC)

IMSC is developed by Meirovitch [9]. The biggest advantage of the algorithm is that it controls the modes separately, but, because of this, the spillover between mode and mode is significant. Figure 2-3 shows the block diagram of the IMSC compensated system. The φ transfers the output into displacement and then calculate a force which equals to the vibration caused force to suppress the vibration [27]. Due to the IMSC structure, one coupled sensor/actuator only can control one mode. In this thesis, only the first three modes will be considered and the physical structure has 3 coupled sensor/actuator, but for more modes control, more sensors/actuators are needed. Besides, in the MIMO system, the φ will become a 9x9 matrix, so the inverse of φ is a very complicated calculation, which multiplies the difficulty of online calculation. Therefore, it is quite difficult to build a suitable IMSC for this system.

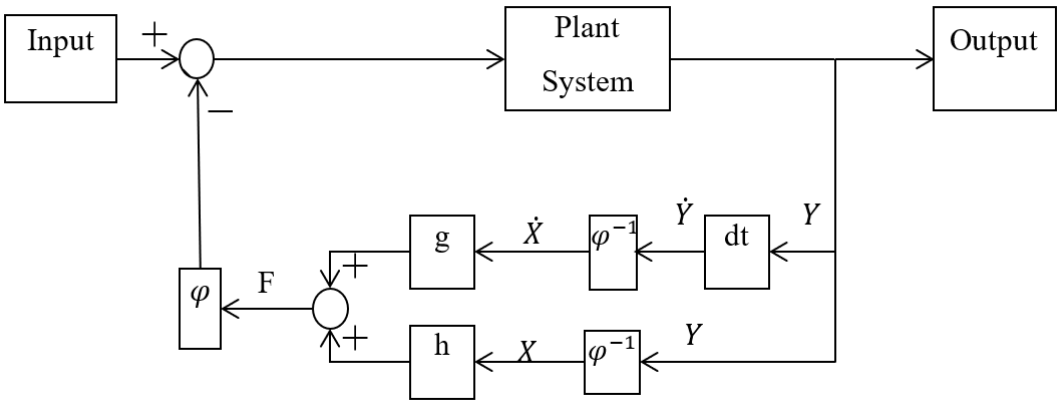

Figure 2-2 – Block Diagram for IMSC compensated system

2.2.4 Positive Position Feedback (PPF) Control

The main advantage of PPF is that it is not sensitive to spillover effect because it is a low-pass filter [1], and the controller design is simple because it has a simple decentralized structure [10]. PPF controller has been proved effectiveness in many algorithms: consensus-PPF [11], fractional-order PPF [12], collocated [10]-[12] and non-collocated PPF [13]. Besides, the PPF controller also used to control different structure systems: sandwich plate [13], clamped beams

[14] and so on. All the above prove that PPF controller has strong adjustability and flexibility. PPF controller has a second-order mathematic model, shown in (2.1).

$$H_{PPF}(s)_i = \frac{g_i\omega_f^2}{s^2+2\zeta_f\omega_f s+\omega_f^2} \tag{2.1}$$

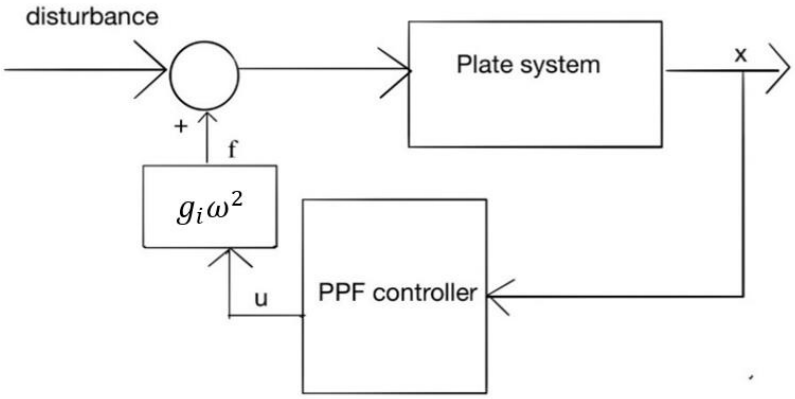

Figure 2-3 - General block diagram with PPF controller

The general compensated system block diagram is shown in Figure 2-2, the $g_i\omega^2$ block transfers displacements to forces, which is proportional to the acceleration [15]. The principle is:

Assume a sinusoidal signal is:

$$x = Asin(\omega t)$$

Where x is displacement of the signal. The velocity (v) is $\dot{x}$, the acceleration (a) is $\ddot{x}$, therefore:

$$v = \dot{x} = A\omega cos(\omega t)$$

$$a = \ddot{x} = -A\omega^2 \sin(\omega t)$$

The MIMO system in this project is a time-varying dynamic system. The adaptive controllers' characteristics request the controller responses the system in time and feedback to control the vibration in force, velocity or acceleration. According to above, several adaptive controller design methods, the PPF controller is suitable to the MIMO plate system, because the PPF transfer function is a second-order function which is same as the mathematic model of the plant system so that the controller design will be much easier. Another advantage of PPF is not sensitive to spillover effects. Besides, the input and output of PPF are displacements, which has a simple dynamic relationship between displacement, velocity, acceleration and force. The

sensor/actuator of the plate system is acceleration actuators, hence, PPF is one choice of the system.

However, although the PPF can use a coupled sensor/actuator to control several modes, it cannot control the mode separately, which makes it difficult to modify the controller as a target control element. In addition, the optimization of PPF parameters needs to be obtained by GA [2], and the calculation time is long. Besides, PPF provides large damping ratio to the closed-loop of flexible structure [17]. Therefore, other control algorithms based on PPF will be proposed to control the vibration.

2.2.5 Independent Model Positive Position Feedback (IMPPF) & Modified Positive Position Feedback (MPPF)

Since the advantages and disadvantages of PPF and IMSC can be complementary, Baz and Hong [16] proposed a new method named Independent Model Positive Position Feedback (IMPPF) in 1997, which includes a first-order filter and a controller gain. It adds the advantage of the IMSC algorithm that can control the mode separately to the PPF controller, so that the controller can not only control multiple modes at the same time, but also control the specified mode separately. The mathematic model of the controller is very simple, that makes it possible to update controller parameters online. However, the simplified mathematical model may result in poor control effect.

In 2010, Nima Mahmoodi et al. [17] added a parallel second-order filter to IMPPF, the second-order filter has the same structure with the conventional PPF, they called the method as Modified Positive Position Feedback (MPPF). It can reduce the damping of the compensator in the PPF control system, thus reducing the steady-state error while maintaining the control performance of PPF over transient vibration and spillover effects. At the same time, due to the large stability range of parameters in MPPF, the MPPF is more robust. This method strengthens the control performance of PPF but also more complex.

According to the above analysis about the advantages and disadvantages of IMPPF and MPPF, a Real-Time Adaptive Control Scheme (RTACS) with the advantages of both controllers can be designed based on these two control algorithms.

2.3 Frequency Estimator

A frequency estimator is needed in the online system because the frequency changes imply the changes in the system. It is an alert to tell whether the controller needs to update parameter now. It has many methods to generate a frequency estimator, such as modal filter method [18], Recursive Least Square method [19], and auto-regressive [20]. This part will simply introduce two methods of frequency estimator.

2.3.1 Zero-crossing

The first one is zero crossing, which is to record the interval time between two adjacent zero crossings of the signal, the time is half of period T. Then the frequency can be calculated based on the T [21]. This method is on time-domain space, it only can find one frequency at one time, it much prefers to be used in single damping mode signal. If used in multiple modes signal, it needs many bandpass filters to filter out unwanted frequencies, so that it may cause larger errors and made the structure in more complex.

2.3.2 Fast Fourier Transform (FFT)

FFT can calculate all frequencies in the system at a time and it can reduce the time cost from $O(N^2)$ to $O(NlogN)$, where N is data size. The principle is to continuously divide the data to be processed into two, and reduce the number of Fourier transforms to speed up the operation [22] [23]. However, it also has shortages, such as it has to store all the data of a signal, so need large storage in the computer, that leads time consumption which is unwanted in the adaptive controller. The storage and calculation time can be reduced by using FFT in a very small period signal and then repeat the work in the following time.

2.4 Original Contributions

This thesis has three original contributions:

1. Construct SSR and Second-order Differential Model on the basis of transfer function representation. Both models can be easily extended and applied to more inputs and outputs systems.

2. Upgrade IMPPF and MPPF that can only be used in SISO systems to be implemented in MIMO systems and implement the two controllers to plate system. The stability derivation of compensated MIMO system is the key to the success of this contribution.

3. Design an RTACS. That combined the advantages of IMPPF and MPPF. It can quickly respond to the changes in the system online and give relatively good control effect.

Chapter 3: System Modelling for the Plate Structure

In this chapter, through mathematical derivation, the transfer function representation established by previous students is transformed into the State-Space Representation (SSR) and Second-order Differential Model. The relevant function simplification process on the basis of control purpose is displayed in section 3.1. Section 3.2 and 3.3 show the mathematical derivation process from transfer function representation to SSR and Second-order Differential Model in detail.

3.1 Mathematical Model Simplification

The plate system is three inputs and three outputs system, so the transfer function representation of the open-loop system can be shown as:

$$\begin{bmatrix} Y_1(s) \\ Y_2(s) \\ Y_3(s) \end{bmatrix} = \begin{bmatrix} G_{11}(s) & G_{12}(s) & G_{13}(s) \\ G_{21}(s) & G_{22}(s) & G_{23}(s) \\ G_{31}(s) & G_{32}(s) & G_{33}(s) \end{bmatrix} \times \begin{bmatrix} U_1(s) \\ U_2(s) \\ U_3(s) \end{bmatrix} \tag{3.1}$$

where $Y_i(s), i = 1,2,3$ are the three outputs of the system, $U_i(s), i = 1,2,3$ are the three inputs of the system, $G_{\mathrm{ij}}(s), i,j = 1,2,3$ are the transfer functions for the i^{th} output and j^{th} input. The number follows the label of transducers shown in Figure 1.1. The block diagram is expressed by Figure 3-1 based on (3.1).

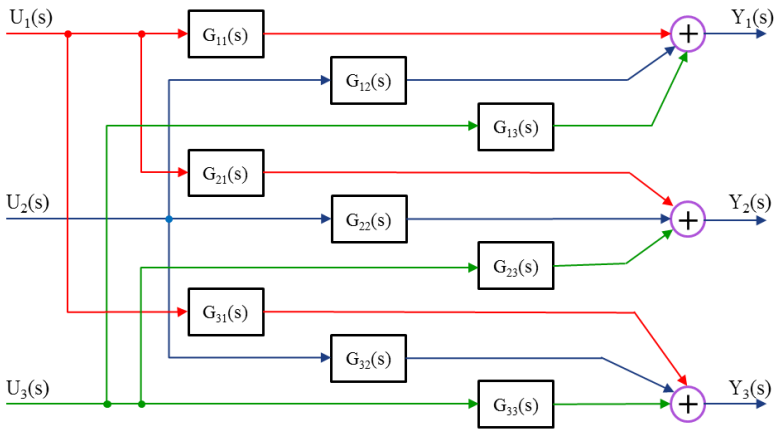

Figure 3-1 - Block Diagram of Open-Loop System

A sweep sinusoidal signal between 20 Hz to 200 Hz are inserted into three transducers respectively as input and the output signals generated in three transducers are measured. Those signals data are acquired by NI DAQ module, then transport the data to software ModalVIEW, the inputs and outputs relationships are produced in nine frequency response function (FRF)

plots by ModalVIEWsoftware [1]. The FRF curves are represented the 9 transfer functions in the real world which are shown as the blue curves in Figure 3-2. In the physical model, each transfer function has a very large number of modes when the top plate vibrating. To simplify, a Multiple Degree of Freedom (MDOF) polynomial curve fitting method in ModalVIEWcan generate similar curve as a substitute function of the real large-order transfer function. The substitute curves are displayed as the origin curves in Figure 3-2. In Figure 3-2, the horizontal axis is frequency (Hz) and the vertical axis is the magnitude which is corresponding voltage to the acceleration because the data from sensor and actuator is measured by accelerometers.

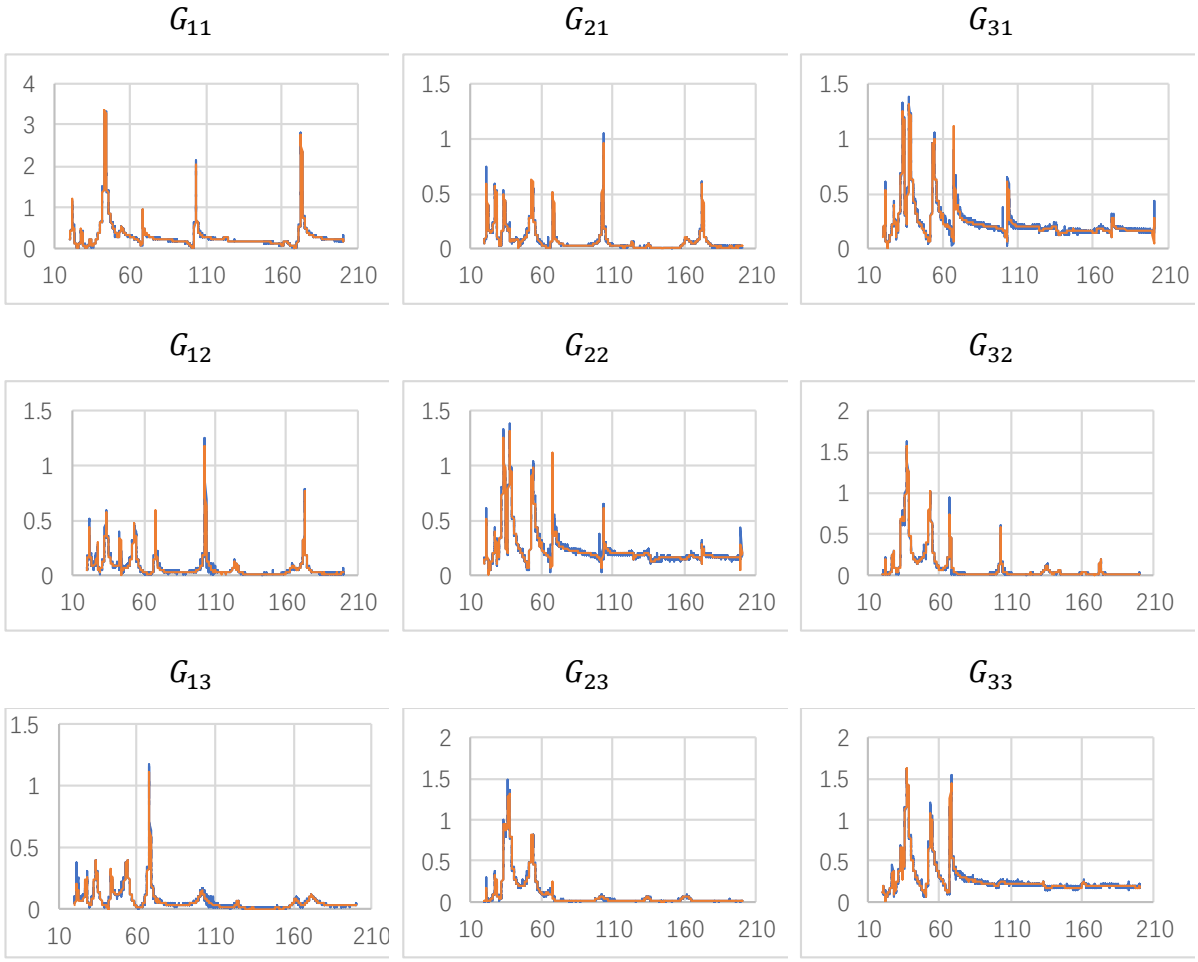

Figure 3-2 - FRF of Open-Loop Transfer Function

(Blue – Real Curve, Origin – Fitting Curve)

The new transfer function is the sum of 23 standard second-order transfer functions which are represented 23 modes. The number 23 was chosen because 23 functions best fit the trend of the original curve for each$G_{\mathrm{ij}}(s)$. Now, the original nine large-order transfer functions are simplified to nine 46-order transfer functions. The new corresponding transfer function $G_{ij}(s)$ can be respected by (3.2).

$$G_{ij}(s) = \sum_{k=1}^{23}\left(\frac{\varphi_{ij}^{k}}{s^2 + 2\zeta_{ij}^{k}\omega_{ij}^{k}s + \omega_{ij}^{k\,2}}\right) \tag{3.2}$$

where, ω_{ij}^{k}, ζ_{ij}^{k} and φ_{ij}^{k} is the frequency, damping ratio and mode shape for the k^{th} mode of i^{th} output j^{th} input.

For further simplification, this thesis only considers the first three modes. Since the low-frequency modes have a greater influence on the system vibration than high-frequency modes [24]. It is discussed about the control method, three low-frequency modes are selected so that the control work can exhibit multi-mode MIMO system control effects. It is easy to extend control effects to more than three modes. The ModalVIEW also provided the frequency, damping ratio and mode shape for the 23 functions. Then (3.2) can be rewritten to (3.3).

$$G_{ij}(s) = \sum_{k=1}^{3}\left(\frac{\varphi_{ij}^{k}}{s^2 + 2\zeta_{ij}^{k}\omega_{ij}^{k}s + \omega_{ij}^{k\,2}}\right) \tag{3.3}$$

The parameters for (3.3) are listed in Table 3-1. The mode shape is calculated by transfer the voltage of acceleration to displacement, so the whole system is considering the displacement changing via the method demonstrated in the paper of Zhang and He [1].

Table 3-1 - Parameters of Transfer Function Model

	Mode No. k	Frequency ω (rads/s)	Damping ζ (%)	Mode shape φ
G_{11}	1	136.7221	1.401	0.0330
	2	174.2327	1.425	0.0127
	3	211.4292	1.318	0.0056
G_{12}	1	135.9053	1.292	0.0113
	2	174.9867	0.9791	0.0055
	3	211.8690	1.725	0.0198
G_{13}	1	134.7743	1.622	0.0062
	2	173.0389	1.423	0.0068
	3	210.7380	1.959	0.0152
G_{21}	1	136.2823	1.238	0.0148
	2	174.7982	1.631	0.0186
	3	211.1779	1.717	0.0169
G_{22}	1	135.9681	0.8888	0.0093
	2	174.7354	1.61	0.0104
	3	210.8009	2.097	0.0515
G_{23}	1	136.2823	0.156	0.0005
	2	174.1071	1.501	0.0097
	3	211.2407	2.245	0.0407
G_{31}	1	137.4133	1.232	0.0134
	2	174.7354	1.554	0.0156
	3	210.9894	1.592	0.0077
G_{32}	1	136.5336	0.001793	0.0002
	2	173.9814	1.365	0.0079
	3	210.1725	2.061	0.0277
G_{33}	1	133.0779	2.342	0.0088
	2	174.4841	1.074	0.0070
	3	212.1203	1.533	0.0155

3.2 State-Space Representation Derivation

State-Space Representation (SSR) is a matrix-based system representation method [25]. It can be used to represent large systems with simple symbols and more convenient to simulate in MATLAB-based controller development. Therefore, this section focuses on transforming the above transfer function representation into SSR.

According to Figure 3-1 and (3.3), the transfer function representation for 3 outputs is shown as:

Output 1:

$$Y_1 = Y_1^1 + Y_1^2 + Y_1^3 \tag{3.4}$$

$$Y_1^1 = G_{11}^1\, U_1 + G_{12}^1\, U_2 + G_{13}^1\, U_3$$
$$= \frac{\varphi_{11}^1}{s^2 + 2\zeta_{11}^1\omega_{11}^1 s + {\omega_{11}^1}^2} U_1 + \frac{\varphi_{12}^1}{s^2 + 2\zeta_{12}^1\omega_{12}^1 s + {\omega_{12}^1}^2} U_2 + \frac{\varphi_{13}^1}{s^2 + 2\zeta_{13}^1\omega_{13}^1 s + {\omega_{13}^1}^2} U_3$$

$$Y_1^2 = G_{11}^2\, U_1 + G_{12}^2\, U_2 + G_{13}^2\, U_3$$
$$= \frac{\varphi_{11}^2}{s^2 + 2\zeta_{11}^2\omega_{11}^2 s + {\omega_{11}^2}^2} U_1 + \frac{\varphi_{12}^2}{s^2 + 2\zeta_{12}^2\omega_{12}^2 s + {\omega_{12}^2}^2} U_2 + \frac{\varphi_{13}^2}{s^2 + 2\zeta_{13}^2\omega_{13}^2 s + {\omega_{13}^2}^2} U_3$$

$$Y_1^3 = G_{11}^3\, U_1 + G_{12}^3\, U_2 + G_{13}^3\, U_3$$
$$= \frac{\varphi_{11}^3}{s^2 + 2\zeta_{11}^3\omega_{11}^3 s + {\omega_{11}^3}^2} U_1 + \frac{\varphi_{12}^3}{s^2 + 2\zeta_{12}^3\omega_{12}^3 s + {\omega_{12}^3}^2} U_2 + \frac{\varphi_{13}^3}{s^2 + 2\zeta_{13}^3\omega_{13}^3 s + {\omega_{13}^3}^2} U_3$$

Output 2:

$$Y_2 = Y_2^1 + Y_2^2 + Y_2^3 \tag{3.5}$$

$$Y_2^1 = G_{21}^1 U_1 + G_{22}^1\, U_2 + G_{23}^1\, U_3$$
$$= \frac{\varphi_{21}^1}{s^2 + 2\zeta_{21}^1\omega_{21}^1 s + {\omega_{21}^1}^2} U_1 + \frac{\varphi_{22}^1}{s^2 + 2\zeta_{22}^1\omega_{22}^1 s + {\omega_{22}^1}^2} U_2 + \frac{\varphi_{23}^1}{s^2 + 2\zeta_{23}^1\omega_{23}^1 s + {\omega_{23}^1}^2} U_3$$

$$Y_2^2 = G_{21}^2 U_1 + G_{22}^2\, U_2 + G_{23}^2\, U_3$$
$$= \frac{\varphi_{21}^2}{s^2 + 2\zeta_{21}^2\omega_{21}^2 s + {\omega_{21}^2}^2} U_1 + \frac{\varphi_{22}^2}{s^2 + 2\zeta_{22}^2\omega_{22}^2 s + {\omega_{22}^2}^2} U_2 + \frac{\varphi_{23}^2}{s^2 + 2\zeta_{23}^2\omega_{23}^2 s + {\omega_{23}^2}^2} U_3$$

$$Y_2^3 = G_{21}^3 U_1 + G_{22}^3\, U_2 + G_{23}^3\, U_3$$
$$= \frac{\varphi_{21}^3}{s^2 + 2\zeta_{21}^3\omega_{21}^3 s + {\omega_{21}^3}^2} U_1 + \frac{\varphi_{22}^3}{s^2 + 2\zeta_{22}^3\omega_{22}^3 s + {\omega_{22}^3}^2} U_2 + \frac{\varphi_{23}^3}{s^2 + 2\zeta_{23}^3\omega_{23}^3 s + {\omega_{23}^3}^2} U_3$$

Output 3:

$$Y_3 = Y_3^1 + Y_3^2 + Y_3^3 \tag{3.6}$$

$$Y_3^1 = G_{31}^1\, U_1 + G_{32}^1\, U_2 + G_{33}^1\, U_3$$
$$= \frac{\varphi_{31}^1}{s^2 + 2\zeta_{31}^1\omega_{31}^1 s + {\omega_{31}^1}^2} U_1 + \frac{\varphi_{32}^1}{s^2 + 2\zeta_{32}^1\omega_{32}^1 s + {\omega_{32}^1}^2} U_2 + \frac{\varphi_{33}^1}{s^2 + 2\zeta_{33}^1\omega_{33}^1 s + {\omega_{33}^1}^2} U_3$$

$$Y_3^2 = G_{31}^2\, U_1 + G_{32}^2\, U_2 + G_{33}^2\, U_3$$
$$= \frac{\varphi_{31}^2}{s^2 + 2\zeta_{31}^2\omega_{31}^2 s + \omega_{31}^2{}^2} U_1 + \frac{\varphi_{32}^2}{s^2 + 2\zeta_{32}^2\omega_{32}^2 s + \omega_{32}^2{}^2} U_2 + \frac{\varphi_{33}^2}{s^2 + 2\zeta_{33}^2\omega_{33}^2 s + \omega_{33}^2{}^2} U_3$$

$$Y_3^2 = G_{31}^2\, U_1 + G_{32}^2\, U_2 + G_{33}^2\, U_3$$
$$= \frac{\varphi_{31}^2}{s^2 + 2\zeta_{31}^2\omega_{31}^2 s + \omega_{31}^2{}^2} U_1 + \frac{\varphi_{32}^2}{s^2 + 2\zeta_{32}^2\omega_{32}^2 s + \omega_{32}^2{}^2} U_2 + \frac{\varphi_{33}^2}{s^2 + 2\zeta_{33}^2\omega_{33}^2 s + \omega_{33}^2{}^2} U_3$$

It can be seen from Table 3-1 that the normal frequency of the same mode has little difference in different transfer functions. For the convenience of expression, for one mode, take mean of the nine frequencies in the nine transfer functions to get ω^1, ω^2 and ω^3. And take the maximum damping ratio in the same way to get ς^1, ς^2 and ς^3. The demonstrator of each output can be the same. The transfer matrix can be built as:

$$\mathbf{Y}(s) = \begin{bmatrix} Y_1(s) \\ Y_2(s) \\ Y_3(s) \end{bmatrix} = \begin{bmatrix} Y_1^1(s) + Y_1^2(s) + Y_1^3(s) \\ Y_2^1(s) + Y_2^2(s) + Y_2^3(s) \\ Y_3^1(s) + Y_3^2(s) + Y_3^3(s) \end{bmatrix} =$$

$$\begin{bmatrix} \frac{\varphi_{11}^1 U_1(s) + \varphi_{12}^1 U_2(s) + \varphi_{13}^1 U_3(s)}{s^2 + 2\varsigma^1\omega^1 s + \omega^1{}^2} + \frac{\varphi_{11}^2 U_1(s) + \varphi_{12}^2 U_2(s) + \varphi_{13}^2 U_3(s)}{s^2 + 2\varsigma^2\omega^2 s + \omega^2{}^2} + \frac{\varphi_{11}^3 U_1(s) + \varphi_{12}^3 U_2(s) + \varphi_{13}^3 U_3(s)}{s^2 + 2\varsigma^3\omega^3 s + \omega^3{}^2} \\ \frac{\varphi_{21}^1 U_1(s) + \varphi_{22}^1 U_2(s) + \varphi_{23}^1 U_3(s)}{s^2 + 2\varsigma^1\omega^1 s + \omega^1{}^2} + \frac{\varphi_{21}^2 U_1(s) + \varphi_{22}^2 U_2(s) + \varphi_{23}^2 U_3(s)}{s^2 + 2\varsigma^2\omega^2 s + \omega^2{}^2} + \frac{\varphi_{21}^3 U_1(s) + \varphi_{22}^3 U_2(s) + \varphi_{23}^3 U_3(s)}{s^2 + 2\varsigma^3\omega^3 s + \omega^3{}^2} \\ \frac{\varphi_{31}^1 U_1(s) + \varphi_{32}^1 U_2(s) + \varphi_{33}^1 U_3(s)}{s^2 + 2\varsigma^1\omega^1 s + \omega^1{}^2} + \frac{\varphi_{31}^2 U_1(s) + \varphi_{32}^2 U_2(s) + \varphi_{33}^2 U_3(s)}{s^2 + 2\varsigma^2\omega^2 s + \omega^2{}^2} + \frac{\varphi_{31}^3 U_1(s) + \varphi_{32}^3 U_2(s) + \varphi_{33}^3 U_3(s)}{s^2 + 2\varsigma^3\omega^3 s + \omega^3{}^2} \end{bmatrix} \quad (3.7)$$

The mode shape φ_{ij}^k can be seen as the product of φ_i^k and φ_j^k due to coupled sensor/actuator, (3.7) can be rewritten as:

$$\mathbf{Y}(s)$$
$$= \begin{bmatrix} \frac{\varphi_1^1(\varphi_1^1 U_1 + \varphi_2^1 U_2 + \varphi_3^1 U_3)}{s^2 + 2\zeta^1\omega^1 s + (\omega^1)^2} + \frac{\varphi_1^2(\varphi_1^2 U_1 + \varphi_2^2 U_2 + \varphi_3^2 U_3)}{s^2 + 2\zeta^2\omega^2 s + (\omega^2)^2} + \frac{\varphi_1^3(\varphi_1^3 U_1 + \varphi_2^3 U_2 + \varphi_3^3 U_3)}{s^2 + 2\zeta^3\omega^3 s + (\omega^3)^2} \\ \frac{\varphi_2^1(\varphi_1^1 U_1 + \varphi_2^1 U_2 + \varphi_3^1 U_3)}{s^2 + 2\zeta^1\omega^1 s + (\omega^1)^2} + \frac{\varphi_2^2(\varphi_1^2 U_1 + \varphi_2^2 U_2 + \varphi_3^2 U_3)}{s^2 + 2\zeta^2\omega^2 s + (\omega^2)^2} + \frac{\varphi_2^3(\varphi_1^3 U_1 + \varphi_2^3 U_2 + \varphi_3^3 U_3)}{s^2 + 2\zeta^3\omega^3 s + (\omega^3)^2} \\ \frac{\varphi_3^1(\varphi_1^1 U_1 + \varphi_2^1 U_2 + \varphi_3^1 U_3)}{s^2 + 2\zeta^1\omega^1 s + (\omega^1)^2} + \frac{\varphi_3^2(\varphi_1^2 U_1 + \varphi_2^2 U_2 + \varphi_3^2 U_3)}{s^2 + 2\zeta^2\omega^2 s + (\omega^2)^2} + \frac{\varphi_3^3(\varphi_1^3 U_1 + \varphi_2^3 U_2 + \varphi_3^3 U_3)}{s^2 + 2\zeta^3\omega^3 s + (\omega^3)^2} \end{bmatrix}$$

$$= \begin{bmatrix} \dfrac{\varphi_1^1[\varphi_1^1 \quad \varphi_2^1 \quad \varphi_3^1]\begin{bmatrix}U_1\\U_2\\U_3\end{bmatrix}}{s^2+2\zeta^1\omega^1 s+(\omega^1)^2} + \dfrac{\varphi_1^2[\varphi_1^2 \quad \varphi_2^2 \quad \varphi_3^2]\begin{bmatrix}U_1\\U_2\\U_3\end{bmatrix}}{s^2+2\zeta^2\omega^2 s+(\omega^2)^2} + \dfrac{\varphi_1^3[\varphi_1^3 \quad \varphi_2^3 \quad \varphi_3^3]\begin{bmatrix}U_1\\U_2\\U_3\end{bmatrix}}{s^2+2\zeta^3\omega^3 s+(\omega^3)^2} \\ \dfrac{\varphi_2^1[\varphi_1^1 \quad \varphi_2^1 \quad \varphi_3^1]\begin{bmatrix}U_1\\U_2\\U_3\end{bmatrix}}{s^2+2\zeta^1\omega^1 s+(\omega^1)^2} + \dfrac{\varphi_2^2[\varphi_1^2 \quad \varphi_2^2 \quad \varphi_3^2]\begin{bmatrix}U_1\\U_2\\U_3\end{bmatrix}}{s^2+2\zeta^2\omega^2 s+(\omega^2)^2} + \dfrac{\varphi_2^3[\varphi_1^3 \quad \varphi_2^3 \quad \varphi_3^3]\begin{bmatrix}U_1\\U_2\\U_3\end{bmatrix}}{s^2+2\zeta^3\omega^3 s+(\omega^3)^2} \\ \dfrac{\varphi_3^1[\varphi_1^1 \quad \varphi_2^1 \quad \varphi_3^1]\begin{bmatrix}U_1\\U_2\\U_3\end{bmatrix}}{s^2+2\zeta^1\omega^1 s+(\omega^1)^2} + \dfrac{\varphi_3^2[\varphi_1^2 \quad \varphi_2^2 \quad \varphi_3^2]\begin{bmatrix}U_1\\U_2\\U_3\end{bmatrix}}{s^2+2\zeta^2\omega^2 s+(\omega^2)^2} + \dfrac{\varphi_3^3[\varphi_1^3 \quad \varphi_2^3 \quad \varphi_3^3]\begin{bmatrix}U_1\\U_2\\U_3\end{bmatrix}}{s^2+2\zeta^3\omega^3 s+(\omega^3)^2} \end{bmatrix}$$

$$= \begin{bmatrix} \varphi_1^1\eta_1 + \varphi_1^2\eta_2 + \varphi_1^3\eta_3 \\ \varphi_2^1\eta_1 + \varphi_2^2\eta_2 + \varphi_2^3\eta_3 \\ \varphi_3^1\eta_1 + \varphi_3^2\eta_2 + \varphi_3^3\eta_3 \end{bmatrix}$$

$$= \begin{bmatrix} \varphi_1^1 & \varphi_1^2 & \varphi_1^3 \\ \varphi_2^1 & \varphi_2^2 & \varphi_2^3 \\ \varphi_3^1 & \varphi_3^2 & \varphi_3^3 \end{bmatrix}\begin{bmatrix}\eta_1\\\eta_2\\\eta_3\end{bmatrix} \tag{3.8}$$

where:

$$\eta_1 \triangleq \frac{[\varphi_1^1 \quad \varphi_2^1 \quad \varphi_3^1]\begin{bmatrix}U_1\\U_2\\U_3\end{bmatrix}}{s^2+2\zeta^1\omega^1 s+(\omega^1)^2}$$

$$\eta_2 \triangleq \frac{[\varphi_1^2 \quad \varphi_2^2 \quad \varphi_3^2]\begin{bmatrix}U_1\\U_2\\U_3\end{bmatrix}}{s^2+2\zeta^2\omega^2 s+(\omega^2)^2}$$

$$\eta_3 \triangleq \frac{[\varphi_1^3 \quad \varphi_2^3 \quad \varphi_3^3]\begin{bmatrix}U_1\\U_2\\U_3\end{bmatrix}}{s^2+2\zeta^3\omega^3 s+(\omega^3)^2} \tag{3.9}$$

To represent the function into SSR, the transfer functions need to be in the time domain [26]. Hence, apply the inverse Laplace transfer function into (3.9), the result will be seen as:

$$\ddot{\eta}_1 + 2\zeta^1\omega^1\dot{\eta}_1 + (\omega^1)^2\eta_1 = [\varphi_1^1 \quad \varphi_2^1 \quad \varphi_3^1]\begin{bmatrix}u_1\\u_2\\u_3\end{bmatrix} \tag{3.10}$$

$$\ddot{\eta}_2 + 2\zeta^2\omega^2\dot{\eta}_2 + (\omega^2)^2\eta_2 = [\varphi_1^2 \quad \varphi_2^2 \quad \varphi_3^2]\begin{bmatrix}u_1\\u_2\\u_3\end{bmatrix} \tag{3.11}$$

$$\ddot{\eta}_3 + 2\zeta^3\omega^3\dot{\eta}_3 + (\omega^3)^2\eta_3 = [\varphi_1^3 \quad \varphi_2^3 \quad \varphi_3^3]\begin{bmatrix}u_1\\u_2\\u_3\end{bmatrix} \tag{3.12}$$

where, u_i is control input in the time domain.

According to (3.10), convert each second-order differential equation into two first-order differential equations. That is shown as:

$$\begin{cases} x_1 = \eta_1 \\ \dot{x}_1 = \dot{\eta}_1 = x_2 \\ \dot{x}_2 = \ddot{\eta}_1 = [\varphi_1^1 \quad \varphi_2^1 \quad \varphi_3^1]\begin{bmatrix}u_1\\u_2\\u_3\end{bmatrix} - 2\zeta^1\omega^1 x_2 - {\omega^1}^2 x_1 \end{cases}$$

$$\begin{bmatrix}\dot{x}_1\\\dot{x}_2\end{bmatrix} = \begin{bmatrix}0 & 1\\-{\omega^1}^2 & -2\zeta^1\omega^1\end{bmatrix}\begin{bmatrix}x_1\\x_2\end{bmatrix} + \begin{bmatrix}0 & 0 & 0\\\varphi_1^1 & \varphi_2^1 & \varphi_3^1\end{bmatrix}\begin{bmatrix}u_1\\u_2\\u_3\end{bmatrix} \tag{3.13}$$

Similar to (3.10), the two first-order differential equations for the (3.11) and (3.12) can be shown as:

$$\begin{bmatrix}\dot{x}_3\\\dot{x}_4\end{bmatrix} = \begin{bmatrix}0 & 1\\-{w^2}^2 & -2\zeta^2 w^2\end{bmatrix}\begin{bmatrix}x_3\\x_4\end{bmatrix} + \begin{bmatrix}0 & 0 & 0\\\varphi_1^2 & \varphi_2^2 & \varphi_3^2\end{bmatrix}\begin{bmatrix}u_1\\u_2\\u_3\end{bmatrix} \tag{3.14}$$

$$\begin{bmatrix}\dot{x}_5\\\dot{x}_6\end{bmatrix} = \begin{bmatrix}0 & 1\\-{w^3}^2 & -2\zeta^3 w^3\end{bmatrix}\begin{bmatrix}x_5\\x_6\end{bmatrix} + \begin{bmatrix}0 & 0 & 0\\\varphi_1^3 & \varphi_2^3 & \varphi_3^3\end{bmatrix}\begin{bmatrix}u_1\\u_2\\u_3\end{bmatrix} \tag{3.15}$$

Together the (3.8) and (3.13) – (3.15), the final SSR of the plant system can be written as:

$$\dot{\boldsymbol{X}} = \mathbf{A}\boldsymbol{X} + \mathbf{B}\boldsymbol{U}$$

$$\boldsymbol{Y} = \mathbf{C}\boldsymbol{X} \tag{3.16}$$

where

$$\boldsymbol{X} = \begin{bmatrix}x_1\\x_2\\x_3\\x_4\\x_5\\x_6\end{bmatrix} \quad \boldsymbol{Y} = \begin{bmatrix}y_1\\y_2\\y_3\end{bmatrix}$$

$$\mathbf{A} = \begin{bmatrix} 0 & 1 & 0 & 0 & 0 & 0 \\ -\omega^{1^2} & -2\varsigma^1\omega^1 & 0 & 0 & 0 & 0 \\ 0 & 0 & 0 & 1 & 0 & 0 \\ 0 & 0 & -\omega^{2^2} & -2\varsigma^2\omega^2 & 0 & 0 \\ 0 & 0 & 0 & 0 & 0 & 1 \\ 0 & 0 & 0 & 0 & -\omega^{3^2} & -2\varsigma^3\omega^3 \end{bmatrix}$$

$$\mathbf{B} = \begin{bmatrix} 0 & 0 & 0 \\ \varphi_1^1 & \varphi_2^1 & \varphi_3^1 \\ 0 & 0 & 0 \\ \varphi_1^2 & \varphi_2^2 & \varphi_3^2 \\ 0 & 0 & 0 \\ \varphi_1^3 & \varphi_2^3 & \varphi_3^3 \end{bmatrix}$$

$$\mathbf{C} = \begin{bmatrix} \varphi_1^1 & 0 & \varphi_1^2 & 0 & \varphi_1^3 & 0 \\ \varphi_2^1 & 0 & \varphi_2^2 & 0 & \varphi_2^3 & 0 \\ \varphi_3^1 & 0 & \varphi_3^2 & 0 & \varphi_3^3 & 0 \end{bmatrix}$$

y_i is output in the time domain.

The parameters in SSR are displayed in Table 3-2 which are selected or calculated as previously demonstrated from Table 3-1.

Table 3-2 - Parameters of Plant System

Mode 1		Mode 2		Mode 3	
ς^1	0.0234	ς^2	0.0163	ς^3	0.0225
ω^1	135.8844	ω^2	174.3444	ω^3	211.1709
φ_1^1	0.1815	φ_1^2	0.1125	φ_1^3	0.0751
φ_2^1	0.0962	φ_2^2	0.1020	φ_2^3	0.2270
φ_3^1	0.0939	φ_3^2	0.0838	φ_3^3	0.1243

3.3 Second-order Differential Model Derivation

To following work considering, a Second-order Differential Model also needs in this thesis. Based on (3.8) and (3.10) - (3.12), the plant system can be written as:

$$\ddot{\boldsymbol{\eta}} + \mathbf{D}\dot{\boldsymbol{\eta}} + \boldsymbol{\Omega}\boldsymbol{\eta} = \boldsymbol{\psi}^{\boldsymbol{T}}\boldsymbol{U}$$

$$\boldsymbol{Y} = \boldsymbol{\psi}\boldsymbol{\eta} \tag{3.17}$$

where

$$\boldsymbol{\eta} = \begin{bmatrix} \eta_1 \\ \eta_2 \\ \eta_3 \end{bmatrix} \quad \boldsymbol{Y} = \begin{bmatrix} y_1 \\ y_2 \\ y_3 \end{bmatrix} \quad \boldsymbol{U} = \begin{bmatrix} u_1 \\ u_2 \\ u_3 \end{bmatrix}$$

$$\mathbf{D} = \begin{bmatrix} 2\zeta^1\omega^1 & 0 & 0 \\ 0 & 2\zeta^2\omega^2 & 0 \\ 0 & 0 & 2\zeta^3\omega^3 \end{bmatrix}$$

$$\boldsymbol{\Omega} = \begin{bmatrix} (\omega^1)^2 & 0 & 0 \\ 0 & (\omega^2)^2 & 0 \\ 0 & 0 & (\omega^3)^2 \end{bmatrix}$$

$$\boldsymbol{\psi} = \begin{bmatrix} \varphi_1^1 & \varphi_1^2 & \varphi_1^3 \\ \varphi_2^1 & \varphi_2^2 & \varphi_2^3 \\ \varphi_3^1 & \varphi_3^2 & \varphi_3^3 \end{bmatrix}$$

All the parameters can be found in Table 3-2.

Chapter 4: Online Adaptive Controller Design

In this chapter, two adaptive control algorithms based on the technique of PPF are proposed in Section 4.1 and 4.2 respectively. Using these two proposed methods, a Real-Time Adaptive Control Scheme (RTACS) module is proposed for the real-time adaptive control for the given plate-structure.

4.1 IMPPF Design

IMPPF was first presented by Poh and Baz [28] in 1990. It absorbs the benefits of IMSC to PPF controller, so it overcomes the disadvantage that PPF cannot control each mode separately. However, the work of Poh and Baz was stopped at SISO system control and it realised the multi-mode control by controlling different mode by time-sharing method. This section extends the algorithm from SISO system to the given MIMO multi-mode plate system in mathematic theory derivation.

4.1.1 IMPPF Concept

The mathematical model of original IMPPF can be expressed as [28]:

$$\begin{cases} \ddot{y}^k + {\omega^k}^2 y^k = f^k = \gamma^k {\omega^k}^2 \left(u^k + u_R^k\right) \\ \tau^k \dot{u}^k + u^k = y^k \end{cases} \tag{4.1}$$

where, ω^k means the natural frequency. There are two parameters need to be designed which are a control gain (γ^k) and a time constant (τ^k). u_R^k and y^k are the input and output of the system respectively. u^k can be seen as control input of the system. The index k means the k^{th} mode of the system.

According to (4.1), the block diagram of the IMPPF for a SISO system can be displayed as Figure 4-1.

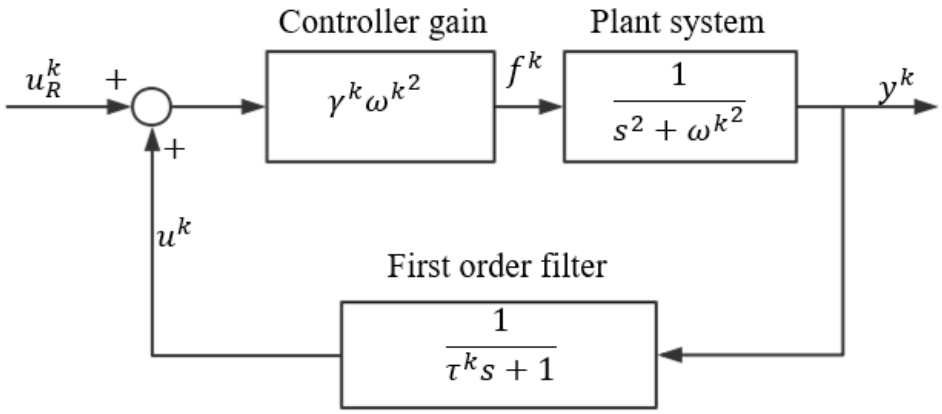

Figure 4-1 - Block Diagram of the Original IMPPF for a SISO System

The whole controller can be divided into three blocks: plant system, controller gain and first-order filter. It assumes the plant system is an undamped system, and sets the location of sensor and actuator by reduced mode shape matrices, so the plant system is no damping ratio and mode shape terms.

The flowchart of the parameters design can be demonstrated as Figure 4-2.

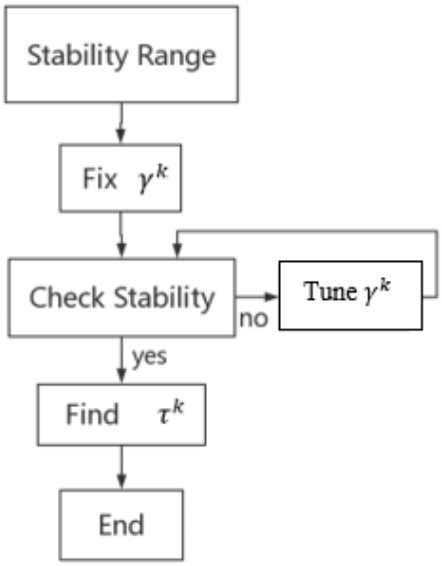

Figure 4-2 - Flowchart of IMPPF Algorithm

Based on Figure 4-3, the parameters design can be explained in mathematic theory in 4.2.2, 4.2.3 and 4.2.4.

4.1.2 Conventional IMPPF Controller

According to Figure 4-2, the closed-loop transfer function (C.L.T.F.) can be represented as:

$$\frac{y^k}{u_R^k} = \frac{\gamma^k {\omega^k}^2 (\tau^k s+1)}{\tau^k s^3 + s^2 + \tau^k {\omega^k}^2 s + (1-\gamma^k){\omega^k}^2} \tag{4.2}$$

a) Stability Range

The closed-loop character equation (C.L.C.E.) is the denominator of (4.2), which is displayed as:

$$C.L.C.E. = \tau^k s^3 + s^2 + \tau^k {\omega^k}^2 s + (1-\gamma^k){\omega^k}^2 \tag{4.3}$$

Apply Routh-Hurwitz's stability criterion to find the stability range of both parameters as Table 4-1 shows.

Table 4-1 - Routh-Hurwitz's Stability Criterion for IMPPF

s^3	τ^k	$\tau^k {\omega^k}^2$
s^2	1	$(1-\gamma^k){\omega^k}^2$
s^1	$\tau^k {\omega^k}^2 - \tau^k(1-\gamma^k){\omega^k}^2$	0
s^0	$(1-\gamma^k){\omega^k}^2$	0

According to the theory of Routh-Hurwitz's stability criterion, the stable system needs the second column of the Table 4-1 do not change the sign [29]. Because in the second row, 1 is a positive number, hence, (4.4) should be met.

$$\begin{cases} \tau^k > 0 \\ \tau^k {\omega^k}^2 - \tau^k(1-\gamma^k){\omega^k}^2 > 0 \\ (1-\gamma^k){\omega^k}^2 > 0 \end{cases} \tag{4.4}$$

From (4.4), the stability ranges of τ^k and γ^k can be found, the ranges are presented as (4.5).

$$\begin{cases} \tau^k > 0 \\ 0 < \gamma^k < 1 \end{cases} \tag{4.5}$$

b) Fix γ^k

The value of γ^k can be fixed into 0.5 by setting steady-state error (e_{ss}) to be zero. Based on (4.1). The steady-state error is measured in the time goes to infinity. To eliminate the e_{ss} requires the $\dot{u}^k(t=\infty)=0$ and $\ddot{y}^k(t=\infty)=0$. Hence, the (4.1) can be rewritten as:

$$\begin{gathered}{\omega^k}^2 y^k(t=\infty)=\gamma^k {\omega^k}^2(u^k(t=\infty)+u_R^k) \\ u^k(t=\infty)=y^k(t=\infty)\end{gathered} \tag{4.6}$$

Substitute u^k to y^k to eliminate the control input, the (4.7) can be found.

$${\omega^k}^2 y^k(t=\infty)=\gamma^k {\omega^k}^2(y^k(t=\infty)+u_R^k) \tag{4.7}$$

If $y^k(t=\infty)=u_R^k$, then $e_{ss}=0$, hence, the $\gamma^k=0.5$. In addition, the value 0.5 is just in the range of $0<\gamma^k<1$. Hence, for the same system, no matter how the system changed, the γ^k is fixed into 0.5.

c) Find τ^k

The suitable value of τ^k can be determined by dividing the numerator and denominator of (4.2) by $\tau\omega^3$, the result can be written as:

$$\frac{y^k}{u_R^k}=\frac{\gamma^k(\bar{s}+\alpha^k)}{\bar{s}^3+\alpha^k\bar{s}^2+\bar{s}+(1-\gamma^k)\alpha^k} \tag{4.8}$$

where $\bar{s}=\frac{s}{\omega^k}$ $\alpha^k=\frac{1}{\tau^k\omega^k}$

Now, there is only one unknown parameter α in C.L.C.E. Therefore, the root locus about α can be drawn in Figure 4-3.

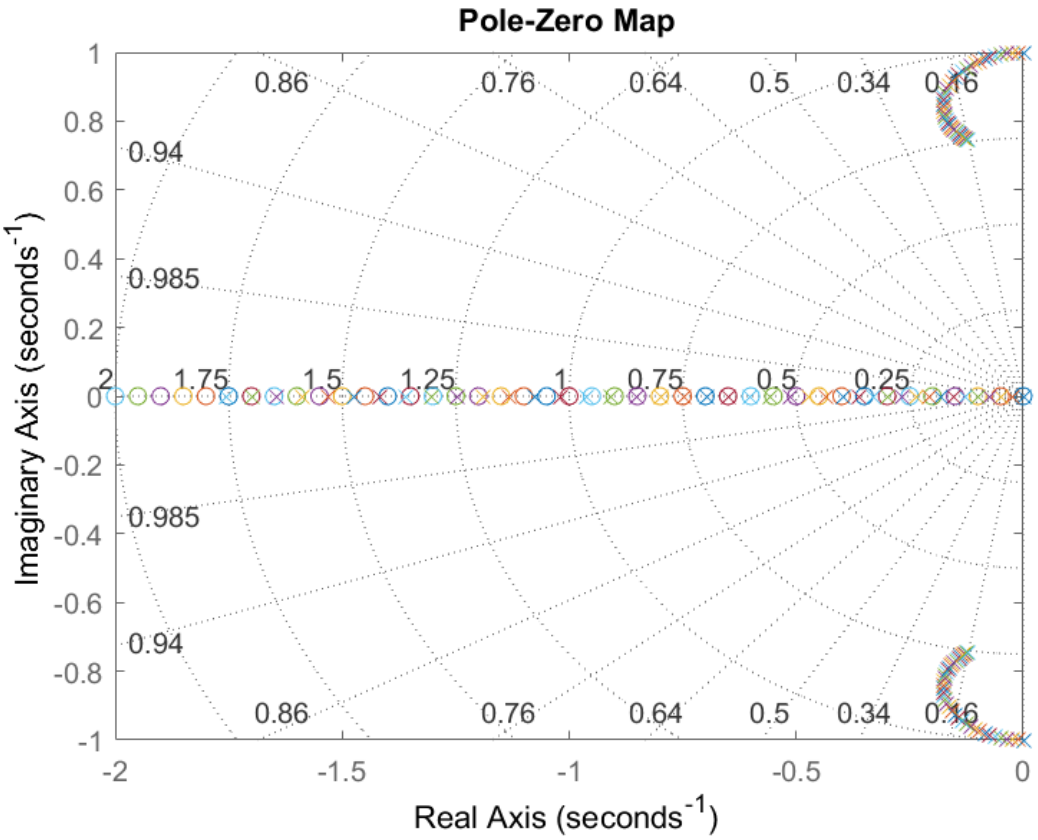

Figure 4-3 - Root Locus about α^k

The poles and zeros are further away from the imaginary axis, the system would be more stable. From the gridline of Figure 4-3, the system becomes more stable when the closed-loop damping ratio become larger. Hence, the suitable value of τ^k can be found when the damping ratio becomes the largest value. The relationship between the α^k and closed-loop damping ratio can be seen as Figure 4-4.

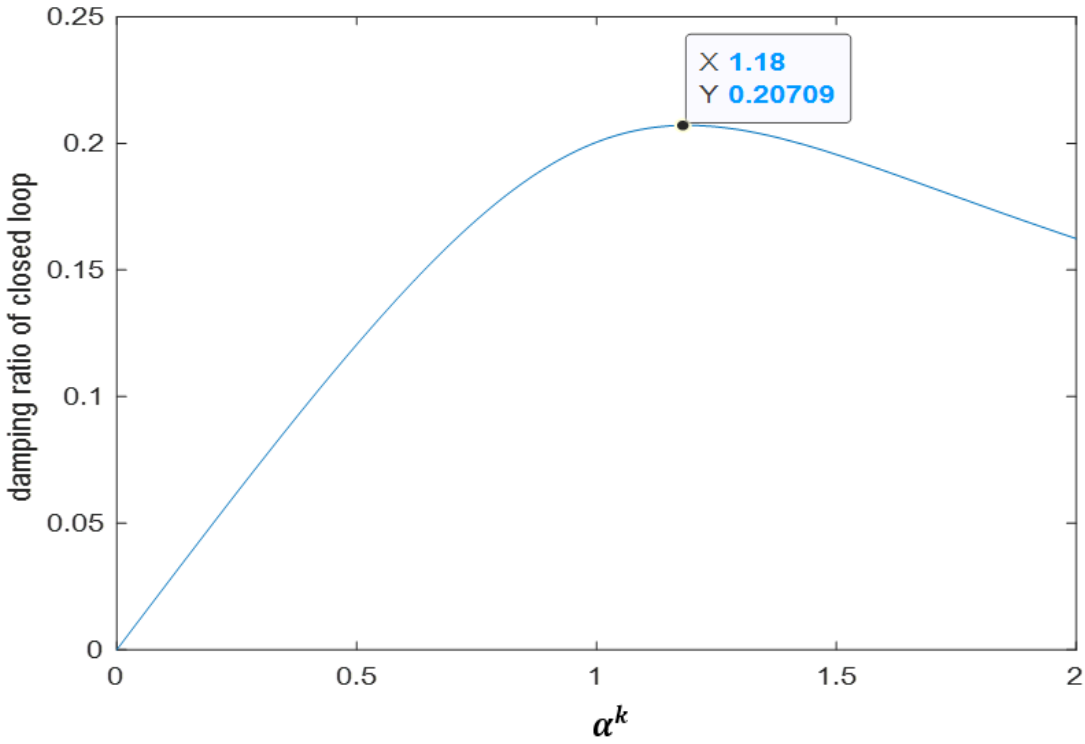

Figure 4-4 - Closed-loop Damping Ratio vs α^k

According to Figure 4-4, the maximum of closed-loop damping ratio is 0.207 where the α^k becomes 1.18. Hence, (4.9) is expressed the value of τ^k.

$$\tau^k = \frac{1}{1.18\omega^k} \tag{4.9}$$

4.1.3 IMPPF for SISO Plate System

The plant system in original IMPPF controller is not same to the plate system listed as (3.2), hence, to extend this method to the plate system, the analysis of IMPPF control in SISO plate system need to be discussed.

Adding the damping ratio (ζ^k) and mode shape (φ^k) to the plant system to Figure 4-1, the C.L.T.F. can be represented as:

$$\frac{y^k}{u_R^k} = \frac{\gamma^k {\omega^k}^2 \varphi^k (\tau^k s+1)}{\tau^k s^3+(2\tau^k\zeta^k\omega^k+1)s^2+(\tau^k{\omega^k}^2+2\zeta^k\omega^k)s+(1-\gamma^k\varphi^k){\omega^k}^2} \tag{4.10}$$

a) Stability Range

The C.L.C.E. is the denominator of (4.10), which is displayed as:

$$C.L.C.E. = \tau^k s^3 + (2\tau^k\zeta^k\omega^k + 1)s^2 + (\tau^k{\omega^k}^2 + 2\zeta^k\omega^k)s + (1-\gamma^k\varphi^k){\omega^k}^2 \tag{4.11}$$

Assume that

$$C.L.C.E. = a_3 s^3 + a_2 s^2 + a_1 s + a_0$$

Apply Routh-Hurwitz's stability criterion to find the stability range of both parameters as Table 4-1 shows.

Table 4-2 - Routh-Hurwitz's Stability Criterion for a Second-order System

s^3	a_3	a_1
s^2	a_2	a_0
s^1	$\frac{1}{a_2}(a_1 a_2 - a_0 a_3)$	0
s^0	a_0	0

Therefore, the (4.12) should be meet.

$$\begin{cases} a_3 > 0 \\ a_2 > 0 \\ a_0 > 0 \\ a_1 a_2 > a_0 a_3 \end{cases} \tag{4.12}$$

Substitute the parameters in (4.11) into (4.12) and reviewing the parameters in plant system are all positive values as shown in Table 3-1, the stability ranges of τ^k and γ^k can be found which are presented as:

$$\begin{cases} \tau^k > 0 \\ -\frac{4{\zeta^k}^2}{\varphi^k} - \frac{2\zeta^k}{\varphi^k \omega^k} < \gamma^k < \frac{1}{\varphi^k} \end{cases} \tag{4.13}$$

b) Fix γ^k

Similar to section 4.1.2. Based on (4.10), the condition to eliminate the e_{ss} in s-domain is that $s = 0, u_R^k = y^k$. (4.10) can be rewritten as:

$$1 = \frac{\gamma^k \varphi^k}{1 - \gamma^k \varphi^k} \tag{4.14}$$

Hence,

$$\gamma^k = \frac{1}{2\varphi^k} \tag{4.15}$$

In addition, the value also can meet the stability request in (4.13), because the values of φ^k in plate structure are positive and less than one, ζ^k and ω^k are also positive.

c) Find τ^k

Substitute (4.15) into (4.10), the C.L.T.F. can be rewritten as:

$$\frac{y^k}{u_R^k} = \frac{0.5\omega^{k^2}(\tau^k s+1)}{\tau^k s^3+(2\tau^k\zeta^k\omega^k+1)s^2+(\tau^k\omega^{k^2}+2\zeta^k\omega^k)s+0.5\omega^{k^2}} \tag{4.16}$$

The parameters in (4.16) are all known, except τ^k, therefore, a root locus about τ^k can be plotted.

For example, considering the first mode of G_{11}, the parameters are listed in the first row of Table 3-1 and the root locus can be seen as Figure 4-5.

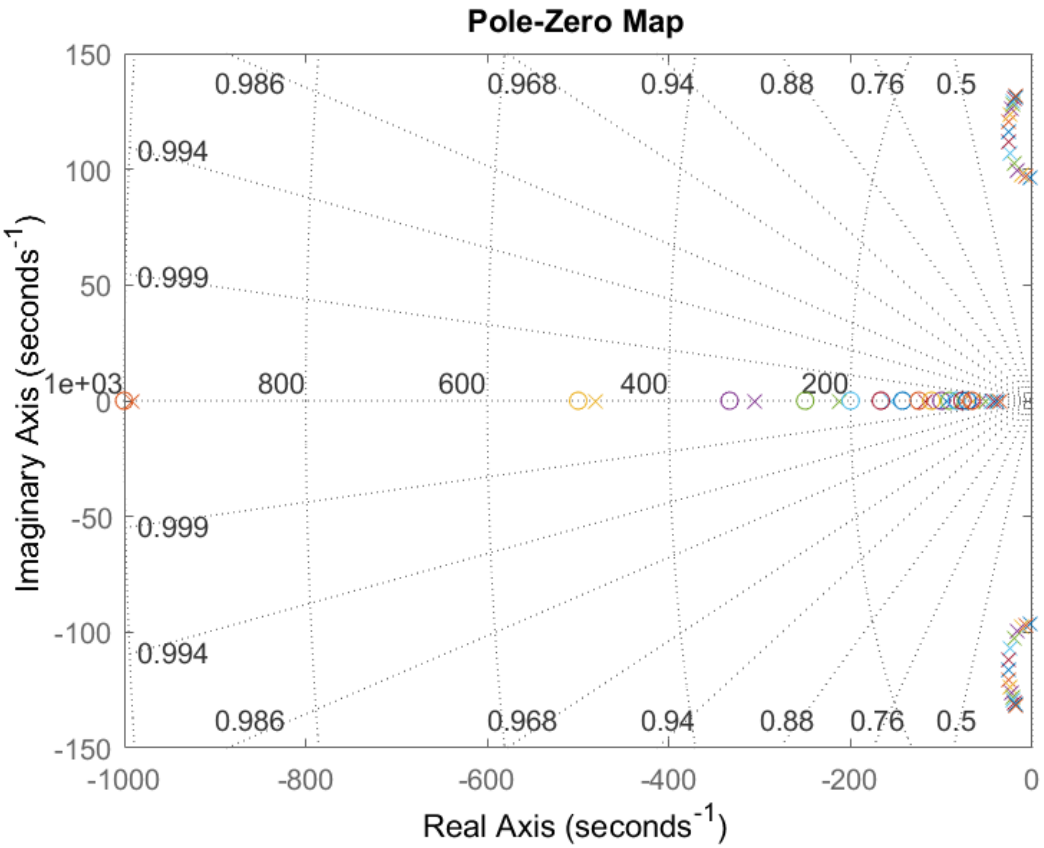

Figure 4-5 - Root Locus about τ_{11}^1

The poles and zeros are further away from the imaginary axis, the system would be more stable. From the gridline of Figure 4-5, the system becomes more stable when the closed-loop damping ratio become larger. Hence, the suitable value of τ^k can be found when the closed-loop damping

ratio becomes the largest value. The relationship between the τ^k and closed-loop damping ratio can be seen as Figure 4-6.

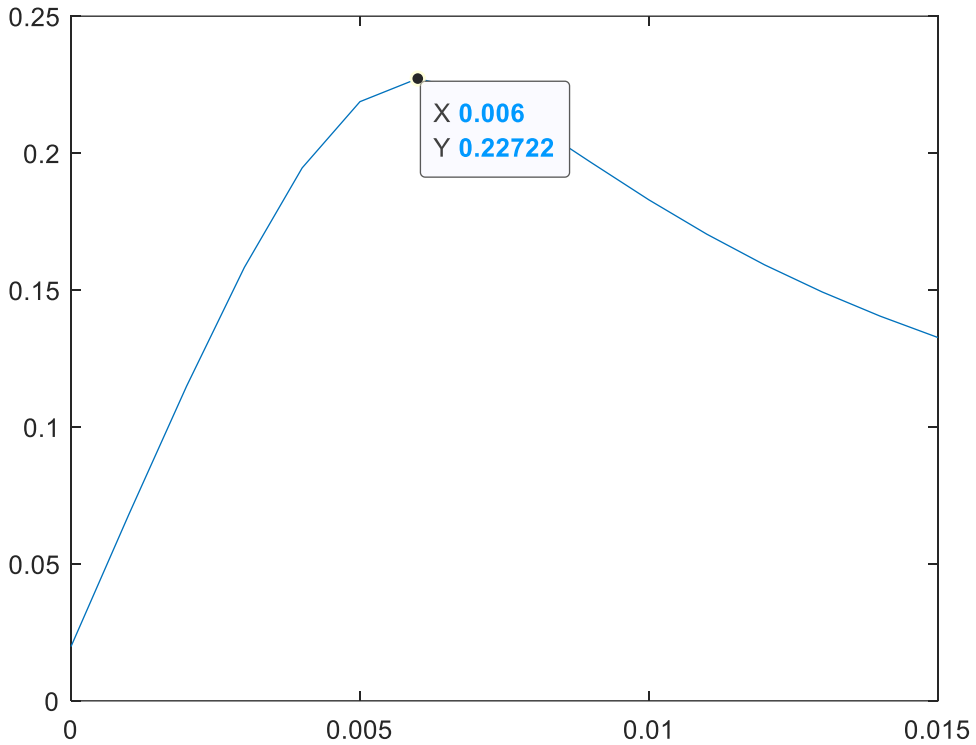

Figure 4-6 - Closed-loop Damping Ratio vs τ_{11}^1

According to Figure 4-6, the maximum of closed-loop damping ratio is 0.2272 where the τ_{11}^1 becomes 0.006.

Figure 4-7 shows the block diagram of IMPPF control SISO plate system.

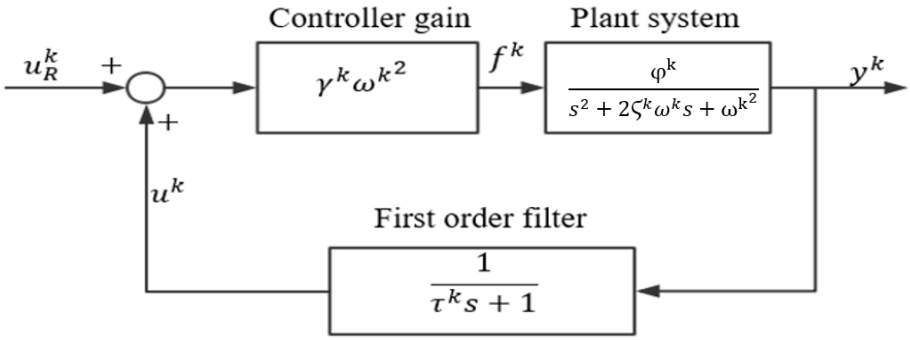

Figure 4-7 - Block Diagram of the IMPPF for a SISO Plate System

The plant system in Figure 4-7 can be seen as any standard second-order plant system. In the plate system, the φ^k and ζ^k is the mode shape and damping ratio of the k^{th} mode. Other parameters are the same as explained in Figure 4-1.

Since vibration cancellations are considered in this thesis, the system input can be assumed as zero. The u_R^k in Figure 4-5 should be zero. Hence, the block of control gain ($\gamma^k \omega^{k^2}$) can be moved alongside the first-order filter block, and can provide the same control effect as Figure 4-7. Then the block diagram shows as Figure 4-8.

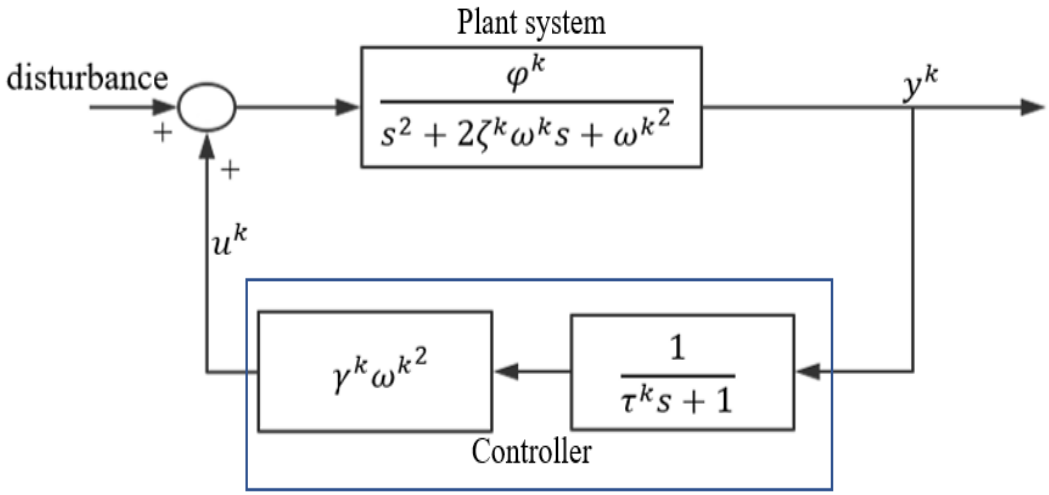

Figure 4-8 - Block Diagram for IMPPF Vibration Cancellation in SISO

The disturbance is caused by the environment the plant system located at. It is added into the plant system to cause the vibration. The y^k is the k^{th} mode output of the system. The u^k is the k^{th} mode control input of the system.

4.1.4 IMPPF for MIMO Plate System

According to (4.16), the value of τ^k is independent of the mode shape. Therefore, using the parameters of the simplified mathematical plant model in Table 3-2, there are three values for τ^k. However, the γ^k still has nine values due to the nine different damping ratios. For simplified expressing, the maximum value of mode shapes for one mode can be extracted. Then the MIMO block diagram can be assumed as Figure 4-9.

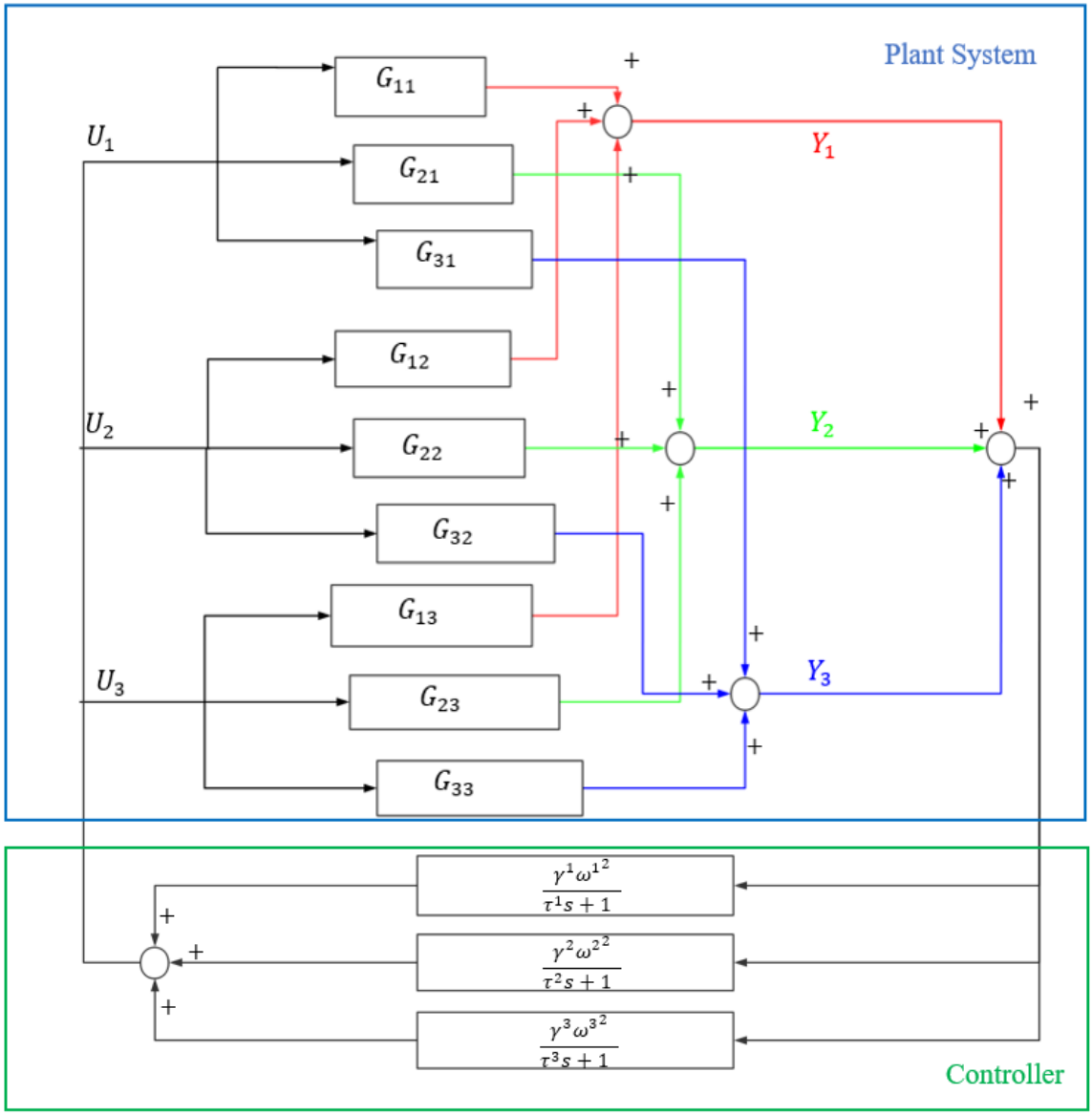

Figure 4-9 - Block Diagram of the IMPPF for the MIMO Plate System

a) Stability Range

The stability range of MIMO plate system can be found by applying Lyapunov function which requests matrix expressions for the compensated system. Therefore, this section provides the details on how to derive the matrix expressions of the closed-loop system and how to apply the Lyapunov function in the compensated system.

Based on Figure 4-9, mathematical expression can be represented in (4.17).

$$U_1 = \frac{\gamma^1\omega^{1^2}}{\tau^1 s+1}(Y_1+Y_2+Y_3) + \frac{\gamma^2\omega^{2^2}}{\tau^2 s+1}(Y_1+Y_2+Y_3) + \frac{\gamma^3\omega^{3^2}}{\tau^3 s+1}(Y_1+Y_2+Y_3) \quad (4.17)$$

where, U_i and Y_i $(i = 1,2,3)$ are the control input and system output in s-domain.

Assume ρ_1, ρ_2, ρ_3 as:

$$\rho_1 = \frac{\gamma^1\omega^1}{\tau^1 s+1}(Y_1 + Y_2 + Y_3) \tag{4.18}$$

$$\rho_2 = \frac{\gamma^2\omega^2}{\tau^2 s+1}(Y_1 + Y_2 + Y_3)$$

$$\rho_3 = \frac{\gamma^3\omega^3}{\tau^3 s+1}(Y_1 + Y_2 + Y_3)$$

Apply the inverse Laplace transform function into (4.18), (4.19) can be obtained.

$$\tau^1\dot{\rho}_1 + \rho_1 = \gamma^1[\omega^1\ \omega^1\ \omega^1]\begin{bmatrix} y_1 \\ y_2 \\ y_3 \end{bmatrix} \tag{4.19}$$

$$\tau^2\dot{\rho}_2 + \rho_2 = \gamma^2[\omega^2\ \omega^2\ \omega^2]\begin{bmatrix} y_1 \\ y_2 \\ y_3 \end{bmatrix}$$

$$\tau^3\dot{\rho}_3 + \rho_3 = \gamma^3[\omega^3\ \omega^3\ \omega^3]\begin{bmatrix} y_1 \\ y_2 \\ y_3 \end{bmatrix}$$

where, y_i $(i = 1,2,3)$ is the system output in time-domain.

Then (4.17) can be rewritten as (4.20) in time-domain.

$$u_1 = \omega^1\rho_1 + \omega^2\rho_2 + \omega^3\rho_3 \tag{4.20}$$

Due to $U_1 = U_2 = U_3$, the matrix expressions in time domain can be shown as:

$$\begin{bmatrix} u_1 \\ u_2 \\ u_3 \end{bmatrix} = \begin{bmatrix} \omega^1 & \omega^2 & \omega^3 \\ \omega^1 & \omega^2 & \omega^3 \\ \omega^1 & \omega^2 & \omega^3 \end{bmatrix}\begin{bmatrix} \rho_1 \\ \rho_2 \\ \rho_3 \end{bmatrix} \tag{4.21}$$

where, u_i $(i = 1,2,3)$ is the control input in time-domain.

Based on (4.19) and (4.21), the controller mathematical model can be expressed as:

$$\begin{cases} \boldsymbol{\tau\dot{\rho}} + \boldsymbol{\rho} = \boldsymbol{\gamma W^T Y} \\ \boldsymbol{U} = \boldsymbol{W\rho} \end{cases} \tag{4.22}$$

where,

$$\boldsymbol{Y} = \begin{bmatrix} y_1 \\ y_2 \\ y_3 \end{bmatrix} \quad \boldsymbol{U} = \begin{bmatrix} u_1 \\ u_2 \\ u_3 \end{bmatrix} \quad \boldsymbol{\tau} = \begin{bmatrix} \tau^1 & 0 & 0 \\ 0 & \tau^2 & 0 \\ 0 & 0 & \tau^3 \end{bmatrix} \quad \boldsymbol{\rho} = \begin{bmatrix} \rho_1 \\ \rho_2 \\ \rho_3 \end{bmatrix}$$

$$\boldsymbol{\gamma} = \begin{bmatrix} \gamma^1 & \gamma^1 & \gamma^1 \\ \gamma^2 & \gamma^2 & \gamma^2 \\ \gamma^3 & \gamma^3 & \gamma^3 \end{bmatrix} \quad \boldsymbol{W} = \begin{bmatrix} \omega^1 & \omega^2 & \omega^3 \\ \omega^1 & \omega^2 & \omega^3 \\ \omega^1 & \omega^2 & \omega^3 \end{bmatrix}$$

Recall the Second-order Differential Model of the plant system is displayed as (3.16) in section 3.3.

$$\begin{cases} \ddot{\boldsymbol{\eta}} + \mathbf{D}\dot{\boldsymbol{\eta}} + \boldsymbol{\Omega\eta} = \boldsymbol{\psi}^T \boldsymbol{U} \\ \boldsymbol{Y} = \boldsymbol{\psi\eta} \end{cases} \tag{3.16}$$

Eliminate the $\boldsymbol{Y}$ and $\boldsymbol{U}$ in (4.22) and (3.16). the closed-loop model can be displayed as:

$$\begin{cases} \ddot{\boldsymbol{\eta}} + \boldsymbol{D}\dot{\boldsymbol{\eta}} + \boldsymbol{\Omega\eta} = \boldsymbol{\psi}^T \boldsymbol{W\rho} \\ \boldsymbol{\tau}\dot{\boldsymbol{\rho}} + \boldsymbol{\rho} = \boldsymbol{\gamma W}^T \boldsymbol{\psi\eta} \end{cases} \tag{4.23}$$

Let $\boldsymbol{\rho} = \boldsymbol{\gamma}^T \mathbf{P}$ to ensure the $\boldsymbol{K}$ term in (4.25) to be a symmetric matrix. The (4.23) can be rewritten as:

$$\begin{cases} \ddot{\boldsymbol{\eta}} + \mathbf{D}\dot{\boldsymbol{\eta}} + \boldsymbol{\Omega\eta} = \boldsymbol{\psi}^T \boldsymbol{W\gamma}^T \mathbf{P} \\ \boldsymbol{\tau\gamma}^T \dot{\mathbf{P}} + \boldsymbol{\gamma}^T \mathbf{P} = \boldsymbol{\gamma \mathbf{W}^{\mathrm{T}} \psi\eta} \end{cases} \tag{4.24}$$

Transfer the (4.24) in matrix expressions, the compensated matrix expressions can be given in (4.25).

$$\boldsymbol{M\ddot{q}} + \boldsymbol{C\dot{q}} + \boldsymbol{Kq} = \mathbf{0} \tag{4.25}$$

where,

$$\boldsymbol{q} = \begin{bmatrix} \boldsymbol{\eta} \\ \boldsymbol{P} \end{bmatrix} \quad \boldsymbol{M} = \begin{bmatrix} \boldsymbol{I} & \mathbf{0} \\ \mathbf{0} & \mathbf{0} \end{bmatrix} \quad \boldsymbol{C} = \begin{bmatrix} \boldsymbol{D} & \mathbf{0} \\ \mathbf{0} & \boldsymbol{\tau\gamma}^T \end{bmatrix} \quad \boldsymbol{K} = \begin{bmatrix} \boldsymbol{\Omega} & -\boldsymbol{\psi}^T \boldsymbol{W\gamma}^T \\ -\boldsymbol{\gamma \mathbf{W}^{\mathrm{T}} \psi} & \boldsymbol{\gamma}^T \end{bmatrix}$$

According to Lyapunov Stability Theory [30], the compensated system is stable *if and only if*:

$$\boldsymbol{V}(\boldsymbol{q}) = \frac{1}{2}(\dot{\boldsymbol{q}}^T \boldsymbol{M\dot{q}} + \boldsymbol{q}^T \boldsymbol{Kq}) > 0$$

$$\dot{\boldsymbol{V}}(\boldsymbol{q}) = \dot{\boldsymbol{q}}^T (\boldsymbol{M\ddot{q}} + \boldsymbol{Kq}) = -\dot{\boldsymbol{q}}^T \boldsymbol{C\dot{q}} < 0 \tag{4.26}$$

Based on analysis of the MIMO IMPPF control system, the matrix $\boldsymbol{M}$ is positive semi-definite, $\boldsymbol{C}$ is positive definite. Hence, if $\boldsymbol{K}$ is positive, the system is stable.

Since the stability of the MIMO system is only related to the matrix $\boldsymbol{K}$, the matrix $\boldsymbol{K}$ is independent to matrix $\boldsymbol{\tau}$. Hence, the stability range of the MIMO system is only about the value of $\gamma^k (k = 1,2,3)$.

The range cannot be calculated in several certain inequalities remain unchanged, because of the enormous computation load. However, if there are the fixed values for γ^k, the stability of the system can be checked by substitute the values into the matrix $\boldsymbol{K}$, and to calculate whether the eigenvalues of matrix $\boldsymbol{K}$ are all positive.

b) Find parameters

In MIMO plate system, the method to find the values of τ^k and γ^k can use the same method in 4.2.3. However, because the calculation of γ^k is based on the steady-state error to be zero, the requirement is not so strict that the steady-state error must be eliminated, the small steady-state error is allowed. Hence, the γ^k can be tuned to an acceptable value if it is not in or on the edge of the stability range.

4.2 MPPF Design

MPPF was first proposed by Nima Mahmoodi et al. by adding a first-order filter to the structure of conventional PPF and successfully implemented the MPPF on a beam-structure in 2010[17]. The output signal of a conventional PPF is positively fed to a second-order controller structure with a large damping. The large damping can provide sufficient suppression effects on the transient vibrations. However, the large damping in the compensator will lead to a decrease of the damping frequency of the compensator [17]. This will create the difference between the damping frequency of the compensator and the natural frequency of the structure, which would otherwise be equal to each other in an ideal case. Consequently, a steady-state error of the system output will be generated. Using MPPF, the damping ratio of the conventional PPF compensator can be reduced. The steady state error of the compensated system in MPPF can be reduced close to zero. The detailed derivation of the MPPF will be given in this section and extended the algorithm from SISO system to the given MIMO plate-structure for controlling multi-modes.

4.2.1 MPPF Concept

The mathematical model of the MPPF can be expressed as [17]:

$$\begin{cases} \ddot{y}^k + 2\zeta^k\omega^k\dot{y}^k + {\omega^k}^2 y^k = \varphi^k(g^k\alpha^k + h^k\beta^k + d) \\ \ddot{\alpha}^k + 2\zeta^k\omega^k\dot{\alpha}^k + {\omega^k}^2\alpha^k = {\omega^k}^2 y^k \\ \dot{\beta}^k + \omega^k\beta^k = \omega^k y^k \end{cases} \tag{4.27}$$

where, the ω^k represents the natural frequency of plant system at the k^{th} mode. There are two positive gains need to be designed which are g^k and h^k. u^k and y^k are the control input and output of the system respectively. The d is a disturbance of the system. The index k means the k^{th} mode of the system.

According to (4.27), the block diagram of the MPPF for a SISO system can be displayed as Figure 4-10.

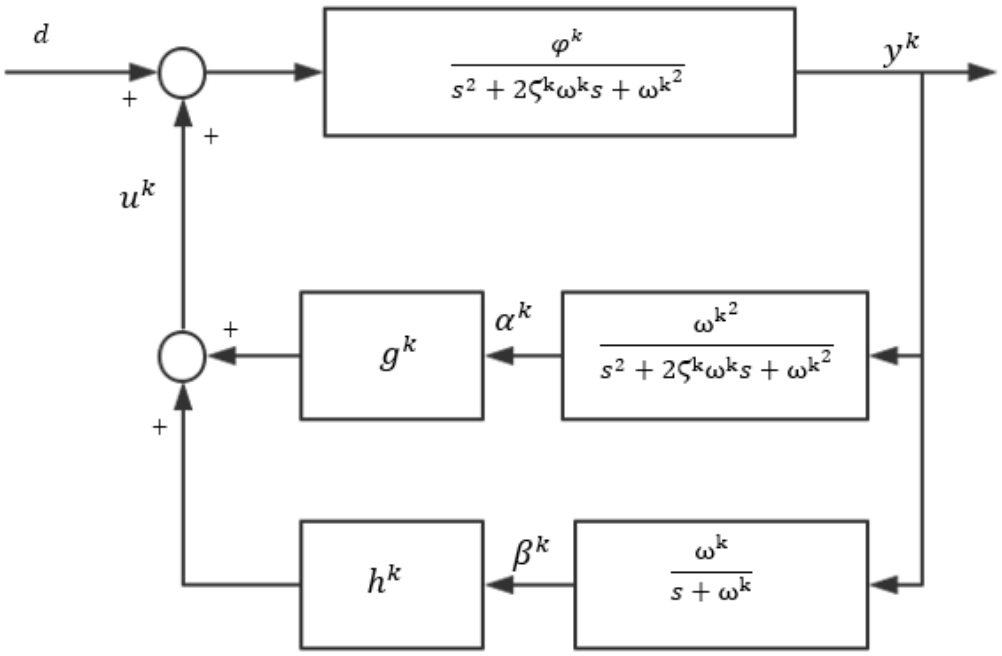

Figure 4-10 - Block Diagram of the MPPF for a SISO System

The MPPF consists of a second-order filter which is used to provide equivalent damping ζ^k with plant system to suppresses transient vibration, and a first-order filter to reduce the system damping. The plant system is a standard second-order system. The frequency parameters of the first-order filter and second-order filter are all equal to the natural frequencies of the plant system.

The flowchart of the parameters design can be demonstrated as Figure 4-11.

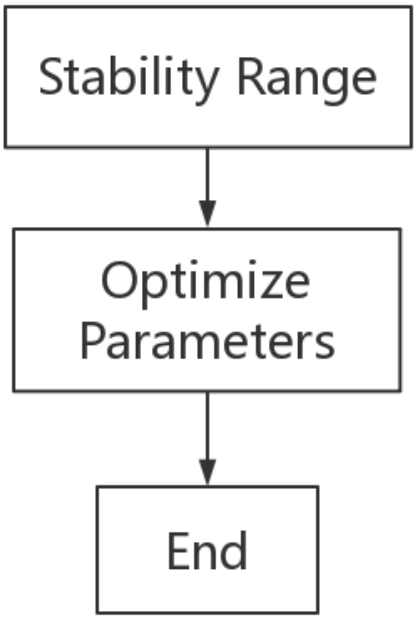

Figure 4-11 - Flowchart of MPPF Algorithm

Based on Figure 4-11, the gains stability range can be explained in mathematic theory in 4.3.2, and 4.3.3.

For two gains optimization of MPPF, the Genetic Algorithm (GA) is used to solve the minimum criterion of the H∞ norm of the closed-loop system, and the optimal parameters of the controller are obtained [2].

4.2.2 MPPF for SISO Plate System

Based on Figure 4-10 and (4.27), setting the α^k and β^k as:

$$\begin{cases} \alpha^k = g^{k\,-\frac{1}{2}}\varphi^{k\,-\frac{1}{2}}\omega^k i^k \\ \beta^k = h^{k\,-\frac{1}{2}}\varphi^{k\,-\frac{1}{2}}\omega^{k\,\frac{1}{2}} j^k \end{cases} \tag{4.28}$$

Substitute (4.28) into (4.27), 4.27 can be rewritten as:

$$\begin{cases} \ddot{y}^k + 2\zeta^k\omega^k\dot{y}^k + \omega^{k\,2}y^k - g^{k\,\frac{1}{2}}\varphi^{k\,\frac{1}{2}}\omega^k i^k - h^{k\,\frac{1}{2}}\varphi^{k\,\frac{1}{2}}\omega^{k\,\frac{1}{2}} j^k - \varphi^k d = 0 \\ \ddot{\imath}^k + 2\zeta^k\omega^k\dot{\imath}^k - \omega^k g^{k\,\frac{1}{2}}\varphi^{k\,\frac{1}{2}}y^k + \omega^{k\,2}i^k = 0 \\ \dot{\jmath}^k - h^{k\,\frac{1}{2}}\varphi^{k\,\frac{1}{2}}\omega^{k\,\frac{1}{2}}y^k + \omega^k j^k = 0 \end{cases} \tag{4.29}$$

(4.29) can be simplified into matrix expressions as:

$$\boldsymbol{N\ddot{p} + E\dot{p} + Gp + H = 0} \tag{4.30}$$

where,

$$\boldsymbol{p} = \begin{bmatrix} y \\ i \\ j \end{bmatrix} \qquad \boldsymbol{N} = \begin{bmatrix} 1 & 0 & 0 \\ 0 & 1 & 0 \\ 0 & 0 & 0 \end{bmatrix} \qquad \boldsymbol{E} = \begin{bmatrix} 2\zeta^k\omega^k & 0 & 0 \\ 0 & 2\zeta^k\omega^k & 0 \\ 0 & 0 & 1 \end{bmatrix}$$

$$\boldsymbol{G} = \begin{bmatrix} {\omega^k}^2 & -g^{k\frac{1}{2}}\varphi^{k\frac{1}{2}}\omega^k & -h^{k\frac{1}{2}}\varphi^{k\frac{1}{2}}\omega^{k\frac{1}{2}} \\ -\omega^k g^{k\frac{1}{2}}\varphi^{k\frac{1}{2}} & {\omega^k}^2 & 0 \\ -h^{k\frac{1}{2}}\varphi^{k\frac{1}{2}}\omega^{k\frac{1}{2}} & 0 & \omega^k \end{bmatrix} \qquad \boldsymbol{H} = \begin{bmatrix} 0 & 0 & -\varphi^k d \\ 0 & 0 & 0 \\ 0 & 0 & 0 \end{bmatrix}$$

Since the value of $-\varphi^k d$ is small, for simplicity, the influence from disturbance is ignored, and (4.30) is displayed as (4.31).

$$\boldsymbol{N}\ddot{\boldsymbol{p}} + \boldsymbol{E}\dot{\boldsymbol{p}} + \boldsymbol{G}\boldsymbol{p} = \boldsymbol{0} \tag{4.31}$$

According to Lyapunov Stability Theory [30], the compensated system is stable *if and only if*:

$$\boldsymbol{V}(\boldsymbol{p}) = \frac{1}{2}(\dot{\boldsymbol{p}}^{\boldsymbol{T}}\boldsymbol{N}\dot{\boldsymbol{p}} + \boldsymbol{p}^{\boldsymbol{T}}\boldsymbol{G}\boldsymbol{p}) > 0$$

$$\dot{\boldsymbol{V}}(\boldsymbol{p}) = \dot{\boldsymbol{p}}^{\boldsymbol{T}}(\boldsymbol{N}\ddot{\boldsymbol{p}} + \boldsymbol{G}\boldsymbol{p}) = -\dot{\boldsymbol{q}}^{\boldsymbol{T}}\boldsymbol{E}\dot{\boldsymbol{q}} < 0 \tag{4.32}$$

Based on analysis of the MIMO IMPPF control system, the matrix $\boldsymbol{N}$ is positive semi-definite, $\boldsymbol{E}$ is positive definite. Hence, if $\boldsymbol{G}$ is positive definite, the system is stable. The conditions required for the positive definite can be written as (4.33), due to Silvester's criterion [31],

$${\omega^k}^2 > 0$$

$$\boldsymbol{det}\begin{vmatrix} {\omega^k}^2 & -g^{k\frac{1}{2}}\varphi^{k\frac{1}{2}}\omega^k \\ -\omega^k g^{k\frac{1}{2}}\varphi^{k\frac{1}{2}} & {\omega^k}^2 \end{vmatrix} > 0$$

$$\boldsymbol{det}\begin{vmatrix} {\omega^k}^2 & -g^{k\frac{1}{2}}\varphi^{k\frac{1}{2}}\omega^k & -h^{k\frac{1}{2}}\varphi^{k\frac{1}{2}}\omega^{k\frac{1}{2}} \\ -\omega^k g^{k\frac{1}{2}}\varphi^{k\frac{1}{2}} & {\omega^k}^2 & 0 \\ -h^{k\frac{1}{2}}\varphi^{k\frac{1}{2}}\omega^{k\frac{1}{2}} & 0 & \omega^k \end{vmatrix} > 0 \tag{4.33}$$

Solve (4.33) provides the result as:

$$g + h < \frac{{\omega^k}^2}{\varphi^k} \tag{4.34}$$

4.2.3 MPPF for MIMO Plate System

The stability range of MIMO plate system can be found by applying Lyapunov function which requests matrix expressions for the closed-loop system. Therefore, in this section, it explains the detail that how to derive the matrix expressions of the closed-loop system and how to apply the Lyapunov function in the compensated system.

Assume the MPPF compensated MIMO plate system is displayed as Figure 4-12

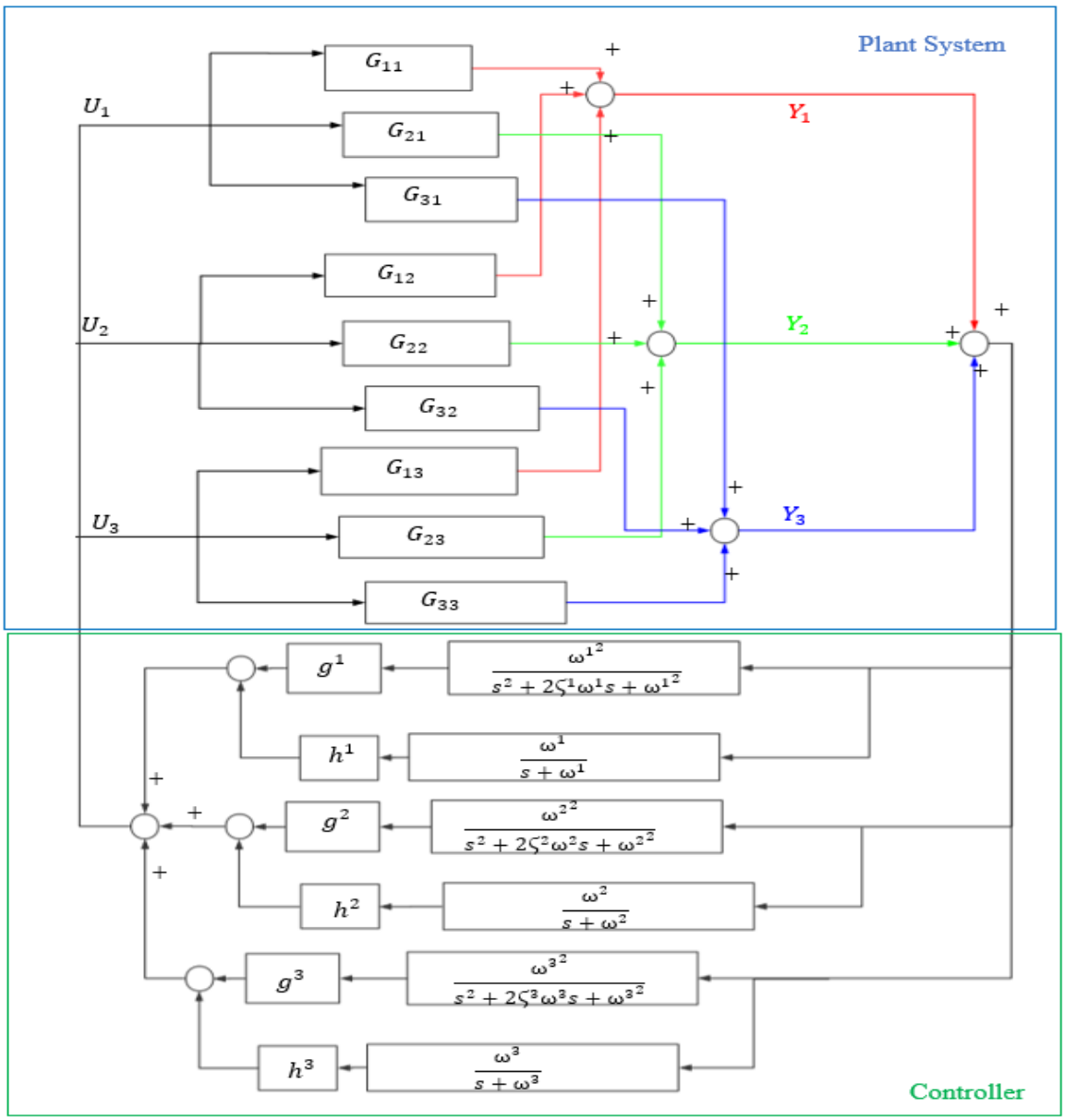

Figure 4-12 - Block Diagram of the MPPF for the MIMO Plate System

Based on Figure 4-12, mathematical expression can be represented in (4.35).

$$U_1 = U_2 = U_3$$

$$U_1 = \left(g^1 \frac{\omega^{1^2}}{s^2+2\zeta^1\omega^1 s+\omega^{1^2}} + h^1 \frac{\omega^1}{s+\omega^1}\right)(Y_1+Y_2+Y_3) + \left(g^2 \frac{\omega^{2^2}}{s^2+2\zeta^2\omega^2 s+\omega^{2^2}} + h^2 \frac{\omega^2}{s+\omega^2}\right)(Y_1 +$$

$$Y_2+Y_3) + (g^3 \frac{\omega^{3^2}}{s^2+2\zeta^3\omega^3 s+\omega^{3^2}} + h^3 \frac{\omega^3}{s+\omega^3})(Y_1+Y_2+Y_3) \quad (4.35)$$

where, U_i and Y_i $(i = 1,2,3)$ are the control input and system output in s-domain.

Define ν_1, ν_2, ν_3 in (4.36):

$$\nu_1 = g^1 \frac{\omega^1}{s^2+2\zeta^1\omega^1 s+\omega^{1^2}}(Y_1+Y_2+Y_3) + h^1 \frac{1}{s+\omega^1}(Y_1+Y_2+Y_3) \quad (4.36)$$

$$\nu_2 = g^2 \frac{\omega^2}{s^2+2\zeta^2\omega^2 s+\omega^{2^2}}(Y_1+Y_2+Y_3) + h^2 \frac{1}{s+\omega^2}(Y_1+Y_2+Y_3)$$

$$\nu_3 = g^3 \frac{\omega^3}{s^2+2\zeta^3\omega^3 s+\omega^{3^2}}(Y_1+Y_2+Y_3) + h^3 \frac{1}{s+\omega^3}(Y_1+Y_2+Y_3)$$

Then (4.35) can be rewritten as (4.37) in time-domain.

$$u_1 = \omega^1\nu_1 + \omega^2\nu_2 + \omega^3\nu_3 \quad (4.37)$$

$$u_2 = \omega^1\nu_1 + \omega^2\nu_2 + \omega^3\nu_3$$

$$u_3 = \omega^1\nu_1 + \omega^2\nu_2 + \omega^3\nu_3$$

where, u_i $(i = 1,2,3)$ is the control input in time-domain.

The matrix expressions of (4.37) can be written as:

$$\boldsymbol{U} = \boldsymbol{W}\boldsymbol{\nu} \quad (4.38)$$

where,

$$\boldsymbol{U} = \begin{bmatrix} u_1 \\ u_2 \\ u_3 \end{bmatrix} \quad \boldsymbol{W} = \begin{bmatrix} \omega^1 & \omega^2 & \omega^3 \\ \omega^1 & \omega^2 & \omega^3 \\ \omega^1 & \omega^2 & \omega^3 \end{bmatrix} \quad \boldsymbol{\nu} = \begin{bmatrix} \nu_1 \\ \nu_2 \\ \nu_3 \end{bmatrix}$$

Set ν_i to be the sum of λ_i and δ_i $(i = 1,2,3)$ as:

$$\nu_1 = \lambda_1 + \delta_1 = g^1 \frac{\omega^1}{s^2+2\zeta^1\omega^1 s+\omega^{1^2}}(Y_1+Y_2+Y_3) + h^1 \frac{1}{s+\omega^1}(Y_1+Y_2+Y_3) \quad (4.39)$$

$$\nu_2 = \lambda_2 + \delta_2 = g^2 \frac{\omega^2}{s^2+2\zeta^2\omega^2 s+\omega^{2^2}}(Y_1+Y_2+Y_3) + h^2 \frac{1}{s+\omega^2}(Y_1+Y_2+Y_3)$$

$$\nu_3 = \lambda_3 + \delta_3 = g^3 \frac{\omega^3}{s^2+2\zeta^3\omega^3 s+\omega^{3^2}}(Y_1+Y_2+Y_3) + h^3 \frac{1}{s+\omega^3}(Y_1+Y_2+Y_3)$$

Apply the inverse Laplace transform function into λ_i and δ_i , (4.40) can be obtained.

$$\begin{cases} \ddot{\lambda}_1 + 2\zeta^1\omega^1\dot{\lambda}_1 + {\omega^1}^2\lambda_1 = g^1\omega^1(y_1 + y_2 + y_3) \\ \dot{\delta}_1 + \omega^1\delta_1 = h^1(y_1 + y_2 + y_3) \end{cases} \quad (4.40)$$

$$\begin{cases} \ddot{\lambda}_2 + 2\zeta^2\omega^2\dot{\lambda}_2 + {\omega^2}^2\lambda_2 = g^2\omega^2(y_1 + y_2 + y_3) \\ \dot{\delta}_2 + \omega^2\delta_2 = h^2(y_1 + y_2 + y_3) \end{cases}$$

$$\begin{cases} \ddot{\lambda}_3 + 2\zeta^3\omega^3\dot{\lambda}_3 + {\omega^3}^2\lambda_3 = g^3\omega^3(y_1 + y_2 + y_3) \\ \dot{\delta}_3 + \omega^3\delta_3 = h^3(y_1 + y_2 + y_3) \end{cases}$$

where, y_i $(i = 1,2,3)$ is the system output in time-domain.

The matrix expressions of (4.40) can be written as:

$$\begin{cases} \ddot{\boldsymbol{\lambda}} + \boldsymbol{D}\dot{\boldsymbol{\lambda}} + \boldsymbol{\Omega}\boldsymbol{\lambda} = \boldsymbol{gWY} \\ \dot{\boldsymbol{\delta}} + \boldsymbol{\Omega}^{\frac{1}{2}}\boldsymbol{\delta} = \boldsymbol{hY} \end{cases} \quad (4.41)$$

where,

$$\boldsymbol{Y} = \begin{bmatrix} y_1 \\ y_2 \\ y_3 \end{bmatrix} \quad \boldsymbol{\lambda} = \begin{bmatrix} \lambda_1 \\ \lambda_2 \\ \lambda_3 \end{bmatrix} \quad \boldsymbol{\delta} = \begin{bmatrix} \delta_1 \\ \delta_2 \\ \delta_3 \end{bmatrix}$$

$$\boldsymbol{g} = \begin{bmatrix} g^1 & g^1 & g^1 \\ g^2 & g^2 & g^2 \\ g^3 & g^3 & g^3 \end{bmatrix} \quad \boldsymbol{h} = \begin{bmatrix} h^1 & h^2 & h^3 \\ h^1 & h^2 & h^3 \\ h^1 & h^2 & h^3 \end{bmatrix} \quad \boldsymbol{W} = \begin{bmatrix} \omega^1 & \omega^2 & \omega^3 \\ \omega^1 & \omega^2 & \omega^3 \\ \omega^1 & \omega^2 & \omega^3 \end{bmatrix}$$

$$\mathbf{D} = \begin{bmatrix} 2\zeta^1\omega^1 & 0 & 0 \\ 0 & 2\zeta^2\omega^2 & 0 \\ 0 & 0 & 2\zeta^3\omega^3 \end{bmatrix} \quad \boldsymbol{\Omega} = \begin{bmatrix} (\omega^1)^2 & 0 & 0 \\ 0 & (\omega^2)^2 & 0 \\ 0 & 0 & (\omega^3)^2 \end{bmatrix}$$

Since, ν_i is the sum of λ_i and δ_i, the term $\boldsymbol{\nu}$ in (4.38) can be eliminate by substituting $\boldsymbol{\lambda}$ and $\boldsymbol{\delta}$ into the (4.38), then (4.42) is given.

$$\boldsymbol{U} = \boldsymbol{W}\boldsymbol{\lambda} + \boldsymbol{W}\boldsymbol{\delta} \quad (4.42)$$

Based on (4.41) and (4.42), the controller can be represented as:

$$\begin{cases} \ddot{\boldsymbol{\lambda}} + \boldsymbol{D}\dot{\boldsymbol{\lambda}} + \boldsymbol{\Omega}\boldsymbol{\lambda} = \boldsymbol{gWY} \\ \dot{\boldsymbol{\delta}} + \boldsymbol{\Omega}^{\frac{1}{2}}\boldsymbol{\delta} = \boldsymbol{hY} \\ \boldsymbol{U} = \boldsymbol{W}\boldsymbol{\lambda} + \boldsymbol{W}\boldsymbol{\delta} \end{cases} \quad (4.43)$$

Recall the Second-order Differential Model of the plant system is displayed as (3.16) in section 3.3.

$$\begin{cases} \ddot{\boldsymbol{\eta}} + \mathbf{D}\dot{\boldsymbol{\eta}} + \boldsymbol{\Omega\eta} = \boldsymbol{\psi}^T \boldsymbol{U} \\ \boldsymbol{Y} = \boldsymbol{\psi\eta} \end{cases} \tag{3.16}$$

Eliminate the $\boldsymbol{U}$ and $\boldsymbol{Y}$ in (3.16) and (4.43). the closed-loop model can be displayed as:

$$\begin{cases} \ddot{\boldsymbol{\eta}} + \boldsymbol{D}\dot{\boldsymbol{\eta}} + \boldsymbol{\Omega\eta} = \boldsymbol{\psi}^T \boldsymbol{W}(\boldsymbol{\lambda} + \boldsymbol{\delta}) \\ \ddot{\boldsymbol{\lambda}} + \boldsymbol{D}\dot{\boldsymbol{\lambda}} + \boldsymbol{\Omega\lambda} = \boldsymbol{gW\psi\eta} \\ \dot{\boldsymbol{\delta}} + \boldsymbol{\Omega}^{\frac{1}{2}}\boldsymbol{\delta} = \boldsymbol{h\psi\eta} \end{cases} \tag{4.44}$$

Transfer the (4.44) in matrix expressions, the compensated matrix expressions can be given in (4.45).

$$\begin{bmatrix} \boldsymbol{I} & \mathbf{0} & \mathbf{0} \\ \mathbf{0} & \boldsymbol{I} & \mathbf{0} \\ \mathbf{0} & \mathbf{0} & \mathbf{0} \end{bmatrix} \begin{bmatrix} \ddot{\boldsymbol{\eta}} \\ \ddot{\boldsymbol{\lambda}} \\ \ddot{\boldsymbol{\delta}} \end{bmatrix} + \begin{bmatrix} \boldsymbol{D} & \mathbf{0} & \mathbf{0} \\ \mathbf{0} & \boldsymbol{D} & \mathbf{0} \\ \mathbf{0} & \mathbf{0} & \boldsymbol{I} \end{bmatrix} \begin{bmatrix} \dot{\boldsymbol{\eta}} \\ \dot{\boldsymbol{\lambda}} \\ \dot{\boldsymbol{\delta}} \end{bmatrix} + \begin{bmatrix} \boldsymbol{\Omega} & -\boldsymbol{\psi}^T\boldsymbol{W} & -\boldsymbol{\psi}^T\boldsymbol{W} \\ -\boldsymbol{gW\psi} & \boldsymbol{\Omega} & \mathbf{0} \\ -\boldsymbol{h\psi} & \mathbf{0} & \boldsymbol{\Omega}^{\frac{1}{2}} \end{bmatrix} \begin{bmatrix} \boldsymbol{\eta} \\ \boldsymbol{\lambda} \\ \boldsymbol{\delta} \end{bmatrix} = \mathbf{0} \tag{4.45}$$

Let $\boldsymbol{\lambda} = \boldsymbol{g}^{\frac{1}{2}}\boldsymbol{\Lambda}$ and $\boldsymbol{\delta} = \boldsymbol{h}^{\frac{1}{2}}\boldsymbol{W}^{-\frac{1}{2}}\boldsymbol{\Delta}$ to ensure the $\boldsymbol{K}$ term in (4.47) to be symmetric matrix. The (4.44) can be rewritten as:

$$\begin{cases} \ddot{\boldsymbol{\eta}} + \boldsymbol{D}\dot{\boldsymbol{\eta}} + \boldsymbol{\Omega\eta} = \boldsymbol{\psi}^T\boldsymbol{W}\boldsymbol{g}^{\frac{1}{2}}\boldsymbol{\Lambda} + \boldsymbol{\psi}^T\boldsymbol{W}^{\frac{1}{2}}\boldsymbol{h}^{\frac{1}{2}}\boldsymbol{\Delta} \\ \ddot{\boldsymbol{\Lambda}} + \boldsymbol{D}\dot{\boldsymbol{\Lambda}} + \boldsymbol{\Omega\Lambda} = \boldsymbol{g}^{\frac{T}{2}}\boldsymbol{W}^T\boldsymbol{\psi\eta} \\ \dot{\boldsymbol{\Delta}} + \boldsymbol{\Omega}^{\frac{1}{2}}\boldsymbol{\Delta} = \boldsymbol{h}^{\frac{T}{2}}\boldsymbol{W}^{\frac{T}{2}}\boldsymbol{\psi\eta} \end{cases} \tag{4.46}$$

Transfer the (4.46) in matrix expressions, the compensated matrix expressions can be given in (4.47).

$$\boldsymbol{M}\ddot{\boldsymbol{q}} + \boldsymbol{C}\dot{\boldsymbol{q}} + \boldsymbol{Kq} = \mathbf{0} \tag{4.47}$$

where,

$$\boldsymbol{q} = \begin{bmatrix} \boldsymbol{\eta} \\ \boldsymbol{\Lambda} \\ \boldsymbol{\Delta} \end{bmatrix} \quad \boldsymbol{M} = \begin{bmatrix} \boldsymbol{I} & \mathbf{0} & \mathbf{0} \\ \mathbf{0} & \boldsymbol{I} & \mathbf{0} \\ \mathbf{0} & \mathbf{0} & \mathbf{0} \end{bmatrix} \quad \boldsymbol{C} = \begin{bmatrix} \boldsymbol{D} & \mathbf{0} & \mathbf{0} \\ \mathbf{0} & \boldsymbol{D} & \mathbf{0} \\ \mathbf{0} & \mathbf{0} & \boldsymbol{I} \end{bmatrix}$$

$$\boldsymbol{K} = \begin{bmatrix} \boldsymbol{\Omega} & -\boldsymbol{\psi}^T\boldsymbol{W}\boldsymbol{g}^{\frac{1}{2}} & -\boldsymbol{\psi}^T\boldsymbol{W}^{\frac{1}{2}}\boldsymbol{h}^{\frac{1}{2}} \\ -\boldsymbol{g}^{\frac{T}{2}}\boldsymbol{W}^T\boldsymbol{\psi} & \boldsymbol{\Omega} & \mathbf{0} \\ -\boldsymbol{h}^{\frac{T}{2}}\boldsymbol{W}^{\frac{T}{2}}\boldsymbol{\psi} & \mathbf{0} & \boldsymbol{\Omega}^{\frac{1}{2}} \end{bmatrix}$$

According to Lyapunov Stability Theory [30], the compensated system is stable *if and only if*:

$$\boldsymbol{V(q)} = \frac{1}{2}(\boldsymbol{\dot{q}^T M \dot{q} + q^T K q}) > 0$$

$$\boldsymbol{\dot{V}(q)} = \boldsymbol{\dot{q}^T(M\ddot{q} + Kq)} = -\boldsymbol{\dot{q}^T C \dot{q}} < 0 \qquad (4.48)$$

Based on analysis of the MIMO IMPPF control system, the matrix $\boldsymbol{M}$ is positive semi-definite, $\boldsymbol{C}$ is positive definite. Hence, if $\boldsymbol{K}$ is positive, the system is stable.

The range cannot be calculated in several certain inequalities, because of the enormous computation load. However, if there are the values of g and h, the stability of the system can be checked by substitute the values into the matrix $\boldsymbol{K}$, and calculate whether the eigenvalues of matrix $\boldsymbol{K}$ are all positive.

4.3 RTACS Design

After the IMPPF and MPPF control methodologies are developed above, a RTACS is finally proposed to realize the online adaptive control of the given MIMO plate-structure.

The RTACS is mainly constructed by three parts: Plant, Frequency Estimator and Controller as shown in Figure 4-13.

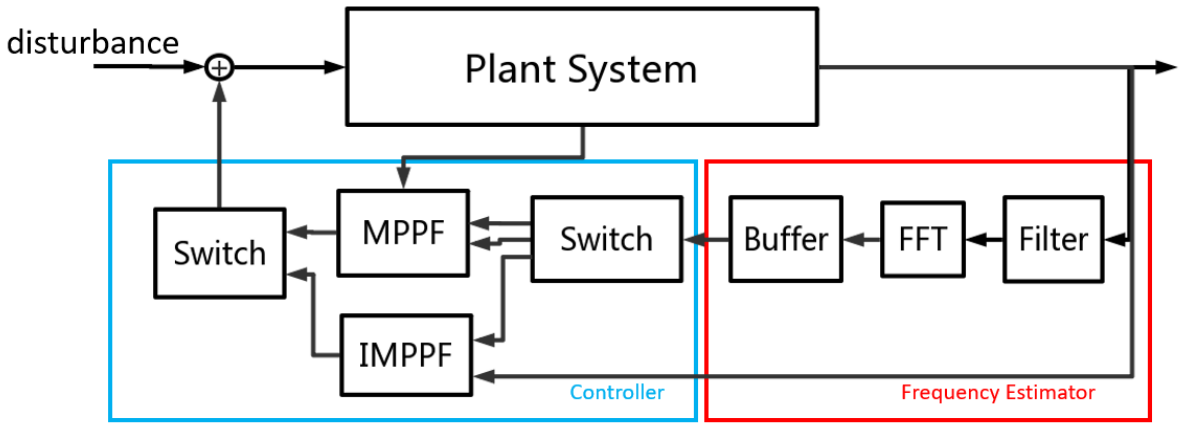

Figure 4-13 – Block Diagram of RTACS

The Frequency Estimator as shown in the red box in Figure 4-13 is used to online identify the natural frequencies of the modes by FFT method within the frequency range of concern (20Hz to 40 Hz). The identifying work is completed by FFT and required frequency range can be obtained by Filter. A Buffer like arrangement is constructed to store the current estimated frequencies which will be compared online continuously with the latest estimated frequencies.

If their differences are within a small threshold value, the stored frequencies will remain unchanged, until a noticeable difference is witnessed.

The estimated frequencies are sending to a Switch, that determines the flow of the new parameters to which controller. The other Switch will be used to determine which controller is going to be connected to form the closed-loop system. If the frequencies in the Buffer remain unchanged, MPPF will be used to form the closed-loop system as its damping performance is better compared to IMPPF. Once the frequencies in the Buffer are changed, the corresponding new frequencies will be sent to IMPPF to calculate a new IMPPF online to replace the previous MPPF. In the meantime, the MPPF controller parameters will be optimized online and will replace the IMPPF once the parameters are obtained.

Chapter 5: Simulation

Numerical simulation is conducted in this chapter to verify the effectiveness of the proposed IMPPF, MPPF and RTACS via MATLAB Simulink©. System parameters obtained in Chapter 3 and compensator parameters designed in Chapter 4 are utilized to build the simulation model in Simulink©. Simulation results are then generated both in frequency-domain and time-domain to validate the effectiveness of the proposed control algorithms.

5.1 Simulation Study of IMPPF

In this section, the IMPPF control effects are demonstrated by discussing the results of the IMPPF designed for a SISO system by time-domain results and bode plots and for the plate MIMO system by time-domain results, respectively. The MIMO system bode plots analysis is demonstrated at Figure 5.19 at Section 5.3 in yellow curve.

5.1.1 IMPPF for SISO System

Using the compensator parameters (time constant τ and control gain γ) obtained following the procedures detailed in Section 4.1.3, each transfer function of plate system G_{ij} (where $i = j$) in (3.1) is regarded as three SISO systems, detailed data can be found in Table 5-1.

Table 5-1 - Parameters of IMPPF for SISO Plate System

	Mode No. k	τ	γ
G_{11}	1	0.006	15.1699
	2	0.005	39.5232
	3	0.004	88.6745
G_{22}	1	0.006	53.9831
	2	0.005	48.0465
	3	0.004	9.7035
G_{33}	1	0.006	56.6747
	2	0.005	71.2435
	3	0.004	32.3373

It is noted that, even though the calculation of time constant τ is related to both the damping ratio and natural frequency of the plant system, but its value is a constant value corresponding to different modes. This method can be easily implemented online by only computing the value of γ with low computation load.

G_{11} will be selected in this thesis to demonstrate the control performance of the IMPPF for a SISO plate system. The closed-loop system is constructed in MATLAB Simulink© as shown in Fig. 5-1.

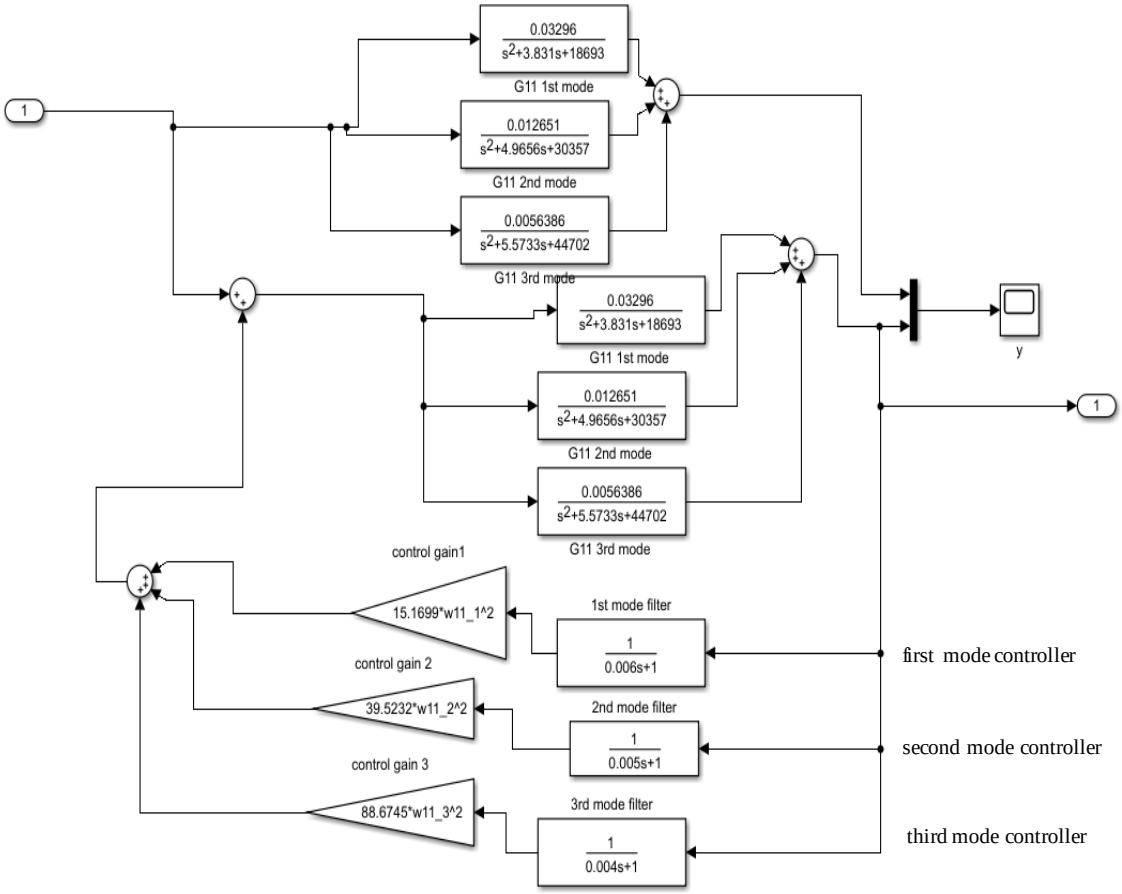

Figure 5-1 – IMPPF SISO System Construction in Simulink©

Based on (3.3), the G_{11} can be written as the sum of 3 second-order functions, each function is built based on one mode. In Figure 5-1, the three functions are represented by 3 blocks which are called 'G11 1st mode', 'G11 2nd mode' and 'G11 3rd mode'. The parameters' values of these three functions can be found in the first three rows of Table 3-1. The whole IMPPF controller can be divided into 3 parallel semi-controllers which are presented as 3 first-order filters and 3 control gains. Each semi-controller is used to control each mode separately. To clearly express the purpose, the 3 paralleled semi-controllers are called first mode controller, second mode controller and third mode controller. The values of γ^k and τ^k can be found from the first three rows of Table 5-1.

To observe the differences between the compensated system and uncompensated system, the 'Scope' block 'y' can display two systems in the time domain (Figure 5-2 is an example), one for uncompensated system and another for the compensated system.

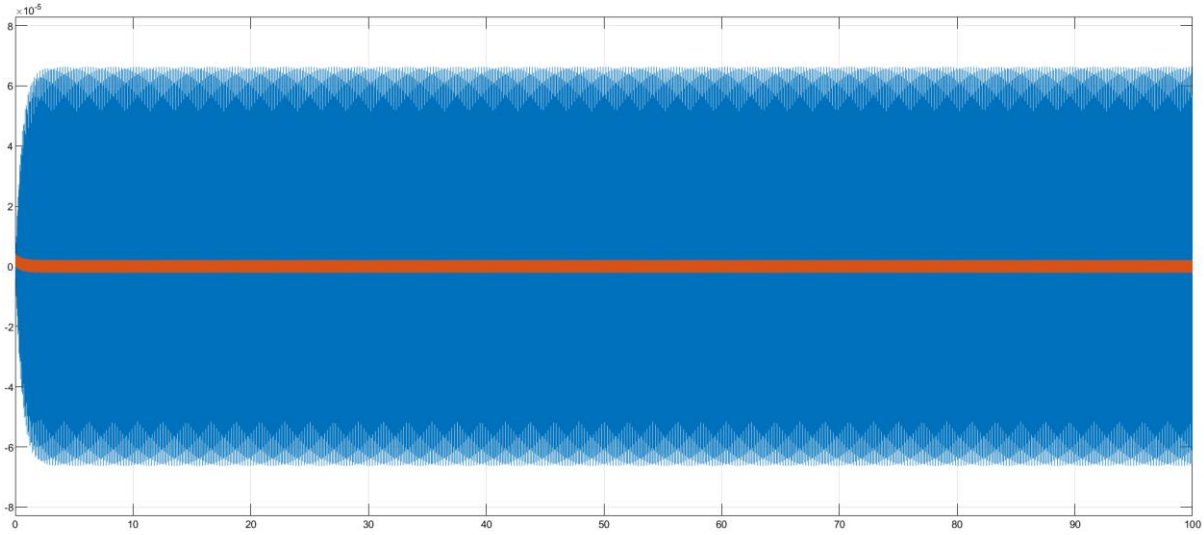

Figure 5-2 – IMPPF SISO System in Time Domain

(blue – uncompensated system, orange – compensated system)

Figure 5-2 shows the separated first mode controller compensation effects for the G_{11}. The first mode controller is separated by disconnecting the second and third mode controllers in Figure 5-1. The compensated system can decrease the amplitude of uncompensated G_{11} by about 30 times. The unit of the horizontal axis is second (s) and the unit of the vertical axis is meter/meter.

Because only less information can be provided from the time domain plots, for further exploring the IMPPF control influences, the bode plots are introduced to see each mode attenuations. The results of IMPPF control effects in SISO system can be displayed by four plots. The effectiveness of separated first, second and third mode controller for G_{11} is observed in Figure 5-3, 5-5 and 5-6 respectively, and then see the total three modes controllers' effectiveness for G_{11} in Figure 5-7.

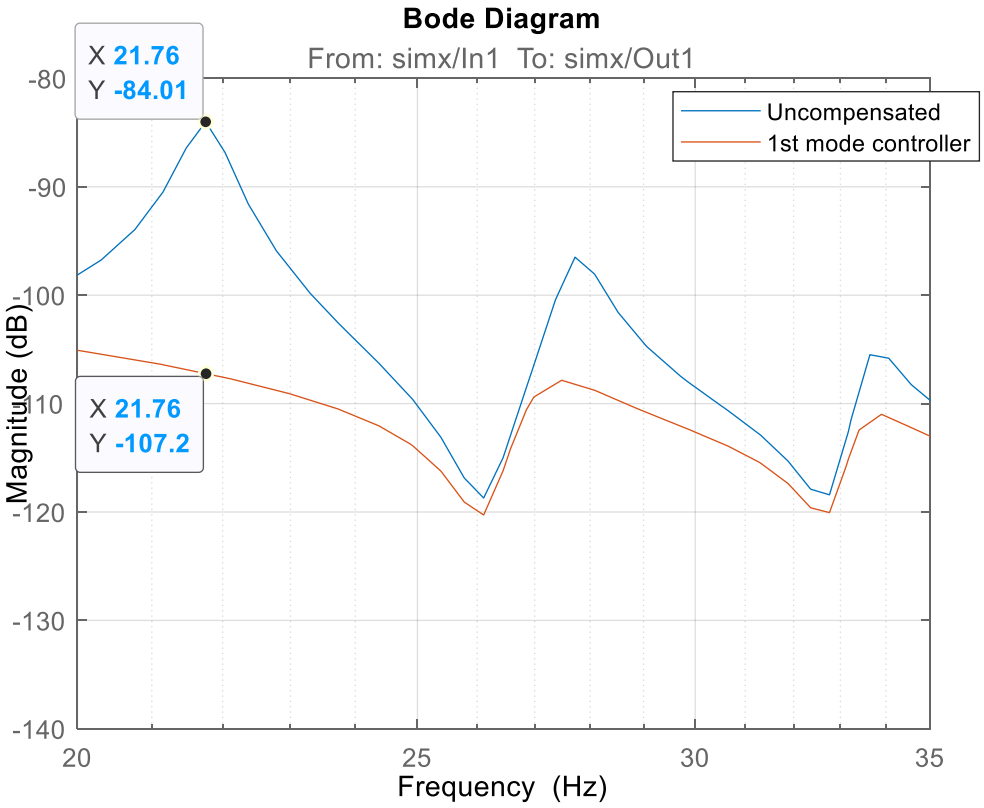

Figure 5-3 - Bode Plot for IMPPF First Mode Controller

From Figure 5-3, the first mode can be decayed up to 23dB. In addition, although the first mode controller is designed only to control the first mode, it also has good attenuation effects for second and third modes. The reason can be found from the Figure 5-4 which is presented the bode plots of a conventional IMPPF and PPF designed for same plant system. Both IMPPF and PPF are low-pass filters. However, the slope of IMPPF in stopband is about 20dB/dec, while slope of PPF is about 40dB/dec, so IMPPF has a more significant vibration reduction on high-frequency mode.

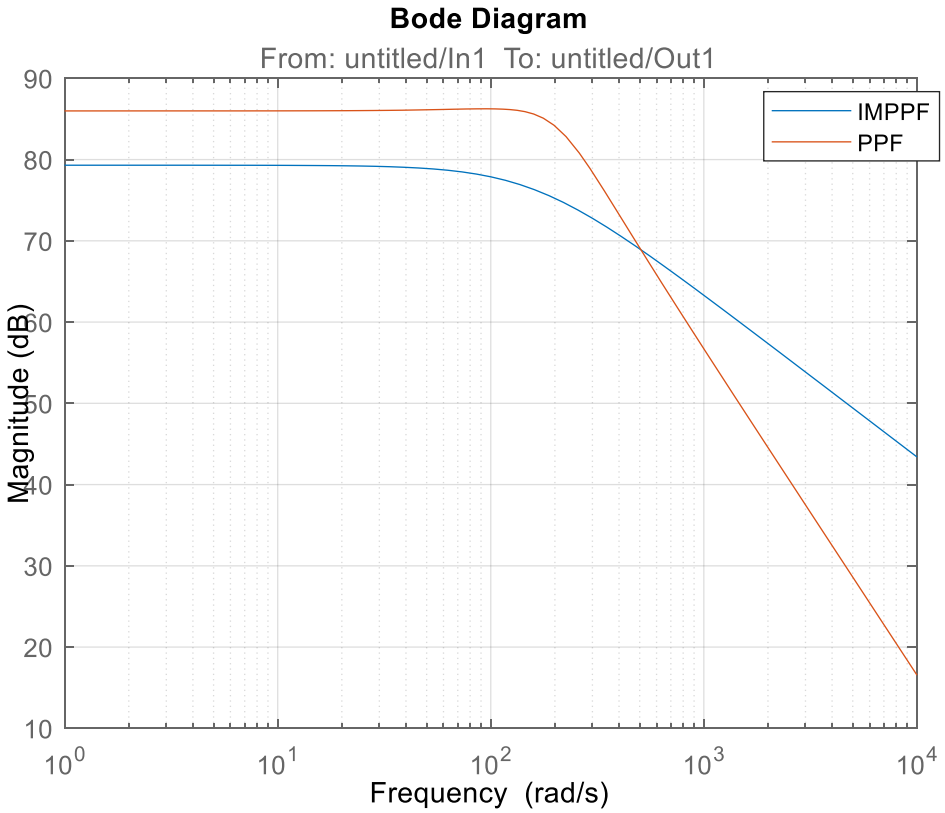

Figure 5-4 - Bode Plot for conventional IMPPF and PPF

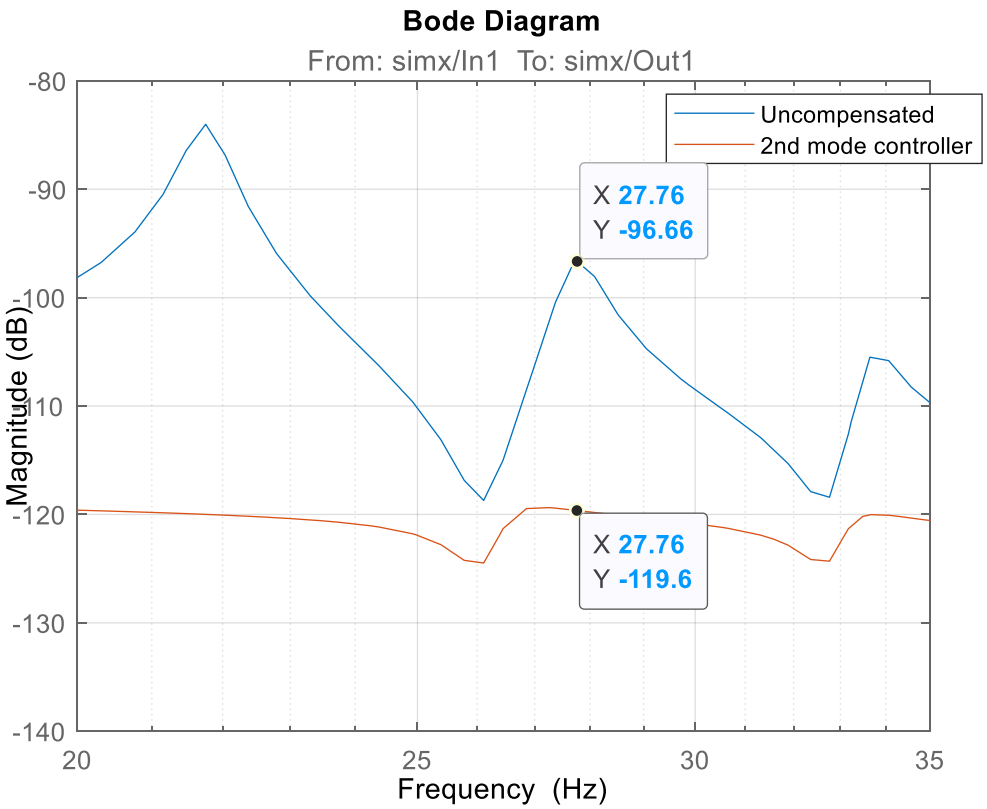

Figure 5-5 - Bode Plot for IMPPF Second Mode Controller

According to Figure 5-5, the second mode can be reduced by 23dB. The attenuation of the second mode is greater than Figure 5-3. However, the natural frequency of the first mode is less than the second mode, but the second mode controller also has good control performance for the first mode. The attenuation of the first mode controlled by second mode controller even is greater than first mode controller. This result is contrary to the common sense of low-pass filter. The reason for this phenomenon is that the second mode controller provides a lower gain than the first mode controller.

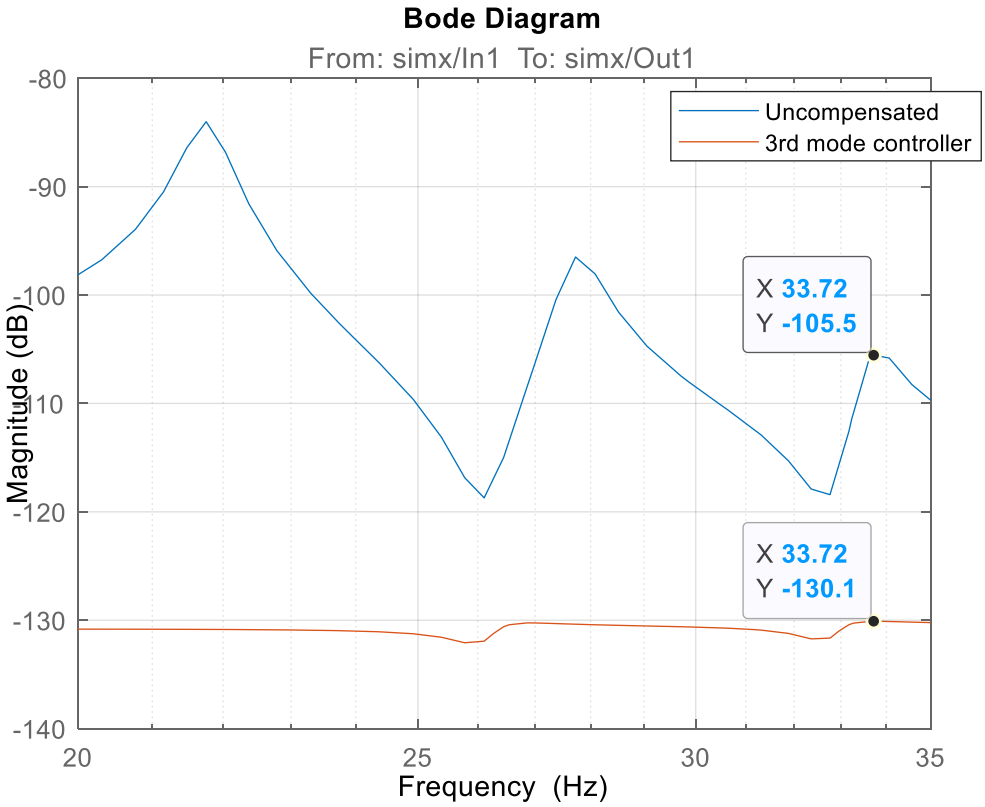

Figure 5-6 - Bode Plot for IMPPF Third Mode Controller

Based on Figure 5-6, the third mode can be shrunk by 25dB. The attenuation of the third mode is greater than 5-3 and 5-5. The third mode controller has better control performance on the first two modes. The attenuations of first two modes controlled by the third mode controller are greater than the previous two semi-controllers, because the third mode controller provides a lower gain than the former two separated controllers.

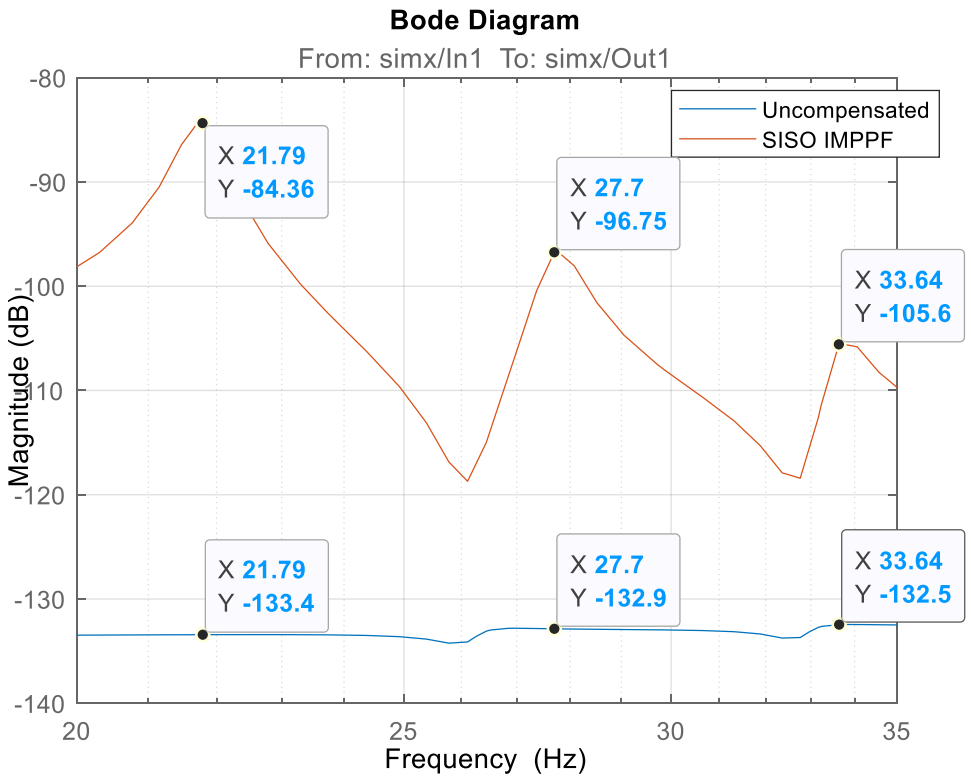

Figure 5-7 - Bode Plot for IMPPF Controller in SISO System

In Figure 5-7, the IMPPF controller has a significant effect on the control of the three modes. The first, second, and third modes are attenuated by 49dB, 36dB, and 27dB, respectively. The effect is better than three separated semi-controllers control systems. This plot fully demonstrates the effectiveness of IMPPF in the SISO system.

5.1.2 IMPPF for MIMO System

Since from SISO to MIMO system, the stability range of the parameters will be relativity narrowed. Substituting the data in Table 5-1 into the (4.26), it leads to the instability of the MIMO system. Thus, the control effect has to be sacrificed in order to achieve the stability of the close-loop system. It is assumed that the plate system is an undamped system to design the IMPPF controller, then the design process will be consistent with Section 4.1.2, where the parameter γ^k is fixed at 0.5. Substituting γ^k with 0.5 in (4.26), the result shows that the MIMO system is stable. As discussed in Section 4.1.4 for (4.26), the parameter τ^k is independent of MIMO system stability, therefore, the same method can be used to obtain the value of τ^k. The process is presented in Section 4.1.2. At this time, the time constant $\tau^k = \frac{1}{1.18\omega^k}$. The value is indicated in Table 5-2.

Table 5-2 - Parameters of IMPPF for MIMO Plate System

Mode No. k	γ^k	$\tau^k(\times 10^{-3})$
1	0.5	6.2366
2	0.5	4.8608
3	0.5	4.01314

According to the block diagram 4-9, the system can be constructed as Figure 5-8 in Simulink©.

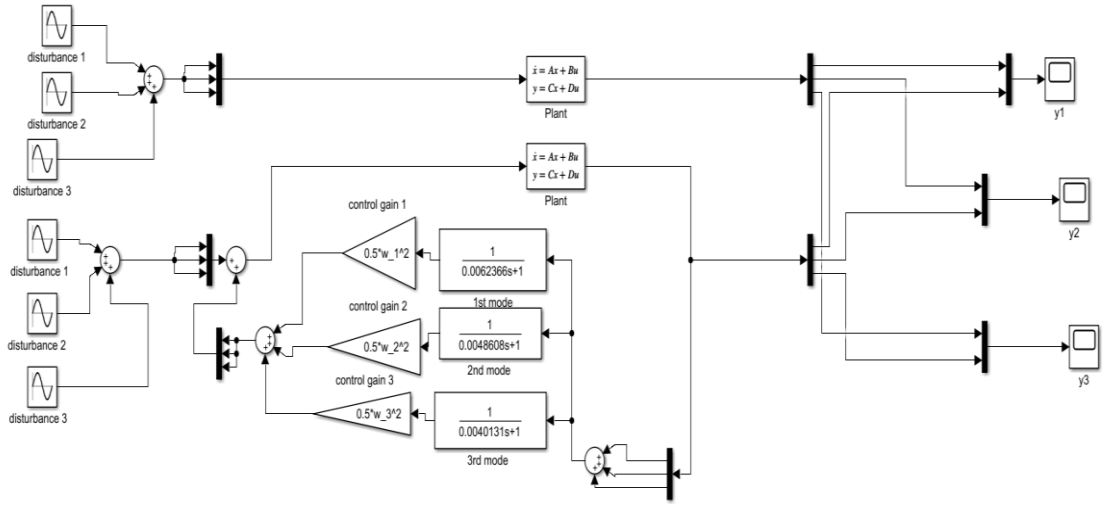

Figure 5-8 - IMPPF MIMO System Construction in Simulink©

In Figure 5-8, the plant system is presented by SSR. The construction of the SSR and the parameter values can be obtained by deriving (3.16) and Table 3-2, respectively. The IMPPF can be divided into 3 semi-controllers, which are designed for each mode. As mentioned above, the control gain for different modes is a fixed value of 0.5, while the time constant values are built according to the frequency of the different modes.

To observe the differences between the compensated system and uncompensated system, the 'Scope' block 'y1', 'y2' and 'y3' can display two systems in the time domain.

y1

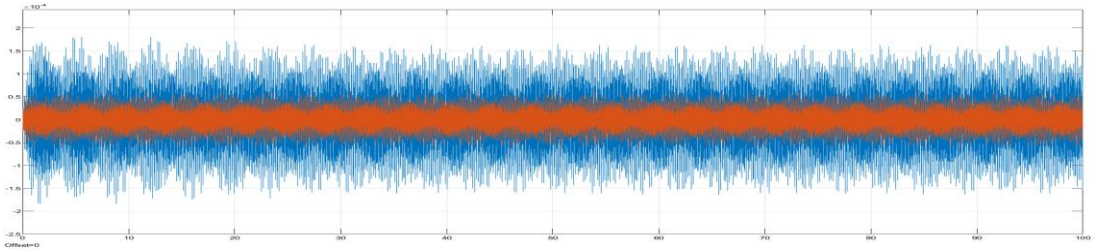

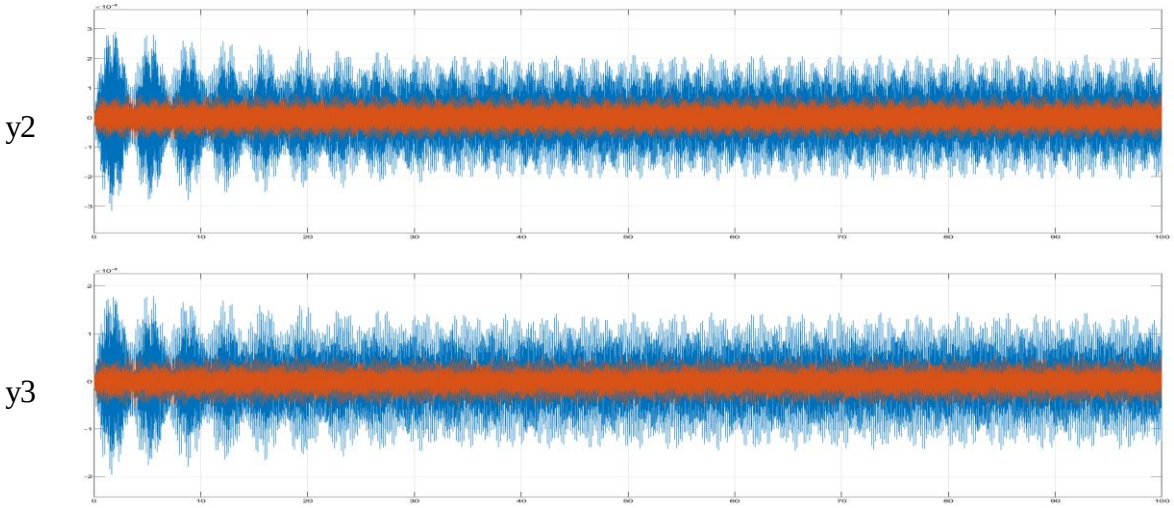

Figure 5-9 - IMPPF MIMO System in Time Domain

(blue – uncompensated system, orange – compensated system)

Figure 5-9 shows the IMPPF compensation effects for the MIMO plate system. The compensated system can shrink the amplitude of the uncompensated system by about 5 times for y1 and y3 and 6 times for y2. The result is not as good as the SISO system. The reason for the poor performance is that in the design process of the controller, to ensure the stability of the system, the system is roughly assumed to be an undamped system, but the generated controller actually controls a damped system.

The bode plots analysis for IMPPF is shown in Section 5.3 which also displays the comparison between IMPPF and MPPF control effects.

5.2 Simulation Study of MPPF

In this section, the MPPF control effects are demonstrated by discussing the results of the MPPF for a SISO system in time domain and bode plots, and for the plate MIMO system in time domain. The MIMO system bode plots analysis is demonstrated at Figure 5.19 at Section 5.3 in purple curve.

5.2.1 MPPF for SISO System

Based on the derived SISO stability (4.34), the sum of the two gains g^k and h^k of MPPF must be less than $\frac{\omega^{k^2}}{\varphi^k}$. In the SISO system exploration, both g^k and h^k are selected to be $\frac{0.25\omega^{k^2}}{\varphi^k}$. This value is chosen to make the value of the parameters close to the intermediate of the stability range and to make the system more stable. The values of both gains can be indicated in Table 5-3.

Table 5-3 - Parameters of MPPF for SISO Plate System

	Mode No. k	g^k $(\times 10^5)$	$h^k(\times 10^5)$
G_{11}	1	1.4179	1.4179
	2	5.9990	5.9990
	3	19.820	19.820
G_{22}	1	4.9900	4.9900
	2	7.3349	7.3349
	3	2.1560	2.1560
G_{33}	1	5.0185	5.0185
	2	10.845	10.845
	3	7.2751	7.2751

The G_{11} is an example of the plant system to show the control effects of the MPPF in SISO system. The system construction in Simulink© can be shown as Figure 5-10. The construction of G_{11} is explained in Section 5.1.1.

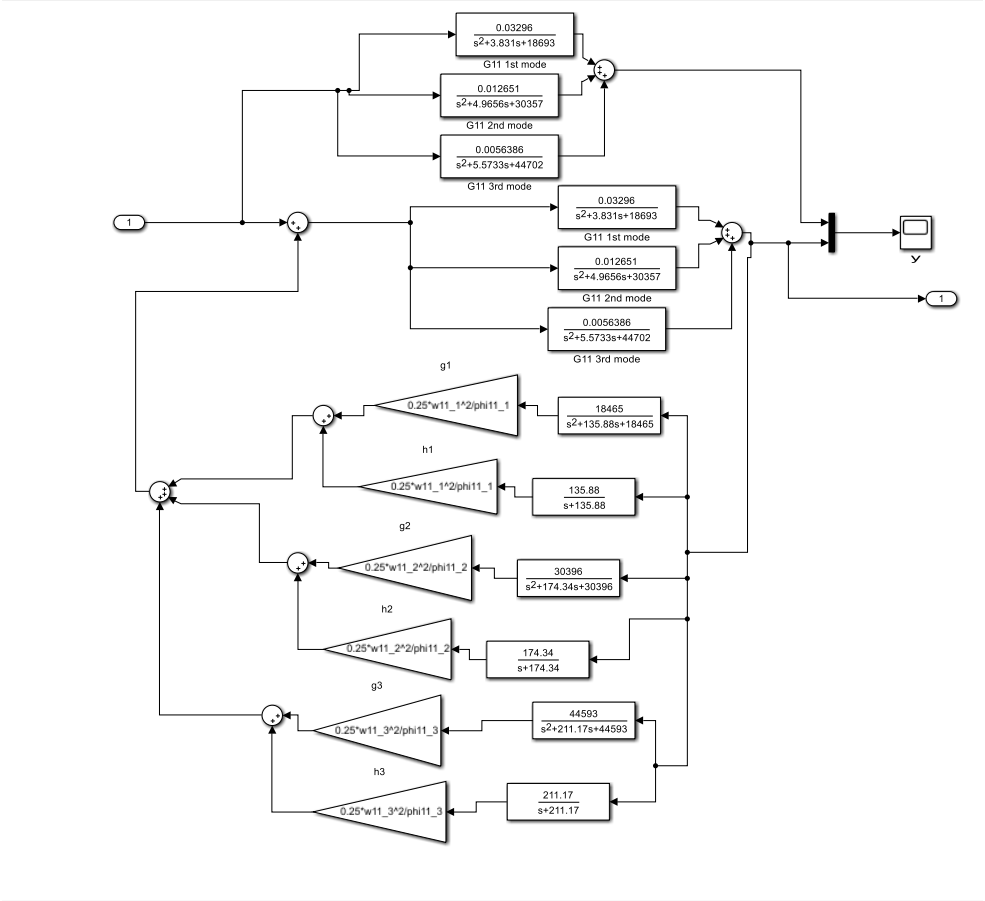

Figure 5-10 - MPPF SISO System Construction in Simulink©

In Figure 5-10, the whole MPPF controller also can be divided into 3 parallel semi-controllers, with each semi-controller consisting of 1 second-order filter (with 1 controller gain) and 1 first order filter (with 1 controller gain). Each semi-controller is used to control each mode separately. To clearly express purpose, the 3 parallel semi-controllers are called first mode controller, second mode controller and third mode controller. To observe the differences between the compensated system and uncompensated system, the 'Scope' block 'y' can display two systems in the time domain as Figure 5-11.

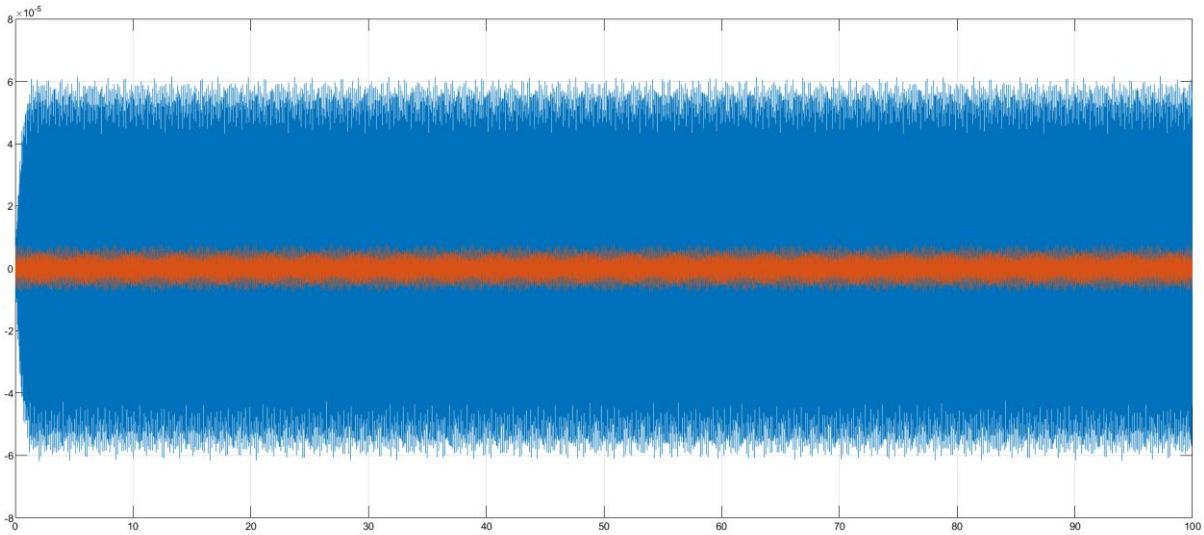

Figure 5-11 - MPPF SISO System in Time Domain

(blue – uncompensated system, orange – compensated system)

Figure 5-11 shows the control performance of the separated first mode controller for the G_{11}. The compensated system can reduce the amplitude of uncompensated G_{11} by about 30 times.

The effectiveness of separated first, second and third mode controller for G_{11} are shown in Figure 5-12, 5-14 and 5-15, respectively, and then the total three semi-controllers' performance for G_{11} is displayed in Figure 5-16.

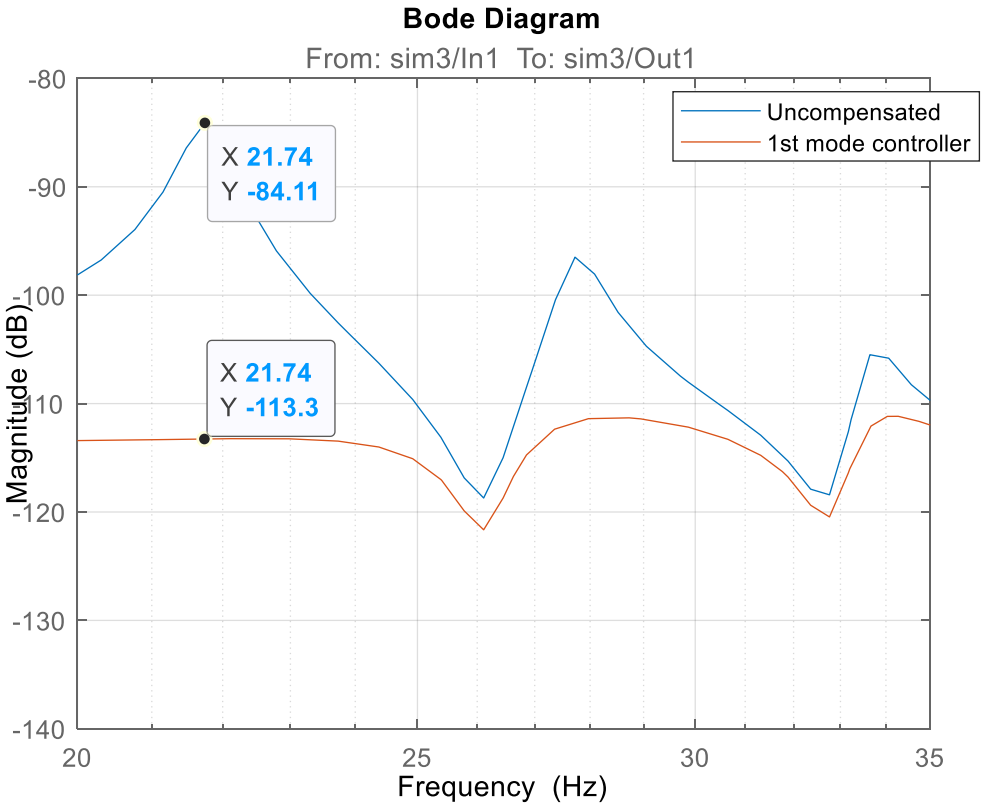

Figure 5-12 - Bode Plot for MPPF First Mode Controller

From Figure 5-12, the first mode can be decayed up to 29dB. That shows the performance of MPPF is better than the IMPPF. Besides, the MPPF first mode controller is the same as IMPPF, also can reduce the vibration of second and third modes. The reason is displayed in Figure 5-13 which is same as analysis for Figure 5-4.

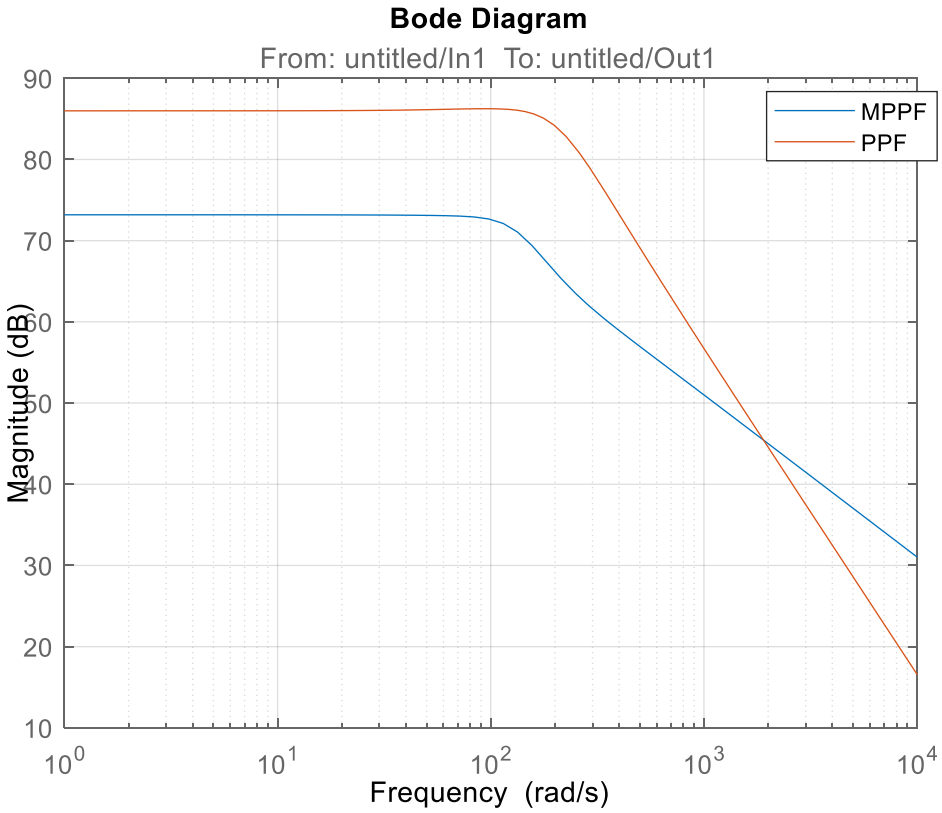

Figure 5-13 - Bode Plot for conventional MPPF and PPF

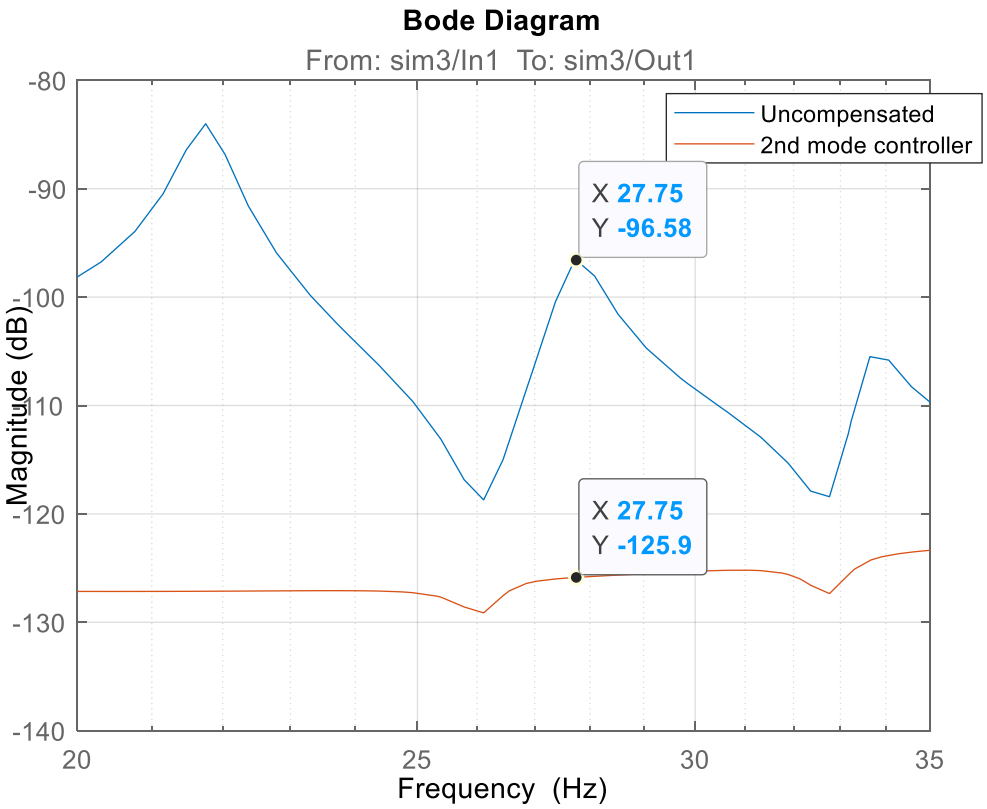

Figure 5-14 - Bode Plot for MPPF Second Mode Controller

According to Figure 5-14, the second mode can be shrunk by about 30dB. The attenuation of the second mode is greater than Figure 5-12 and also greater than the IMPPF attenuation effect in Figure 5-5. Similar to Figure 5-5, since the gain provided by the second mode controller is lower than that of the first mode controller, the semi-controller provides a better control effect on first mode than that of Figure 5-12.

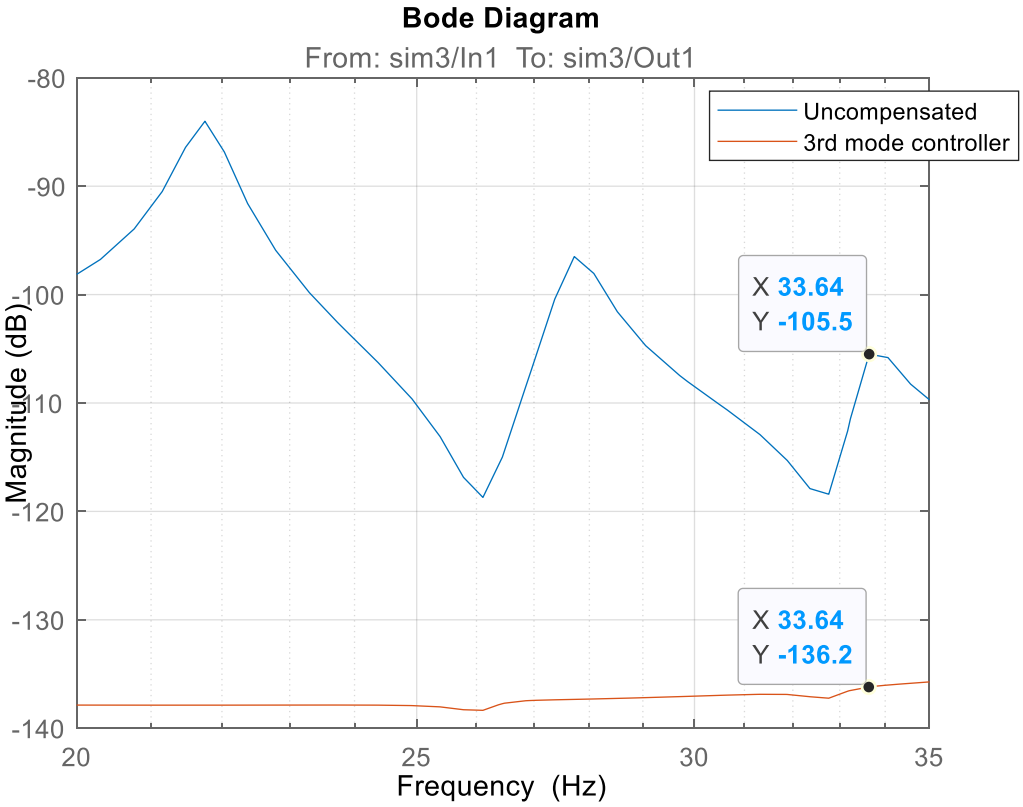

Figure 5-15 - Bode Plot for MPPF Third Mode Controller

Based on Figure 5-15, the third mode can be attenuate by 31dB. The attenuation effect of the third mode is greater than 5-12 and 5-14. The third mode controller has better control performance on the first two modes. The attenuations of the first two modes controlled by this semi-controller is greater than previous two semi-controllers. That because the third mode controller provides a lower gain than previous two semi-controllers.

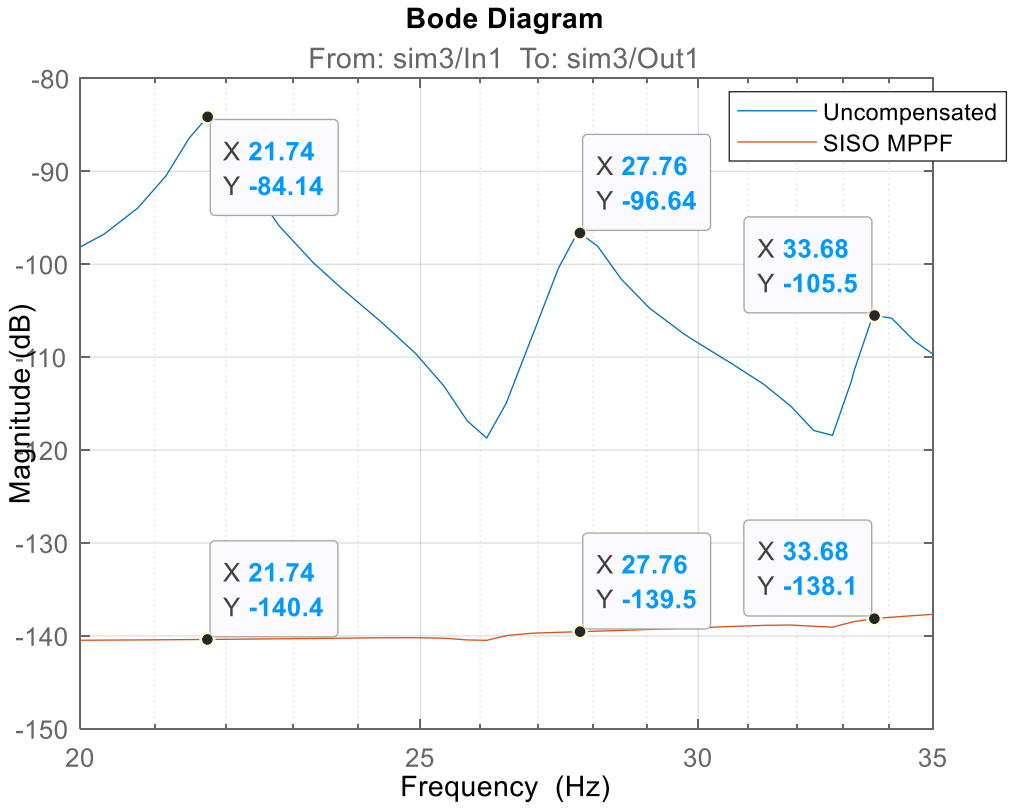

Figure 5-16 - Bode Plot for MPPF Controller in SISO System

In Figure 5-16, the MPPF controller has a significant effect on the control of the three modes. The first, second, and third modes are attenuated by 56dB, 43dB, and 33dB, respectively. The effect is better than three separated semi-controllers control systems and also better than the performance of IMPPF. Figure 5-16 fully demonstrates the effectiveness of MPPF in the SISO system.

5.2.2 MPPF for MIMO System

Since from SISO to MIMO system, the stability range of the gains will be narrowed. Substituting the g and h by $\frac{0.25\omega^{k^2}}{\varphi^k}$ into the (4.48), it leads to the instability of the MIMO system. Thus, the GA and H∞ are used to calculate the optimal values of both gains. The values are displayed in Table 5-4.

Table 5-4 - Parameters of MPPF for MIMO Plate System

Mode No. k	g^k	h^k
1	5476.8	5205.9
2	9061.2	1000
3	13284	13373

According to the block diagram 4-12, the system can be constructed as Figure 5-17 in Simulink©.

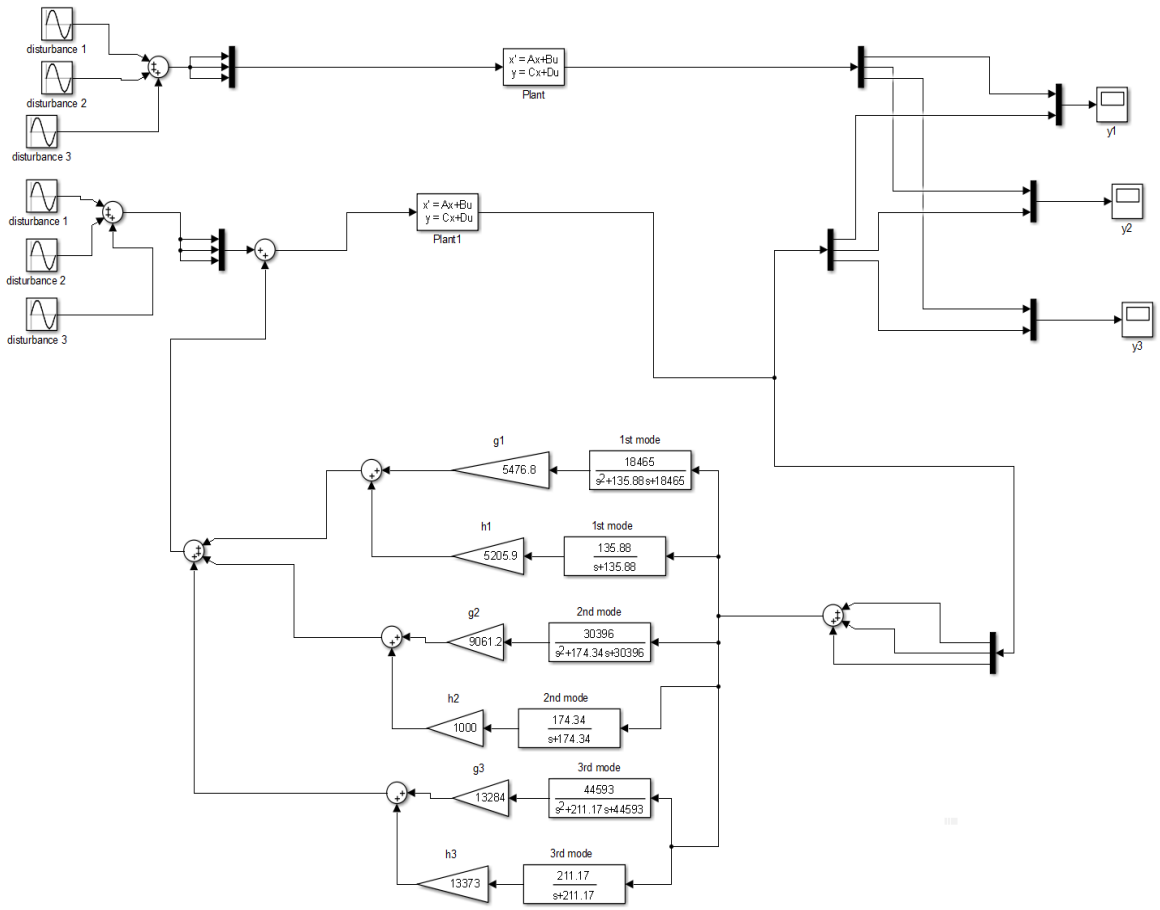

Figure 5-17 - MPPF MIMO System Construction in Simulink©

In Figure 5-17, the plant system is presented by SSR. The construction of the SSR and the parameter values can be obtained by deriving (3.16) and Table 3-2, respectively. The MPPF can be divided into 3 semi-controllers, which are designed for each mode.

To observe the differences between the compensated system and uncompensated system, the 'Scope' block y1, y2 and y3 can display two systems in the time domain.

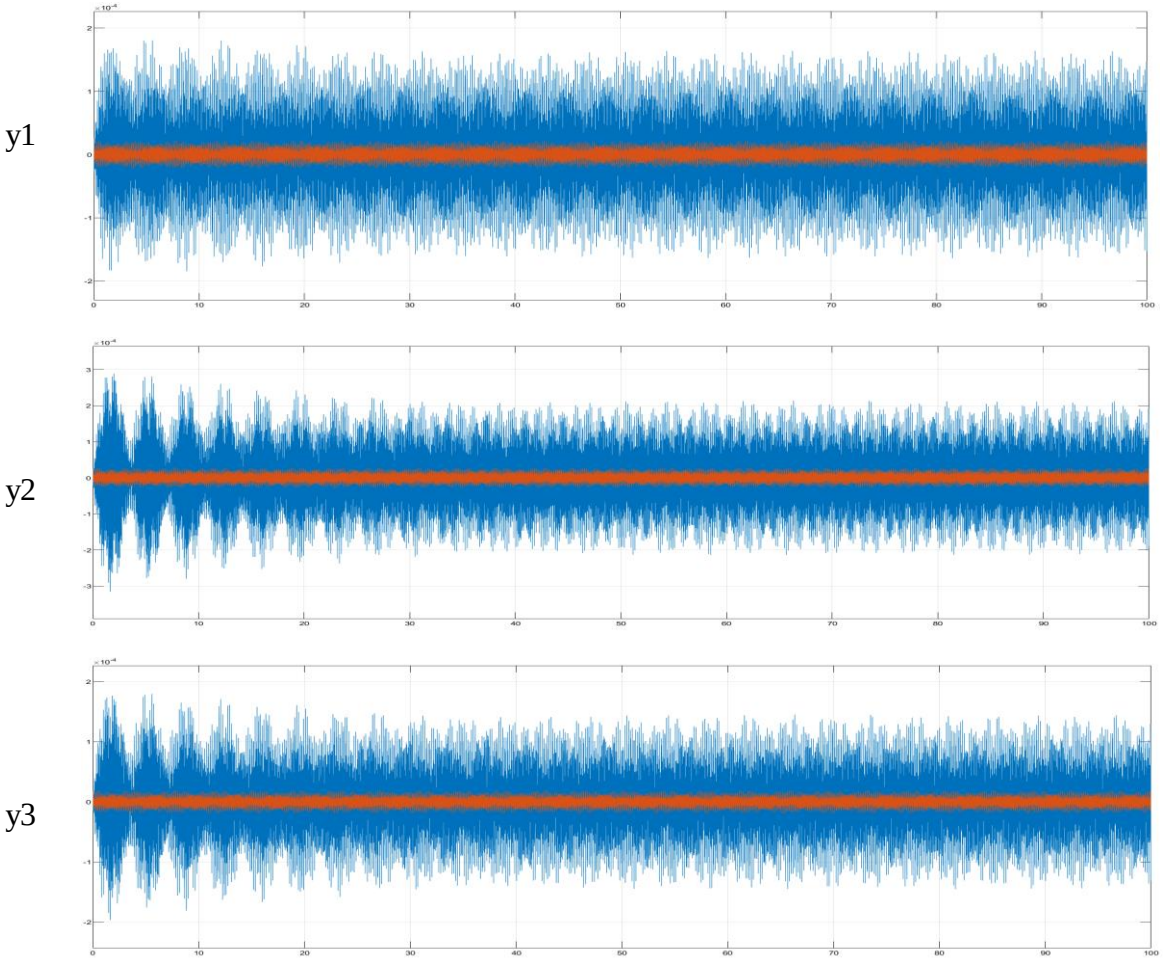

Figure 5-18 - IMPPF MIMO System in Time Domain

(blue – uncompensated system, orange – compensated system)

Figure 5-18 shows the MPPF compensation effects for the MIMO plate system. The compensated system can reduce the amplitude of the uncompensated system by about 8 times for y1 and y3 and 15 times for y2. The result is not good as the SISO system. The reason for the poor performance is that the GA method uses the random values to check whether the H∞ can meet the condition, once the condition is met, it will stop and assign the values to gains. For online design considering, GA can reduce the calculation time, but it cannot give accurate optimized values. However, the performance is better than IMPPF control effect in Figure 5-9.

The bode plots analysis for MPPF is also shown in Section 5.3.

5.3 PPF, IMPPF and MPPF Simulation Results Comparison

By analyzing the IMPPP and MPPF in the MIMO plate system in the time domain, it can be found that the MPPF has better control effect on the vibration than the IMPPP. To verify

whether the RTACS hypothesis is feasible in the MIMO plate system, the comparison of the control performance among the IMPPF, MPPF and the conventional PPF is needed. The control performance of PPF, IMPPF and MPPF are shown in red, yellow and purple curve respectively in Figure 5-19 for three outputs when applying same disturbance to the system. The parameters of IMPPF are shown in Table 5-2 and MPPF's gains are indicated in Table 5-4.

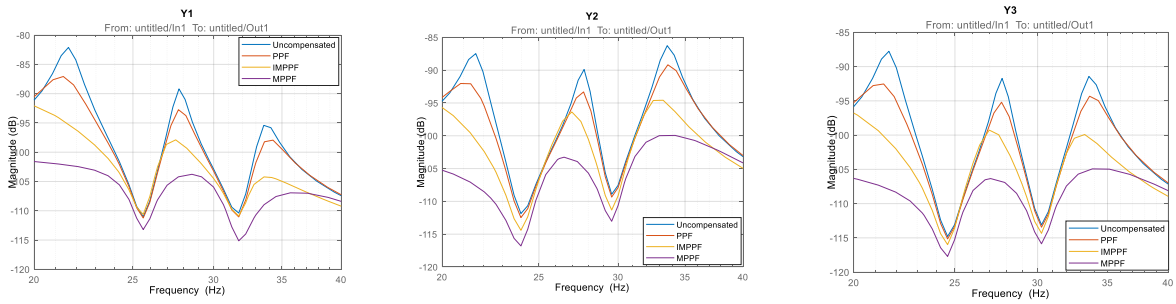

Figure 5-19 - Bode Plots Comparison

It is noted in Figure 5-19 that all three controllers have good control performance over the plate system. Both MPPF and IMPPF are better than traditional PPF control, and MPPF has better control effects. The control performance in numerical values is shown in Table 5-5.

Table 5-5 - Vibration Control Effects Comparison

(dB)	Y1			Y2			Y3		
Mode No.	PPF	IMPPF	MPPF	PPF	IMPPF	MPPF	PPF	IMPPF	MPPF
1	5	12	18	6	13	20	4	13	19
2	4	10	16	3	9	13	3	8	14
3	3	9	14	3	10	14	2	9	13

Table 5-5 shows the attenuation effects of the three controllers. PPF, IMPPP and MPPF can reduce the vibration up to 6dB, 13dB and 20dB, respectively.

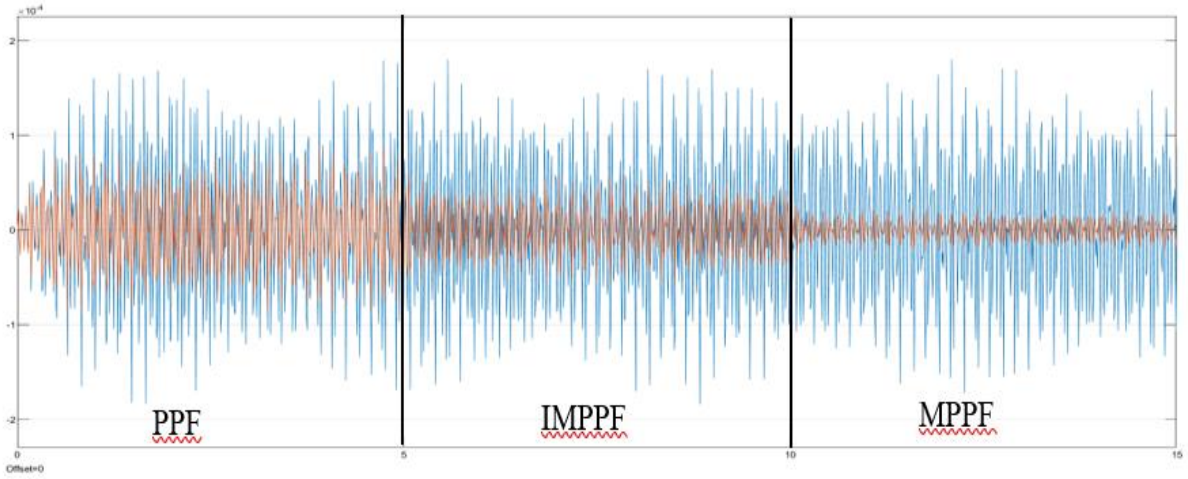

Figure 5-20 - Time Domain Comparison

(blue – uncompensated system, orange – compensated system)

Figure 5-20 compares the performance of three controllers in the time domain. The system is initially controlled by the PPF, converted to IMPPP at 5 s, and switched to MPPF at 10 s. The results agree with frequency domain analysis.

Therefore, according to the results, as proposed by Section 4.3, ARTCS can abandon PPF and only include MPPF and IMPPP.

To further explore whether the ARTCS assumption is correct, it also needs to compare the control effects of IMPPF and MPPF before and after the system changes. Because, if the control effect of MPPF with the previous parameter is better than the IMPPF with updated the parameter, then the entire ARTCS can be controlled only by MPPF, although it updates the parameter slowly, the effect is the best.

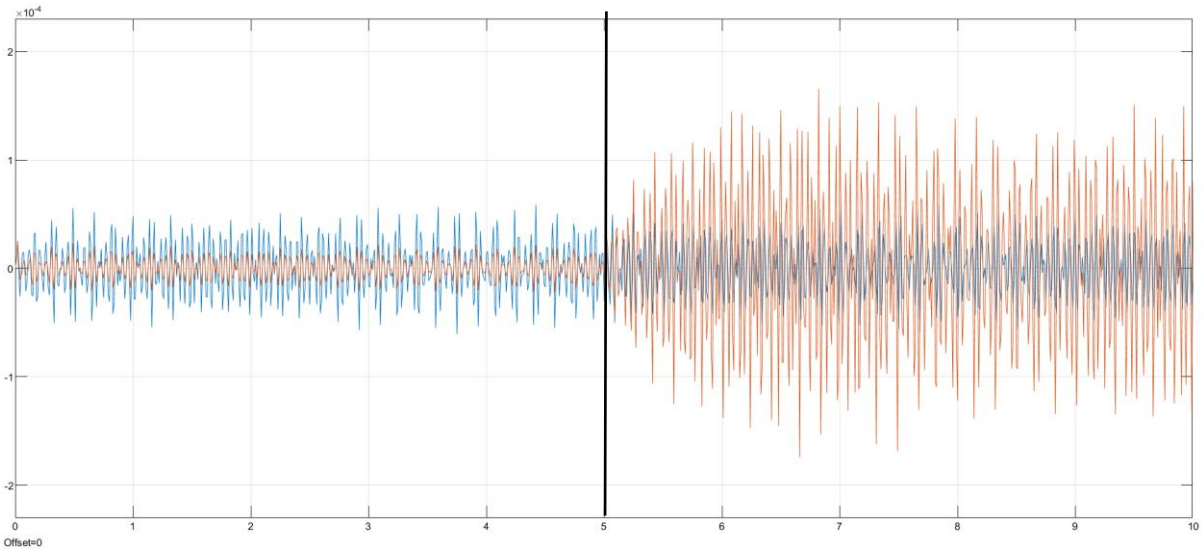

Figure 5-21 - IMPPF vs MPPF at System Change

(blue – IMPPF, orange – MPPF)

As shown in Figure 5-21, before the system changes at 5s, IMPPF performance is worse than MPPF, but after the system changes, IMPPP can quickly update parameters, thus maintaining a relatively good control effect. At the same time, although MPPF can use the previous parameters to control the plate system, the control effect is significantly worse than IMPPP.

Therefore, the RTACS can be implemented on the plate system. This scheme combines the advantages that IMPPF can quickly update parameters online and MPPF can provide sufficient damping effect so that it can respond quickly to dynamic systems and maintain relatively good attenuations.

5.4 Simulation of RTACS

According to block diagram 4-13 proposed in Section 4.3, Figure 5-22 can be constructed in Simulink© to simulate implement RTACS in MIMO plate system. The FFT Estimator, the parameter calculation process of MPPF and IMPPF, and the assignment of new parameters will be implemented by a main programming file in MATLAB. The file also simultaneously controls the start and stop of this Simulink©. The switch in Figure 5-22 is implemented by a MATLAB function that controls which controller should be applied at a time.

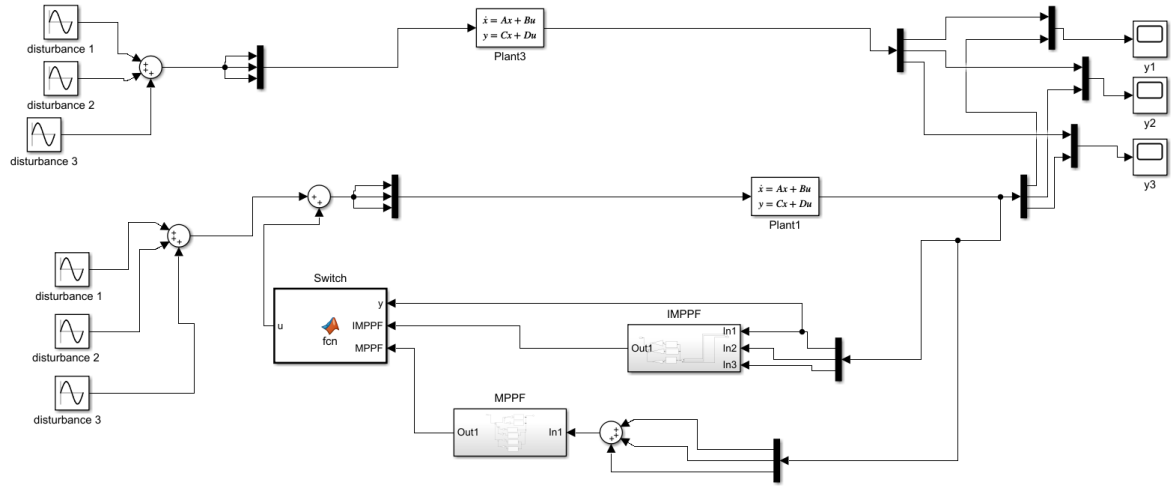

Figure 5-22 – RTACS Construction in Simulink©

The results of the simulation system in the time domain are shown in Figure 5-23. In the initial state, the system is controlled by MPPF. The plant system changes are introduced at t_1, the IMPPF that quickly updates the parameters replaces the MPPF control plate system immediately, then when the MPPF parameters are ready at t_2, it is transferred to the MPPF control system. The scheme can reduce the amplitude of the original vibration of the system by at least 50%.

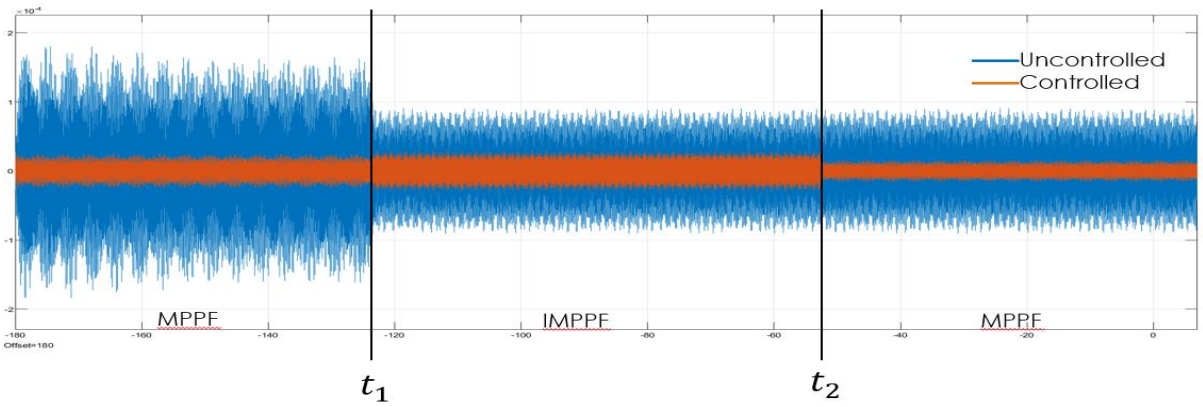

Figure 5-23 – RTACS in Time Domain

Chapter 6: Experiment Result

This chapter uses dSPACE to transmit the constructed compensator in Chapter 5 to the actual physical plate system to control its vibration, and observe the effect of the controller through ModalVIEW.

6.1 Laboratory System

The experiment system setup and block diagram are shown in Figure 6-1 and 6-2, respectively. The signal generator generates a 150mV sinusoidal sweep signal (10Hz ~ 60Hz, 10s per period) to T4. This signal acts as a disturbance to vibrate the initially stationary top plate. Then the noise signal is transmitted to the sensors T1, T2, and T3 through the base plate as input signals u_j (j = 1, 2, 3). In the same position of the three sensors, there are three accelerometers for measuring the three output signals y_i (i = 1, 2, 3). These three output signals are recorded by the NI DAQ and sent to dSPACE, which processes the signals and return the controlled signal to the three actuators located at T1, T2 and T3 to cancel or reduce the vibration of the top plate. The system changes are represented by the top plate load objects.

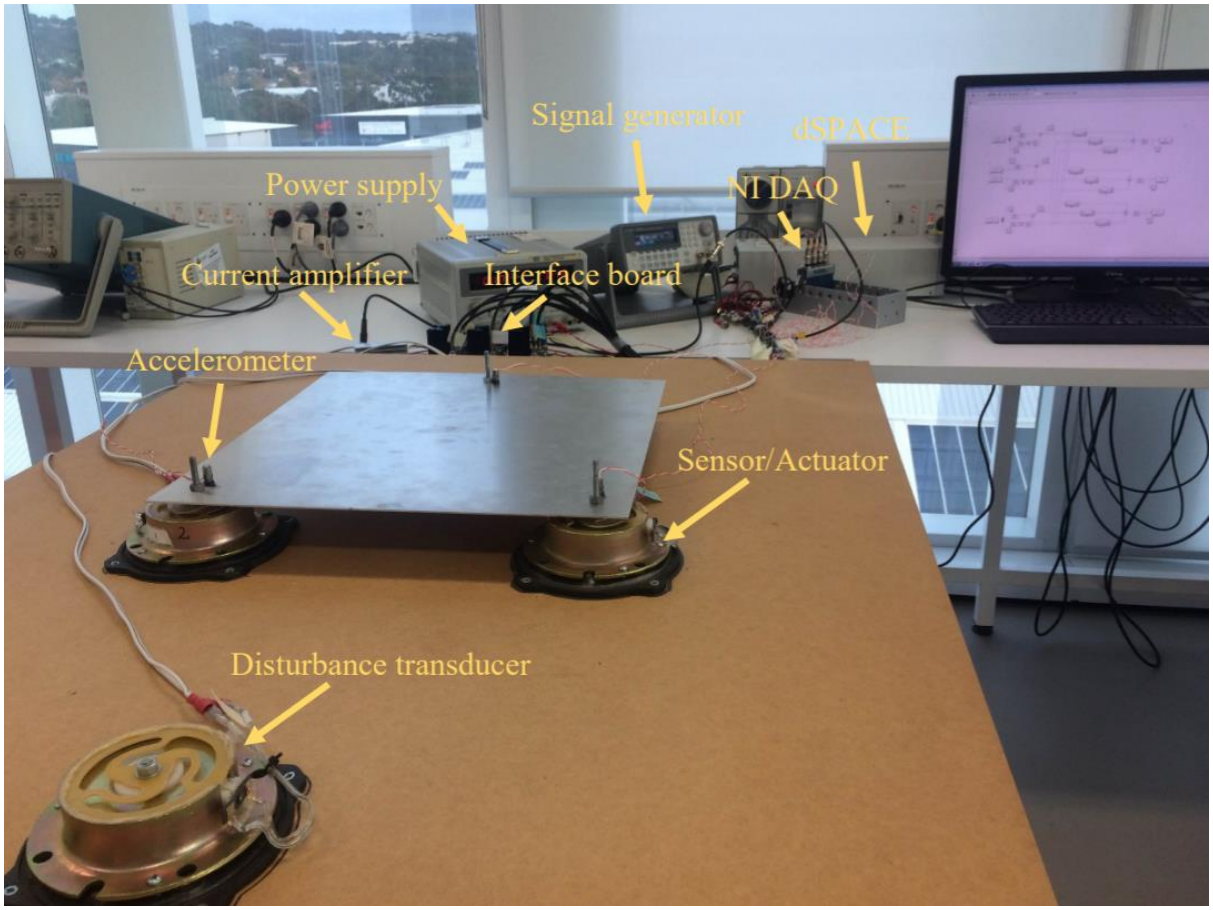

Figure 6-1 - Experiment System Setup

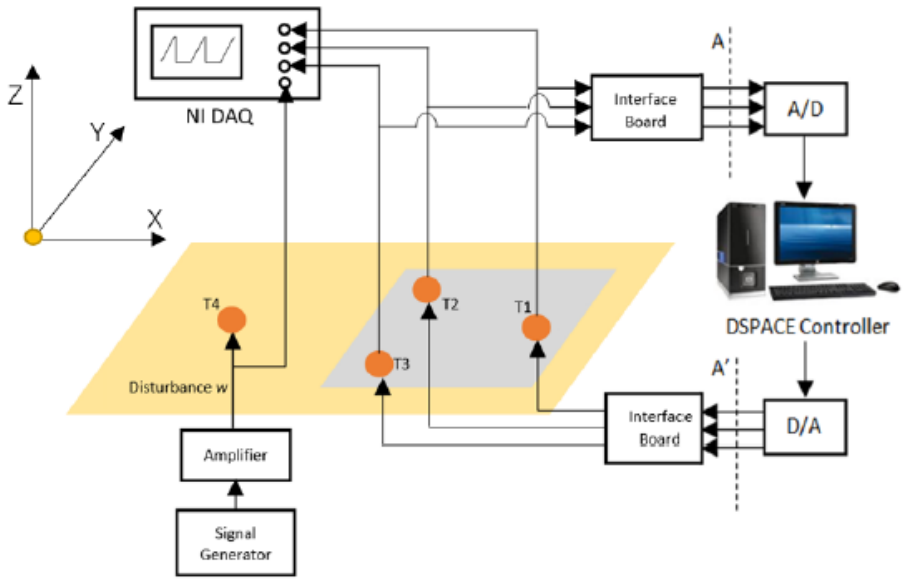

Figure 6-2 - Block Diagram of Experiment System

6.2 PPF, IMPPF and MPPF Experiment Results Comparison

To verify whether the IMPPF and MPPF designed according to a simplified plant model can be effective in the real model, this section experiment is implemented with an unloaded top plate. The unload top plate is regarded as a static system. Figure 6-3 indicates the bode plots of three outputs. The vertical axis is presented the amplitude corresponding to the displacement.

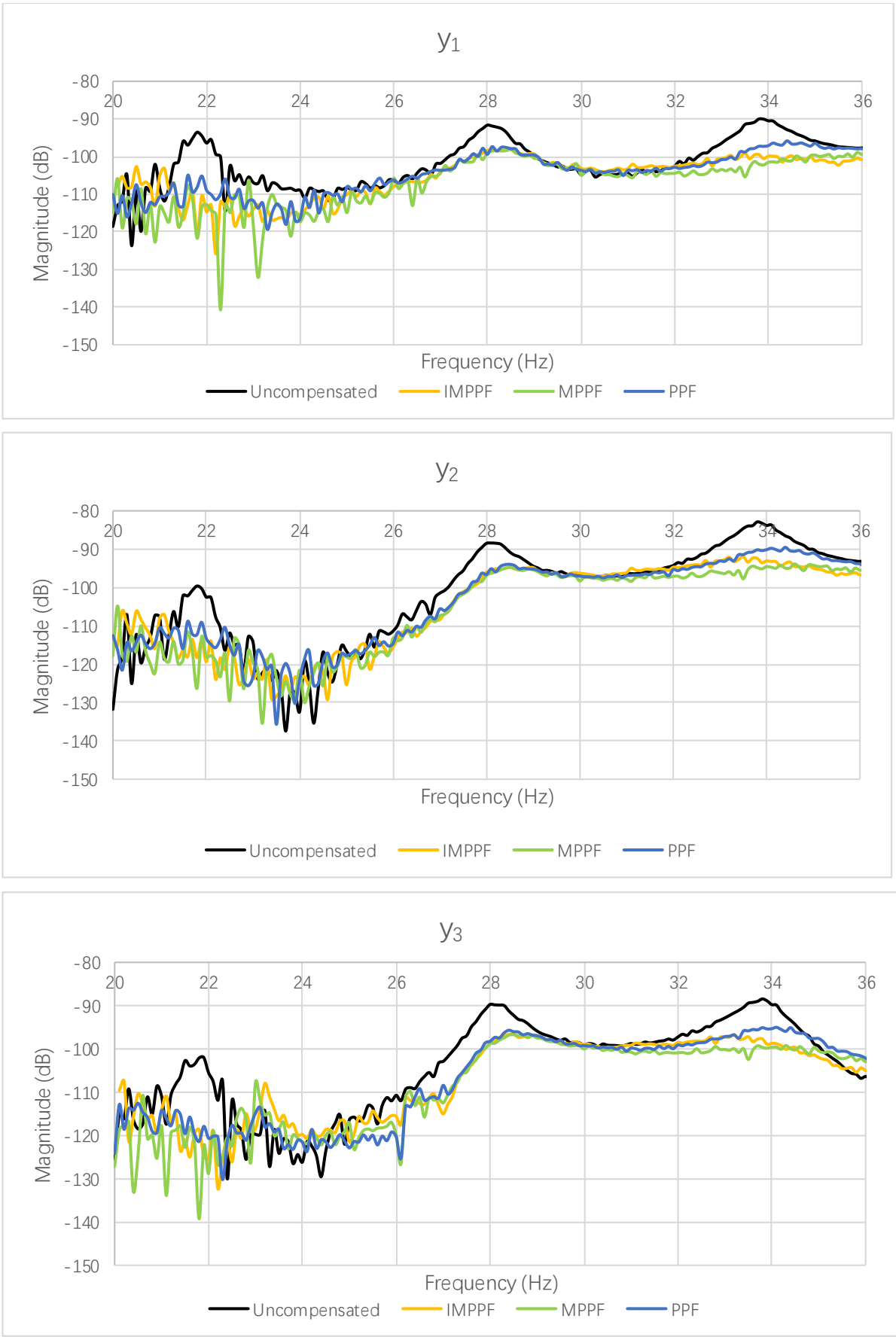

Figure 6-3 - IMPPF, MPPF and PPF Control Effect in Real Model Comparison

According to Figure 6-3, the result can be listed as Table 6-1.

Table 6-1 - Laboratory Vibration Control Effects Comparison

(dB)	Y1			Y2			Y3		
Mode No.	PPF	IMPPF	MPPF	PPF	IMPPF	MPPF	PPF	IMPPF	MPPF
1	12	17	20	9	14	14	13	16	16
2	7	8	8	9	9	9	11	10	10
3	7	10	12	7	10	14	7	9	10

The result shows that the PPF can suppress the vibration from 6dB to 13dB. This achieved attenuation is relatively less than the attenuation of 20dB achieved by Zhang and He [1]. This is because the D term is ignored in this study when the PPF controller is constructed via SSR. The MPPF can reduce the vibration from 7dB to 20dB. Although an attenuation of 37dB is achieved in Nima Mahmoodi et al.'s experiment [17], their cantilever beam system is only a SISO system. The plate structure, however, in the thesis is a MIMO system where the omitted D term includes cross-couplings between all inputs. This may affect the attenuation result.

The difference in control effects of the three compensators is only 0dB ~ 8dB. The result does not coincide with the result of simulation. That may be because of three reasons:

1. In simulation, the D term of SSR is ignored when the simplified plant system model was built. The D term refers to the higher frequencies' effects. Different controllers may have different sensitivities to the effects.
2. The input signal has to enlarge by 10 times to excite the normal performance of the controller in the whole experimental process, the signal is amplified and then shrunk after passing through the controller. Therefore, uncontrollable factors are added to the system, and some unwanted noises will be introduced to deviate the experimental results.
3. The three modes of the plate system are not well apart from each other, so the mode may affect each other in the experiment. The influence may deviate the result.

However, it can still be seen that MPPF can provide the best control effect, and IMPPF and MPPF are better than PPF. The control performance of IMPPF and MPPF can reach up to 17dB and 20dB, respectively. Therefore, RTACS can still be applied to the real plate system, but the

result of switching between controllers is not obvious. However, for some systems that require high precision, controllers switching is still necessary.

6.3 Experiment of RTACS

The results of the real plate system in the time domain are shown in Figure 6-4. However, it does not allow MATLAB to be directly assigned new parameter to dSPACE, so the time before and after the change is divided into two experiments. For the clear expression of the result, the two experiments are integrated into one figure.

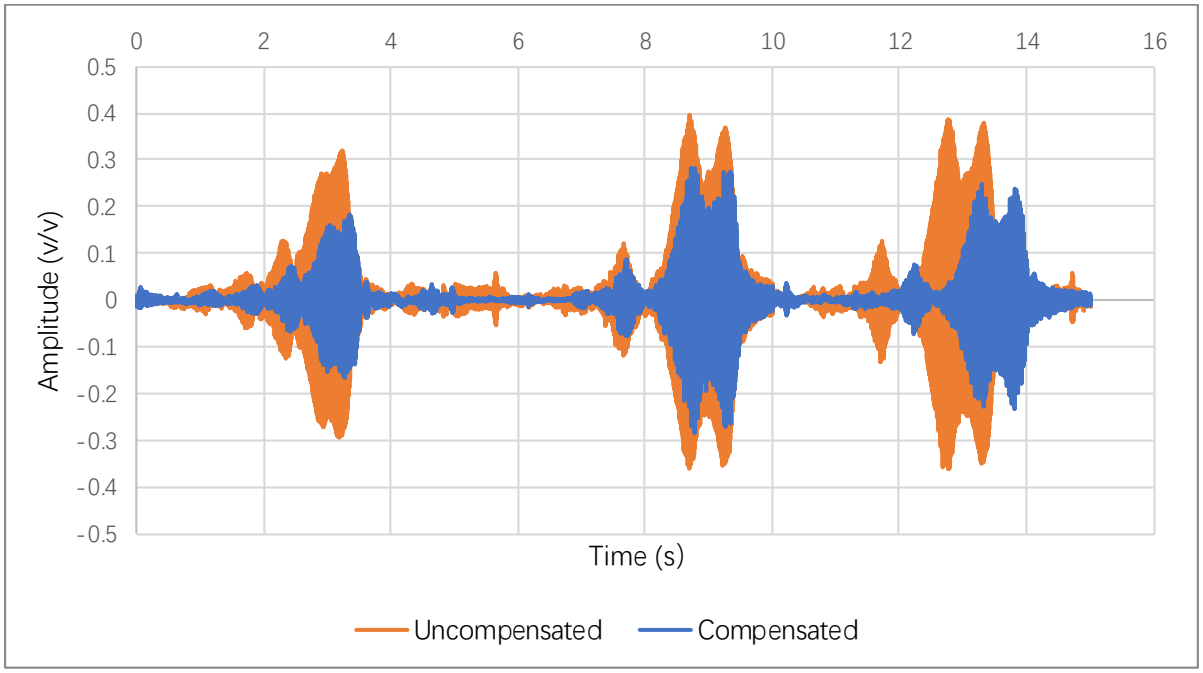

Figure 6-4 - RTACS Performance in Time Domain

In the initial state, the system is controlled by MPPF. The plant system is loaded a 700g object at 5s, the IMPPF that quickly updates the parameters replaces the MPPF control plate system immediately, then when the MPPF parameters are ready at 10s, the switch turns back to the MPPF system.

The unit of the horizontal axis is second (s) and the unit of the vertical axis is volt/volt. The voltage corresponds to the acceleration. It is not converted to displacement because the frequency is required to displacement conversion formula, and the frequency value at each time cannot be obtained in the time domain.

Figure 6-4 displays the RTACS can effectively reduce the vibration about 30%~50% and the result agrees to the simulation results in Section 5.4.

Chapter 7: Conclusion

7.1 Project Conclusion

In this thesis, a simplified transfer function representation of the MIMO plate system is built via taking the first three most significant modes. Then, based on the transfer function representation, a State-Space Representation and a Second-order Differential Model are derived. Both representations are built on a matrix basis. This makes this method easy to extend into any system with more outputs, inputs and more modes.

The IMPPF and MPPF control algorithms are proposed in theoretical analysis. For IMPPF, it consists of a first-order filter and a control gain. The control gain can be obtained by eliminating the steady-state error of the closed-loop system. The time constant τ^k of the first-order filter can be solved through the analysis of root locus: the optimization formula of τ^k can be obtained when the damping ratio of compensated closed-loop system reaches its maximum value (Figure 4-4). Although the process is complicated, all the work can be done offline. Only the final formula for τ^k in (4.9) for the time constant is applied to the online controller. Therefore, it can response the dynamic system quickly. However, in order to stabilize the system, IMPPF design in the MIMO system has to assume that the MIMO system is undamped, that results in worse damping effect. In MPPF, since it consists of a conventional PPF and a first-order filter, it not only maintains the PPF control effect, but also reduces the steady-state error, thus it can provide a relatively good control effect. The two gains can be optimized by the GA and H∞ norm methods, which result in longer parameter acquisition times.

The theories of two controllers are verified by simulation in MATLAB Simulink©. The vibration attenuation effects of the IMPPF and MPPF can reach up to 13dB and 20dB, respectively. Both perform better than 6dB provided by PPF. According to these results, and the control effect analysis of IMPPF and MPPF after system changing, this thesis makes a reasonable RTACS design. The effectiveness of the RTACS is verified by MATLAB Simulink©, the results shows that the vibration is reduced by at least 50%.

Finally, IMPPF and MPPF, which are designed according to the simplified system, are applied to the actual system. IMPPP and MPPF still have good control effects, and the attenuation effects can reach up to 16dB and 18dB, respectively. These effects are still better than PPF.

Based on the success of the previous experiments, the RTACS is also implemented in a real system, and the damping effect of RTACS can at least reach up to 30%.

It is concluded that the RTACS is effective in vibration cancellation of the MIMO plate system.

7.2 Recommendations

The control effect difference between IMPPF and MPPF in Chapter 6 is small. Therefore, it is recommended to use IMPPF as the controller in general devices, which can quickly detect and respond to changes in the system. However, for instruments that are sensitive to vibration and require high accuracy, it is recommended to use the RTACS to control the whole system.

Due to time and equipment limitations, current RTACS cannot simultaneously calculate MPPF parameters while monitoring whether the system changes again. If there are two CPUs, running monitoring and calculation parameters separately, this problem may be solved in future work.

Appendix A: MATLAB Code

The MATLAB codes for each section are kept within the Advanced Control Research Group, Flinders University. The MATLAB codes can be provided upon request.

Bibliography

[1] Zhang, P & He, F 2017, 'Experimental Implementation of Multiple-input Multiple-output Active Vibration Control on Vibration Isolation Systems', in *24th International Congress on Sound and Vibration*.

[2] Chen, G, 2018, 'Online Optimization of Adaptive Vibration Control System of Dynamically Loaded Flexible Structures', Master thesis, Flinders University, Adelaide, Australia.

[3] Cus, F & Balic, J 2003, 'Optimization of cutting process by GA approach', *Robotics and Computer-Integrated Manufacturing*, vol. 19, no. 1-2, pp. 113-21.

[4] Gan, Z, Hillis, AJ & Darling, J 2015, 'Adaptive control of an active seat for occupant vibration reduction', *journal of sound and vibration*, vol. 349, pp. 39-55.

[5] Fang, Y, Fei, J & Hu, T 2018, 'Adaptive backstepping fuzzy sliding mode vibration control of flexible structure', *Journal of Low Frequency Noise, Vibration and Active Control*, vol. 37, no. 4, pp. 1079-96.

[6] Zhao, X, Shi, P & Zheng, X 2015, 'Fuzzy adaptive control design and discretization for a class of nonlinear uncertain systems', *IEEE transactions on cybernetics*, vol. 46, no. 6, pp. 1476-83.

[7] Li, Y, Tong, S & Li, T 2015, 'Hybrid fuzzy adaptive output feedback control design for uncertain MIMO nonlinear systems with time-varying delays and input saturation', *IEEE Transactions on Fuzzy Systems*, vol. 24, no. 4, pp. 841-53.

[8] Yin, S, Shi, P & Yang, H 2015, 'Adaptive fuzzy control of strict-feedback nonlinear time-delay systems with unmodeled dynamics', *IEEE transactions on cybernetics*, vol. 46, no. 8, pp. 1926-38.

[9] Meirovitch, L. *Dynamics and Control of Structures*. Wiley, New York, 1990.

[10] Rew, K-H, Han, J-H & Lee, I 2002, 'Multi-modal vibration control using adaptive positive position feedback', *Journal of intelligent material systems and structures*, vol. 13, no. 1, pp. 13-22.

[11] Omidi, E & Mahmoodi, SN 2015, 'Consensus positive position feedback control for vibration attenuation of smart structures', *Smart Materials and Structures*, vol. 24, no. 4, p. 045016.

[12] Niu, W, Li, B, Xin, T & Wang, W 2018, 'Vibration active control of structure with parameter perturbation using fractional order positive position feedback controller', *journal of sound and vibration*, vol. 430, pp. 101-14.

[13] Ferrari, G & Amabili, M 2015, 'Active vibration control of a sandwich plate by non-collocated positive position feedback', *journal of sound and vibration*, vol. 342, pp. 44-56.

[14] Hong, C, Shin, C & Jeong, W 2010, 'Active vibration control of clamped beams using PPF controllers with piezoceramic actuators', *Proc. 20th Int. Congr. on Acoustics (Sydney, Australia, ICA 2010 23–27 August 2010)*.

[15] Yuan, M, Qiu, J, Ji, H, Zhou, W & Ohayon, R 2015, 'Active control of sound transmission using a hybrid/blind decentralized control approach', *Journal of Vibration and Control*, vol. 21, no. 13, pp. 2661-84.

[16] Baz, A & Hong, JT 1997, 'Adaptive control of flexible structures using modal positive position feedback', *International journal of adaptive control and signal processing*, vol. 11, no. 3, pp. 231-53.

[17] Nima Mahmoodi, S, Ahmadian, M & Inman, DJ 2010, 'Adaptive modified positive position feedback for active vibration control of structures', *Journal of intelligent material systems and structures*, vol. 21, no. 6, pp. 571-80.

[18] Lim, TW, Bosse, A & Fisher, S 1996, 'Structural damage detection using real-time modal parameter identification algorithm', *AIAA journal*, vol. 34, no. 11, pp. 2370-6.

[19] Lim, TW, Bosse, A & Fisher, S 1997, 'Adaptive filters for real-time system identification and control', *Journal of guidance, control, and dynamics*, vol. 20, no. 1, pp. 61-6.

[20] Piombo, B, Fasana, A, Marchesiello, S & Ruzzene, M 2000, 'Modelling and identification of the dynamic response of a supported bridge', *Mechanical Systems and Signal Processing*, vol. 14, no. 1, pp. 75-89.

[21] Kedem, B 1986, 'Spectral analysis and discrimination by zero-crossings', *Proceedings of the IEEE*, vol. 74, no. 11, pp. 1477-93.

[22] Heideman, MT, Johnson, DH & Burrus, CS 1985, 'Gauss and the history of the fast Fourier transform', *Archive for history of exact sciences*, vol. 34, no. 3, pp. 265-77.

[23] Frigo, M & Johnson, SG 2005, 'The design and implementation of FFTW3', *Proceedings of the IEEE*, vol. 93, no. 2, pp. 216-31.

[24] Moheimani, SR 2000, 'Minimizing the effect of out-of-bandwidth dynamics in the models of reverberant systems that arise in modal analysis: implications on spatial H∞ control', *Automatica*, vol. 36, no. 7, pp. 1023-31.

[25] Friedland, B 2012, *Control system design: an introduction to state-space methods*, Courier Corporation.

[26] Keviczky, L, Bars, R, Hetthéssy, J & Bányász, C 2019, 'State-Space Representation of Continuous Systems', in *Control Engineering: MATLAB Exercises*, Springer, pp. 55-70.

[27] Fang, J, Li, Q & Jeary, A 2003, 'Modified independent modal space control of mdof systems', *journal of sound and vibration*, vol. 261, no. 3, pp. 421-41.

[28] Poh, S & Baz, A 1990, 'Active control of a flexible structure using a modal positive position feedback controller', *Journal of intelligent material systems and structures*, vol. 1, no. 3, pp. 273-88.

[29] Morin, P & Samson, C 2000, 'Control of nonlinear chained systems: From the Routh-Hurwitz stability criterion to time-varying exponential stabilizers', *IEEE Transactions on Automatic Control*, vol. 45, no. 1, pp. 141-6.

[30] Nikravesh, SKY 2018, *Nonlinear systems stability analysis: Lyapunov-based approach*, CRC Press.

[31] Gilbert, GT 1991, 'Positive definite matrices and Sylvester's criterion', *The American Mathematical Monthly*, vol. 98, no. 1, pp. 44-6.

[32] Gwadabe, TR, Salman, MS & Abuhilal, H 2014, 'A modified leaky-LMS algorithm', *International Journal of Computer and Electrical Engineering*, vol. 6, no. 3, p. 222.